Aus dem Institut für Genome Stability in Ageing and Disease
der Universität zu Köln
Direktor: Prof. Dr. Björn Schumacher

The cell cycle gene repressor DRM- complex modulates DNA damage response in *Caenorhabditis elegans*

Inaugural- Dissertation zur Erlangung der Doktorwürde
der Medizinischen Fakultät
der Universität zu Köln

vorgelegt von
Georg Sendtner
aus Würzburg

promoviert am 23.05.2022

Gedruckt mit Genehmigung der Medizinischen Fakultät der Universität zu Köln

Druckjahr 2022

Dekan: Universitätsprofessor Dr. med. G.R. Fink

1. Gutachter: Universitätsprofessor Dr. rer. nat. B. Schumacher

2. Gutachter: Professorin Dr. rer. nat. Aleksandra Trifunovic

Erklärung

Ich erkläre hiermit, dass ich die vorliegende Dissertationsschrift ohne zulässige Hilfe Dritter und ohne Benutzung anderer als der angegebenen Hilfsmittel angefertigt habe; die aus fremden Quellen direkt oder indirekt übernommenen Gedanken sind als solche kenntlich gemacht.

Bei der Auswahl und Auswertung des Materials sowie bei der Herstellung des Manuskriptes habe ich Unterstützungsleistungen von folgenden Personen erhalten:

Arturo Bujarrabal

Weiter Personen waren an der geistigen Herstellung der vorliegenden Arbeit nicht beteiligt. Insbesondere habe ich nicht die Hilfe einer Promotionsberaterin/ eines Promotionsberaters in Anspruch genommen. Dritte haben von mir weder unmittelbar noch mittelbar geldwerte Leistungen für Arbeiten erhalten, die im Zusammenhang mit dem Inhalt der vorgelegten Dissertationsschrift stehen.

Die Dissertationsschrift wurde von mir bisher weder im Inland noch im Ausland in gleicher oder ähnlicher Form einer anderen Prüfungsbehörde vorgelegt.

Die dieser Arbeit zugrunde liegende RNA sequencing Analyse mit dem *lin-52(n771)* Mutanten im Vergleich zum Wildtyp wurde ohne meine Mitarbeit in dem Institut für Genome Stability in Ageing and Disease/ CECAD Köln AG Schumacher von Herrn Bujarrabal ermittelt und zur Verfügung gestellt.

Die in dieser Arbeit verwendeten Primer paare und Kreuzungen wurden teilweise ohne meine Mitarbeit in dem Institut für Genome Stability in Ageing and Disease/ CECAD Köln AG Schumacher zur Verfügung gestellt. Im näheren in den Methoden angegeben.

Der in dieser Arbeit verwendete *E. coli* Bakterien Stamm TOP10 und das Plasmid px330A wurde ohne meine Mitarbeit in dem Institut ZMMK, Köln von Sara de la Cruz Molina zur Verfügung gestellt.

Die in dieser Arbeit angegebenen Experimente sind nach entsprechender Anleitung durch Herrn Bujarrabal von mir selbst durchgeführt worden.

Erklärung zur guten wissenschaftlichen Praxis:

Ich erkläre hiermit, dass ich die Ordnung zur Sicherung guter wissenschaftlicher Praxis und zum Umgang mit wissenschaftlichem Fehlverhalten (Amtliche Mitteilung der Universität zu Köln AM 24/2011) der Universität zu Köln gelesen habe und verpflichte mich hiermit, die dort genannten Vorgaben bei allen wissenschaftlichen Tätigkeiten zu beachten und umzusetzen.

Köln, den 23.06.2021

Acknowledgements:

I am very thankful to Prof. Dr. Schumacher for giving me the opportunity to do this experimental work in his laboratory and for his support at all stages of my thesis. Arturo Bujarrabal was not only supporting me as a mentor during the whole process of my thesis and encouraging me with good ideas when experiments did not work. He was also a good sports partner for climbing on many occasions. Thanks also to my parents and my two sisters, Barbara and Elisabeth, who supported me with energy, good advice and food, whenever I was in need during my research work. I also would like to acknowledge the support of Aileen, my girlfriend, who encouraged me strongly during the hard times while writing this thesis. Many thanks also to all people in the laboratory, in particular Ash, Markus, Najmeh, Simon, Robert, João and Paulo, giving me advice for experiments, staying with me on weekends in lab, showing me how to climb and making fun several times to cheer someone up, and thus to bring this work to success.

Table of contents

Abbreviations

6-4PP	Pyrimidine (6-4) pyrimidone photoproduct
ARF	Alternative reading frame
B-MYB/MYBL2	MYB proto-oncogene like 2
bp	base pairs
C. elegans	*Caenorhabditis elegans*
CDE	Cell cycle dependent element
CHR	Cell cycle gene homology region
CPD	Cyclobutane pyrimidine dimer
CSA-1/*csa-1*/CSA	Cockayne syndrome protein A
CSB-1/*csb-1*/CSB	Cockayne syndrome protein B
dd	double distillated
DDB	DNA damage binding protein
DDR	DNA damage response
DNA Pol	DNA polymerases
DP	Dimerization partner
DREAM	DP, RB- like, E2F and MuvB- complex (Human)
dREAM	DP, RB- like, E2F and Myb- complex (*Drosophila melanogaster)*
DRM	DP, RB and MuvB- complex (*C. elegans*)
DSB	Double-strand break
DYRK1A	Dual specificity tyrosine (Y)-phosphorylation-regulated kinase 1A
e.g.	exempli gratia/ for example
E. coli	*Escherichia coli*
EdU	5-Ethynyl-2´Deoxyuridin

ERCC1	Excision repair 1 protein
Fig.	Figure
FOXM1	Forkhead box M1
GG-NER	Global- Genome- nucleotide excision repair
Gy	Gray
HR	Homologous recombination
ICL	Interstrand cross links
IR	Ionizing radiation
LB	Lysogeny broth
mESC	Mouse embryonic stem cells
MMS	Methyl- methanesulphonate
MOPS	3-(N-Morpholino)propanesulfonic acid, 4-Morpholinepropanesulfonic
NER	Nucleotide excision repair
NGM	Nematode growth media
NuRD	Nucleosome remodeling and histone deacetylase (complex)
PBS	Phosphate buffered saline
PBST	Phosphate buffered saline tween
PCNA	Proliferating cell nuclear antigen
RB	Retinoblastoma
RBL2	RB-like 2 protein/ p130
RCF	Relative centrifugal force
RFC	Replication factor C
RPA	Replication protein A
synMuvB	Class B synthetic multivulva
TC-NER	Transcription- Coupled- nucleotide excision repair
TFIIH	Transcription initiation factor IIH

USP7	Ubiquitin specific processing protease 7
UV	Ultraviolet
UVSSA	UV-stimulated scaffold protein A
XPA-1/ *xpa-1*/ XPA	Xeroderma pigmentosum group A
XPB	Xeroderma pigmentosum group B
XPC-1/*xpc-1*/XPC	Xeroderma pigmentosum group C
XPD	Xeroderma pigmentosum group D
XPF	Xeroderma pigmentosum group F
XPG	Xeroderma pigmentosum group F

1.1 Abstract

Cancer is a frequent cause of death. Disturbed or inefficient DNA damage response including DNA repair, cell cycle control and apoptosis, can cause tumorigenesis. The central question for this thesis was to study the relation between DNA repair and cell cycle control. The DPL-1- RB- MuvB (DRM)- complex is a well-characterized gene repressor in the nematode *Caenorhabditis elegans.* Its main task is the regulation of the cell cycle by repression of different genes. Homologous complexes also exist in humans and *Drosophila melanogaster*. For this reason, the DRM- complex was investigated in *Caenorhabditis elegans*. DNA damage was applied to mutants for this complex to study the impact on larval development. Furthermore, these mutant worms were intercrossed with several mutants for DNA repair pathways to investigate the interplay of cell cycle regulation and DNA repair. Using multiple *in-vivo* approaches by applying different types of DNA damage to these worms and *in-vitro* studies with qPCR and western blot analyses provided evidence that DRM- complex mutant worms exhibit an improved response to DNA damage. This is not a consequence of accelerated cell cycle. Mutants with defects in different DNA repair pathways exhibit an arrest in larval development. Interestingly, this could be bypassed partially by intercross with mutants of the DRM- complex. In summary these data indicate that mutants defective for components of DRM- complex exhibit improved response to different DNA damaging agents and that multiple repair mechanisms are involved in this altered developmental response of DRM- complex mutants.

1.2 Zusammenfassung

Krebs ist eine der häufigsten Todesursachen. Eine gestörte oder reduzierte DNS Schadensantwort, welche DNS Reparatur, Zellzykluskontrolle und Apoptose beinhaltet, kann Ursache einer Tumorentstehung sein. Zentrale Fragestellung dieser Doktorarbeit war die Erforschung einer Interaktion zwischen Zellzyklusregulation und DNS Reparatur. Der DPL-1- RB- MuvB (DRM)- Komplex ist ein bekannter Genrepressor im Nematoden *Caenorhabditis elegans.* Dieser Komplex reguliert durch Repression von verschiedenen Genen den Zellzyklus. Ein homologer Komplex ist auch beim Menschen oder der Fliegenart *Drosophila melanogaster* bekannt. Aus diesen Gründen wurde der DRM- Komplex für die experimentelle Forschungsarbeit mit dem Nematoden *Caenorhabditis elegans* ausgewählt. DNS Schäden, induziert durch unterschiedliche Methoden, wurden Mutanten für diesen Komplex zugefügt und der Einfluss auf die Larvenentwicklung untersucht. Des Weiteren

wurden diese Mutanten mit Mutanten, welche genetische Mutationen in unterschiedlichen DNS Reparaturmechanismen zeigten, verkreuzt, um die Interaktion zwischen Zellzyklusregulation und DNS Reparatur zu untersuchen. *In- vivo* Versuche, in denen unterschiedliche Formen von DNS Schaden an Würmern appliziert wurden, und *in-vitro* Versuchsansätze, wie qPCR oder Western Blot, wurden angewandt. Es zeigte sich eine verbesserte DNS Schadensantwort in DRM- Komplex Mutanten. Dies war keine Folge von schnellerer Zellteilung. Mutanten mit Schäden in unterschiedlichen DNS Reparaturmechanismen zeigten eine langsamere Progredienz oder sogar ein Sistieren der Larvenentwicklung. Diese Entwicklung konnte partial verbessert werden, indem DRM-Komplex Mutanten mit den eben genannten Mutanten gekreuzt wurden. Zusammenfassend wurde in dieser Arbeit gezeigt, dass Mutanten mit genetischen Mutationen in Genen des DRM- Komplexes eine verbesserte DNS Schadensantwort auf unterschiedlicher Formen von DNS Schädigung zeigten. Unterschiedliche DNS Reparaturmechanismen konnten für diese verbesserte Antwort identifiziert werden.

2. Introduction

2.1 The DNA damage response

DNA damage can occur in multiple forms in each cell of the human body at any moment. This can have mutagenic consequences and cause carcinogenesis. The control of the DNA damage response (DDR) is important for tumor suppression. This DDR includes many different cellular mechanisms (1). Among these, repair of DNA damage and the regulation of the cell cycle have central relevance.

In mammalian cells several DNA repair mechanisms are known. Loss or dysregulation of these mechanisms can result in tumor development and other cellular pathologies. This becomes apparent for example in the autosomal recessive disorder Xeroderma pigmentosum which is caused by mutations in genes related to nucleotide excision repair (NER) (2). This disorder becomes clinically manifest by photosensitivity, skin cancer after Ultraviolet (UV) exposure (3), ocular abnormalities (4), neurological degeneration (5) and hearing loss (6), which is variable with the different mutations in the corresponding NER genes. These different manifestations indicate that loss of function of a gene product involved in DNA repair can also result in other cellular dysfunctions as a consequence of the unsuccessful DNA repair. This appears even more prominent in patients with the Cockayne syndrome, which is also caused by mutations in genes for the NER (2). This disorder manifests clinically by neurological degenerations and premature aging (2). Thus, this may indicate that DNA repair mechanisms play also a central role in development and aging. How DNA repair pathways are regulated by other cellular mechanisms is not fully understood yet and part of current biomedical research.

The regulation of cell cycle is another important mechanism in the DDR. Multiple cell cycle regulators prevent cells to undergo uncontrolled cell division leading to tumorigenesis. Among these is the retinoblastoma (*RB1)* gene which is functioning in cell cycle regulation and referred as a tumor suppressor gene (7). Carriers of a hereditary mutation in the *RB1* gene in germline cells are at high risk to develop different tumors in case of a second hit mutation in this allele (8).

Investigations of how DNA repair and cell cycle regulation are connected could give more insights in NER- triggered diseases and tumor development but also provide a fundamental understanding of DDR mechanisms in cells.

2.1.1 DNA damage repair

DNA damage is triggered by many factors such as UV- irradiation, ionizing radiation (IR) or chemical substances. Each exposure can cause multiple types of DNA damage and different types of DDRs. UV-B irradiation usually leads to DNA modifications such as cyclobutane pyrimidine dimers (CPDs) and pyrimidine (6-4) pyrimidone photoproducts (6-4PPs) (9). Interestingly, each type of DNA damage itself leads to a different DDR: CPDs, the most common forms of lesion after UV-B irradiation, have higher impact on cell cycle regulation, whereas 6-4PPs have higher potency to induce apoptosis in the cell (10). Previous research also suggests that these types of DNA damage can block replication forks in the cell which can cause DNA double-strand breaks (DSBs) when these blocked replication forks are not resolved (11). This type of lesion is supposed to be the most harmful one (12).

2.1.1.1 The nucleotide excision repair pathway

CPDs and 6-4PPs can be detected and repaired by the NER. This repair mechanism can be further divided in four steps: 1) Lesion detection, 2) damage verification, 3) excision and 4) DNA synthesis/ ligation (13). The first step can be again separated in two different acting pathways which merge again in the second step: The global- genome (GG)- NER and the transcription- coupled (TC)- NER.

The central protein in the GG-NER in humans is the Xeroderma pigmentosum group C protein (XPC) which works together in a complex with hRAD23B and centrin 2 (CETN2) to detect helix distorting lesions (14). This detection process can be markedly increased by the UV-damage DNA-binding protein complex which consists of DNA damage binding protein 1 (DDB) and DDB2. This complex can recognize CPDs and 6-4 PPs and reacts with a bend in the DNA (15,16). This guides XPC towards the lesions. Ubiquitylation processes and complex formation then recruit the transcription initiation factor IIH (TFIIH) (17).

The TC-NER does not actively detect helix distorting lesions but gets recruited by the RNA-polymerase II when it is blocked. Consistent with this, the TC-NER is only detecting lesions at the transcribed strand whereas the GG-NER works in the whole genome (18). When the RNA- polymerase II arrests by DNA blocking lesions, the Cockayne syndrome protein B (CSB) gets recruited which is also supposed to be the key regulator for the TC-NER (18). This protein assembles further proteins of the TC-machinery such as the Cockayne syndrome protein A (CSA), UV-stimulated scaffold protein A (UVSSA) and ubiquitin - specific processing protease 7 (USP7). Subsequently, this TC- machinery recruits the TFIIH (14).

At this point both NER sub-branches merge into a common pathway. The TFIIH consists of 10 protein subunits. Among these are Xeroderma pigmentosum group B (XPB) and Xeroderma pigmentosum group D (XPD) proteins which are responsible for unwinding the DNA. Interestingly, XPB only works as ATPase whereas XPD has an additional helicase function which is supposed to verify DNA damage (17,19). This process is also assisted by the Xeroderma pigmentosum group A protein (XPA) (14,20) which is also involved in the detection of chemical alterations in ssDNA (20,21). Furthermore, XPA is considered as one of the central proteins in the NER as it interacts with multiple other proteins of this repair mechanism (22). After verification processes the damaged DNA strand is incised by the two endonucleases: The 5' strand is incised by the Excision repair 1 protein (ERCC1), acting together with Xeroderma pigmentosum group F protein (XPF). In addition, the 3' strand is incised by the Xeroderma pigmentosum group G protein (XPG) which is dependent on the ERCC1-XPF endonuclease incision (23). This point is also described as the "point of no return" (14) where mistakes in the following repair can be detrimental for the cell. Thereby, modulating function and protection of the non-damaged strand is done by the replication protein A (RPA). The excised damaged DNA fragment is then released together with the bound TFIIH (22). DNA synthesis and ligation of the new DNA strand is then performed by proliferating cell nuclear antigen (PCNA), replication factor C (RFC), different DNA polymerases (DNA Pol) such as DNA Pol δ, DNA Pol ε or DNA Pol κ, and DNA ligase 1 (14). Understanding this DNA repair mechanism is still a central part of ongoing research, as its regulation and how it differs in different cell types is much more complex than described here.

2.1.2 Cell cycle regulation

The cell cycle consists of interphase, including G1, S and G2 phase, and the subsequent mitotic (M) phase. Cells can also arrest cell cycle by entering the G0 phase (24). This process is regulated and controlled by many genes and their corresponding products. Errors in this regulatory network can lead to uncontrolled cell division and carcinogenesis. One specific group of genes known as "tumor suppressors" have their main task in preventing uncontrolled cell division. Retinoblastoma (RB1) is a well-established tumor suppressor gene in human cells, controlling the expression of cell cycle regulatory gene products during the G1/S phase (7). In addition, the RB1 protein plays a central role to maintain persistence in G0 (25). Loss of function mutations in *RB1* are found in many different types of tumors, including retinoblastoma itself, the most frequent eye cancer in childhood (8), but also osteosarcoma, small-cell lung cancer and many others (26). Even though RB1 may be one of the best- known proteins acting in cell cycle repression, it is not the only one. There are

other tumors in which the expression of cell cycle regulators for G2/M (27) or G0 phase are also deregulated (28). The cellular basis for these forms of deregulation of the cell cycle is less well understood.

2.1.2.1 The DREAM- complex

The DP, RB- like, E2F and MuvB (DREAM)- complex is a conserved complex that is found both in invertebrates, such as the nematode *Caenorhabditis elegans* (*C. elegans),* and in vertebrates. Its main function is to repress cell cycle genes during cell quiescence. In addition, subunits of this complex are involved in activating gene expression with peaks in G1/S and G2/M phase. Thus, it differs from the well-characterized RB1 which represses the transcriptional activators E2F1, E2F2 and E2F3 together with corresponding dimerization partners (DP) and acts in a complementary way to cell cycle regulators for the G1/2 phase (29).

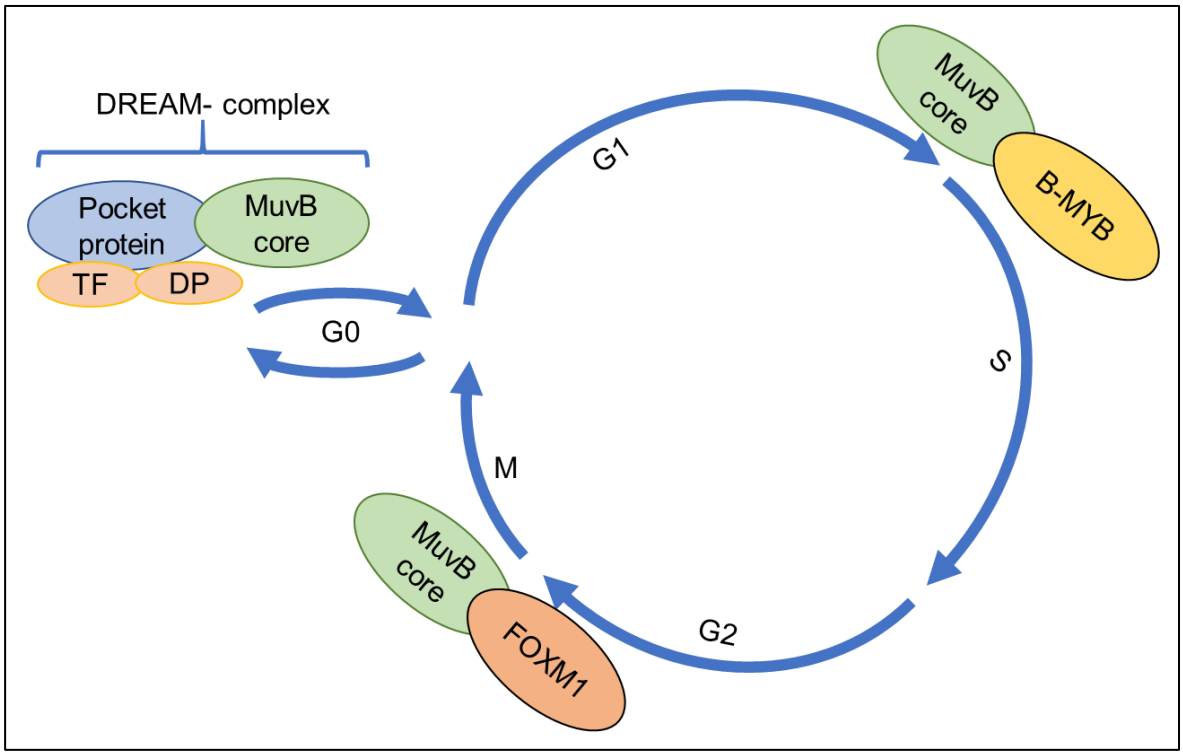

Figure 1. **Schema of the DREAM- complex and other subcomplexes functioning in the cell cycle in mammalian cells**

DREAM- complex in mammalian cells represses genes to promote G0 phase and cell quiescence. During cell division the MuvB core complex which consists of LIN9, LIN54, LIN37, LIN52 and RBBP4 can act together with B-MYB to activate genes with peaks in G1/S phase. Among these is also the protein coding gene FOXM1 which adopts the function of B-MYB in G2/M phase to activate genes together with the MuvB core complex. Schema was adapted from: Sadasivam, et al. 2013. Figure 1b.

As part of the mammalian DREAM- complex, the RB-like 2 protein p130 (RBL2) is able to bind to the transcription repressors E2F4 and E2F5, together with their DPs, and forms the p130-DP-E2F4 complex. The p130 pocket protein also interacts with the MuvB core, which contains LIN9, LIN54, LIN37, LIN52 and RBBP4 (30). The interaction of these three subunits (p130 pocket protein, transcription factor and dimerization partner, MuvB core) then results in the so-called DREAM- complex (Fig. 1).

A key regulation for the p130 and MuvB core unit interaction is the phosphorylation at serine 28 in the LIN52 protein by the dual specificity tyrosine (Y)-phosphorylation-regulated kinase 1A (DYRK1A) (31). This phosphorylation is necessary for binding of LIN52 to the p130 pocket protein, resulting in the active DREAM- complex. A loss or inhibition of this serine 28 phosphorylation in LIN52 does not result in reduced MuvB core assembly, but it affects the recruitment of p130 to the MuvB core unit. This then causes decreased induction of RAS- induced senescence and cell quiescence (31). The assembly of the DREAM- complex can promote cell quiescence by inhibiting several genes during G0 phase (30). Inhibition of gene expression in G0 phase is mediated by the transcription factor E2F4 via E2F binding sites (30) but also by the MuvB component LIN54, via cell cycle gene homology regions (CHRs) (32).

Interestingly the MuvB core in mammalian cells can also interact with the transcription factors MYB proto-oncogene like 2 (B-MYB/MYBL2) and Forkhead box M1 (FOXM1). Interaction between these proteins and MuvB core unit promotes and activates the expression of genes which are repressed by the DREAM- complex in G0 (33). The MuvB-B-MYB interaction leads to activation of genes with peaks in G1/S phase, whereas the MuvB- FOXM1 interaction leads to activation of genes with peaks in G2/M phase (Fig. 1). Interestingly, the MuvB- B-MYB complex itself regulates the expression of FOXM1 in S phase (34) while B-MYB degrades by a proteasome mediated process at the same time (35). Thus, the MuvB core unit has a dual function: Repression of genes through the DREAM- complex and activation of genes through B-MYB and FOXM1 interactions.

2.2 The role of DREAM- complex in the DNA damage response

The DREAM- complex is also involved in the DDR by inhibiting cell cycle progression. This process is surprisingly mediated through the activation of the DNA damage key modulator p53 in the p53-p21-DREAM-E2F/CHR pathway (36). Activation of p53 by DNA damage leads to upregulation of p21/CDKN1A which inactivates cyclin dependent kinases which are normally phosphorylating p130 and p107. Reduced phosphorylation of p130/p107 is an important factor for DREAM- complex assembly which then leads to cell cycle arrest and repression of gene expression (37). The importance for this regulatory pathway can be

especially seen in cells lacking p53 which exhibit elevated levels of gene expression via B-MYB- MuvB interaction, resulting in uncontrolled cell- division (36,38). Furthermore, p53 switches also the balance from B-MYB- MuvB to the activation of the DREAM- complex when DNA damage is induced by doxorubicin (38).
In addition, it has been shown that genes of the NER are regulated by the DREAM- complex, extending DREAM function in DDR also towards DNA repair regulation. For example, XPC is bound at the promoter level by E2F4 and p130 (39), two members of the DREAM-complex. Interestingly, this E2F4- mediated repression can be disrupted by the activation of the tumor suppressor alternative reading frame (ARF) (40). In this context, ARF acts independently from p53 (40).
These investigations revealed that the DREAM- complex is a main regulator in DDR. Its functions reach even beyond cell cycle regulation. Perturbations of this complex can trigger tumorigenesis via dysfunction of the MuvB- B-MYB/ MuvB- FOXM1 complex. Overexpression of B-MYB but also components of the DREAM- complex such as LIN9 can be found in a variety of tumors, e.g. breast cancer (41). In such cases, this overexpression is correlated with a poor overall prognosis for patients (42). This clinical observation points out the importance for research in DDR because its components could be targets for future cancer therapies. Understanding mechanisms in cell cycle regulation and DNA repair after damage could give more insights in such targets for therapy development. These could be used for better tumor treatment and individualized therapies in cases with defined mutations and overexpression of specific cell cycle genes.

2.3 Research strategy for this project

2.3.1 *Caenorhabditis elegans* as a model for biomedical research

Deeper understanding of the cellular mechanisms underlying tumor development and therapy development depend on the availability of appropriate experimental organisms. These model organisms should be suitable for studying the relation of cell cycle regulation and DNA repair within the DDR. *Caenorhabditis elegans* (*C. elegans)* is well- known for its complex developmental programs that regulate mitosis and differentiation in distinct cell types during development. For this purpose, I decided to use the nematode *C. elegans*. This nematode allows *in-vivo* investigations which give insights in gene expression and cell cycle regulation in the context of cell differentiation under physiological conditions. Experiments with cell culture are less suitable for studying gene- phenotype correlations in the whole organism. For this reason, I decided to do most of my experiments *in-vivo*. The conditions for maintaining *C. elegans* are also simple: The worms are usually stored at 20°C

on agar plates containing the *Escherichia coli* (*E. coli*) strain OP50 for feeding. Basic experiments such as western blot approach or quantitative real time PCR (qRT-PCR) analysis are also possible with this nematode. DNA damage can be easily induced by irradiating the worms with UV-B light, ionizing radiation or application of chemical drugs. This nematode has two sexes dependent on the number of X- chromosomes: Hermaphrodite have two X- chromosomes and obtain progeny by self- fertilizing. Males have one X- chromosome and can be easily identified by their different sharp- tail (43). With this characteristic phenotype, intercrossing of different mutant strains can easily be achieved. The life cycle of *C. elegans* is quite fast compared to other experimental organisms (Fig. 2). The worms reach adult stage within less than a week when kept under standard conditions (20°C) (43,44). *C. elegans* undergoes development through four larval stages (L1, L2, L3, L4) until adulthood is reached (Fig. 2).

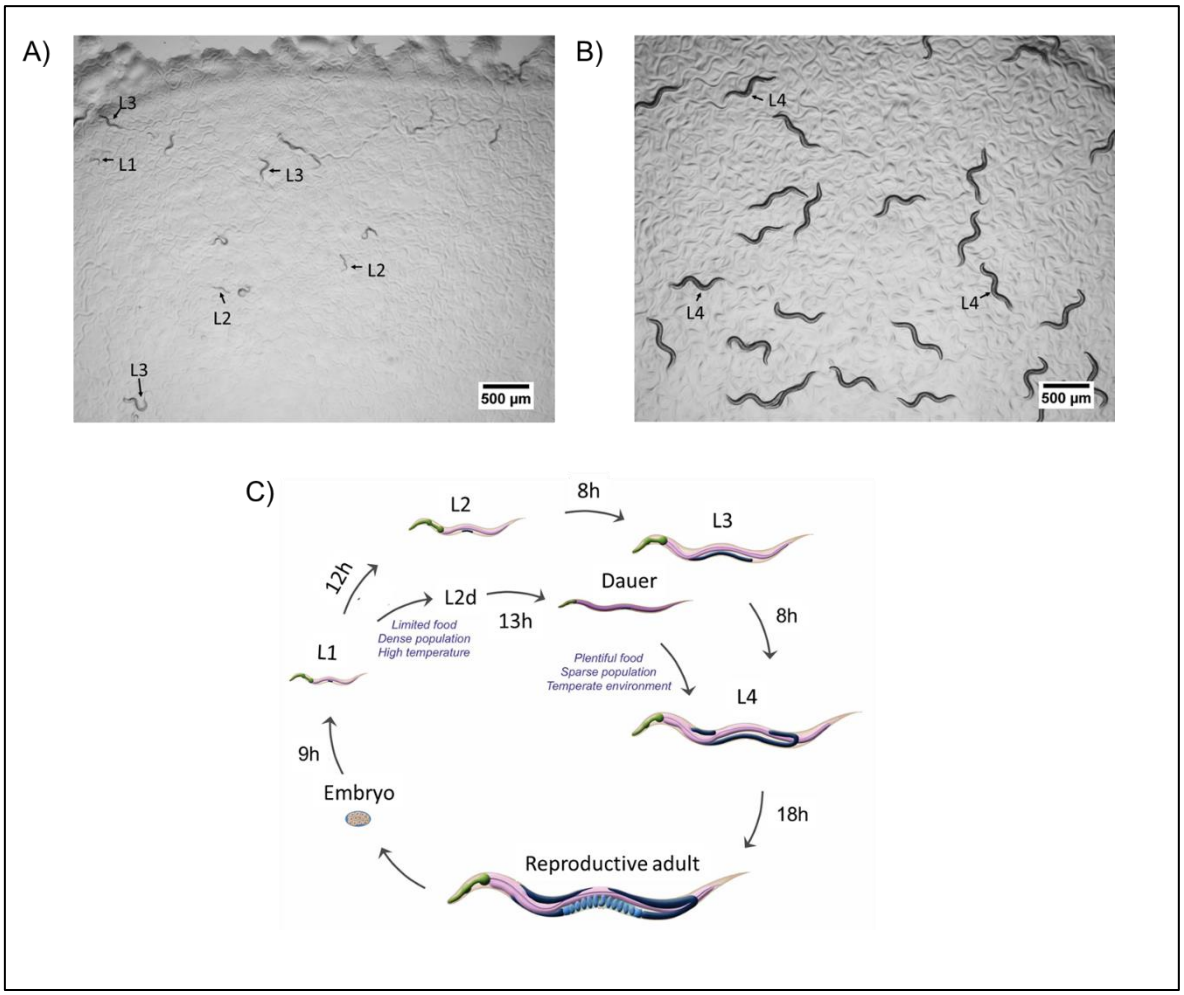

Figure 2. **Representative pictures of larval stages in C. elegans**

2a) Representative pictures of different larval stages of N2 wildtype worms. Worms were applied to 40mJ/cm² of UV-B irradiation in this picture which importance will be clarified later.
2b) Representative picture of L4 wildtype worms. All pictures were done with the same magnification. Overall magnification: 38.5x. Scale bar showing length of 500µm. 2c) Schema of larval development in C. elegans. Picture was adapted from: https://www.wormatlas.org/dauer/introduction/DIntroframeset.html (last access 26.05.2021)

Starting from the egg, hatching can be seen after 10- 12 hours (44). Then the worms enter the first larval stage (L1) which usually takes another 12- 16 hours to reach the second larval stage (L2). The ending of each larval stage is connected to molding. The mean time for further larval stages (L2, L3, L4) is described in literature with 8- 12 hours for each larval stage when kept under standard conditions (43). Examples for different larval stages in *C. elegans* are given in figure 2. This larval development can be only seen when worms are being fed. No food leads to developmental arrest (45) or the “dauer” stage, a special form of L3, for which a specific developmental program is already set at L1 stage, depending on food availability but also temperature and worm density (46). These dauer worms exhibit e.g. different behavior in health span, metabolism and resistance to stress (47). Interestingly, worms can survive in this dauer stage several months and can return to normal development when food is applied again (48). Apart from the dauer stage, each larval stage exhibits different phenotype characteristics such as the length (44) or invagination of the vulva cells, which can be seen in a white spot in the middle of the worm. This phenotype is typical for the L4 stage (49).

The L1 worms consist out of about 550 somatic cells and four gonad precursor cells (50). Thus, experimental approaches at this larval stage are suitable for studying mechanisms that are distinct in somatic and germline cells. Somatic cells in adult worms are supposed to be postmitotic (less cell division can be seen in late L2 worms and during L3) whereas germline cells divide during development (50,51). This difference is important for cellular responses to DNA damage and repair. While affected germline cells can undergo apoptosis, somatic cells usually do not and have to repair DNA damage to maintain their cellular function (52). DNA damage in somatic tissue can lead to a delay in larval development. This delay can be especially seen when DNA repair is disabled, leading to a developmental arrest (53). This specific phenotype will be also important for the experimental work in this thesis.

2.3.2 The nucleotide excision repair in *C. elegans*

In *C. elegans* many NER genes are well characterized to function as orthologs to human genes. This includes genes and gene products for the main repair mechanism for UV-B irradiation related damage (13). As explained above, the NER in humans can be divided in two sub-branches (TC- and GG-NER). Genes of both branches are also expressed in *C. elegans* such as *csb-1*, *xpc-1*, *xpa-1* or *csa-1* which are also orthologs to the human genes *CSB*, *XPC, XPA* and *CSA* (13,54-56). Furthermore, it has been shown that these two sub-branches of the NER do also function likewise in *C. elegans* than in humans (13,54).

Interestingly, the GG-NER has been described to be more relevant for cellular survival and DNA damage repair of germ cells after UV-B irradiation (54). UV-B irradiation of L1 *xpc-1* mutants leads only to a small delay in larval development. Interestingly, the same worms exhibit lack of germline development which results in adult sterility (53,54). In comparison to this, the TC-NER is supposed to be the main repair mechanism for UV-B irradiation damage repair in the somatic tissue (53,54). UV-B irradiation of *csb-1* mutants leads to defects in the somatic tissues resulting in developmental delay. However, germline cells are less affected and even undergo mitosis (53).
This difference in phenotype after UV-B irradiation can be used to test the relation of other genes to the NER sub-branches in an experimental setup. This is the basis for a commonly used paradigm to test larval development after UV-B irradiation (57).

2.3.3 The DRM- complex in *C. elegans*

The DREAM- complex in mammals is named DRM- complex in *C. elegans* and is supposed to act in homologous manner (58), although its function is also slightly different.
The root of DRM- complex research was the discovery of a multivulva (Muv) phenotype in *C. elegans*. This is caused by a hyper- induction of vulva precursor cells in worms. Interestingly, this phenotype could be also observed when worms carry mutations in *lin-8* and *lin-9* genes at the same time. Thus, this phenotype was called synthetic multivulva (synMuv) (59). This discovery started the process of searching for additional genes with related phenotype. It is important to mention that only mutations of genes which refer to the class A synMuv genes (such as *lin-8*) in combination with mutations in genes which refer to the class B synMuv genes (such as *lin-9*) lead to the previous phenotype (60). Single mutations in one class of the synMuv genes results in a wildtype phenotype (60). A subgroup of genes of the class B synMuv group was later identified as one complex containing LIN-9, LIN-35, LIN-37, LIN-52, LIN-53, LIN-54, DPL-1 and EFL-1 which also functions apart from other synMuvB genes (58). This complex was further named as the DRM (DP, RB, MuvB)- complex (58). Similar subunits of this complex were also identified in the dREAM- complex in *Drosophila melanogaster* (61) and the DREAM- complex in mammalians (29). A comparison between these complexes in different organisms can be found in figure 3a.
LIN-35 in *C. elegans* resembles the RB- like proteins p130/p107, and *lin-53* encodes for a protein with similar function as RbAp48 (62). EFL-1 is most similar to the transcription factor E2F4 and E2F5 in mammals (63). This protein is acting together with the dimerization partner DPL-1. These investigations reveal homology genes in DRM- complex and DREAM-complex.

A)

Subcomplex	Pocket protein	Transcription factor	Dimerization partner	MuvB core	MuvB core	MuvB core	MuvB core	MuvB core	B-MYB	FOXM1
Human	RBL1(p107) RBL2(p130)	E2F4 E2F5	DP1 DP2 DP3	LIN9	LIN37	LIN52	RBBP4	LIN54	MYBL2/ B-MYB	FOXM1
Drosophila melanogaster	Rbf1 Rbf2	E2f2	Dp	Mip130	Mip40	Lin52	Caf1	Mip120	Myb	-
C. elegans	LIN-35	EFL-1	DPL-1	LIN-9	LIN-37	LIN-52	LIN-53	LIN-54	-	-

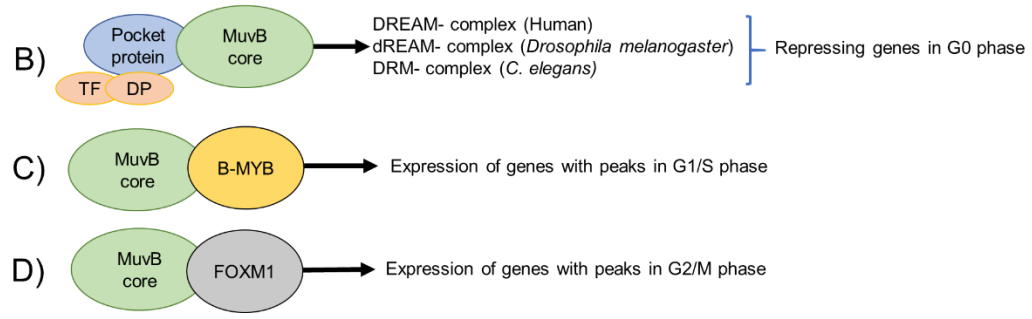

Figure 3. **Comparison between the DREAM/dREAM/DRM- complex in different organisms**

3a) Table showing comparison of different subunits of the DREAM- (Human), dREAM- (*Drosophila melanogaster*) and DRM- complex (*C. elegans*). Furthermore, in human and drosophila cells the transcription factor B-MYB/ Myb and FOXM1 (only in humans) can be found. 3b) Schema of the DREAM-/ dREAM- and DRM- complex. The main function of this complex is the repression of genes to admit G0- phase. TF = Transcription factor, DP = Dimerization partner. 3c) Schema of B-MYB/Myb acting together with the MuvB core unit to promote gene expression with peaks in G1/S phase. 3d) Schema of FOXM1, a transcription factor only known in human cells, promoting gene expression with peaks in G2/M phase together with the MuvB core unit.

Chromatin immunoprecipitation sequencing (ChIP- seq) data of late *C. elegans* embryos show a high overlap of peaks of EFL-1 and DPL-1 with other members of the DRM- complex, indicating that these subcomplexes function together in gene regulation (64). The same study also provided evidence that different subcomplexes might be involved in different tasks, similar to the DREAM- complex in mammals. In this context, the DRM- complex can be separated in three subcomplexes: The transcription factor (EFL-1) together with its dimerization partner (DPL-1), the MuvB- core- complex as the main mediator (consisting out of LIN-9, LIN-37, LIN-52, LIN-53 and LIN-54) and LIN-35 as the core regulation unit/ pocket protein (Fig. 3a and 3b). However, the exact mechanism of DRM- complex assembling, its molecular structure and the way of gene repression are still not fully understood.

Although these proteins that build the DREAM/dREAM/DRM- complex in different species may reveal similar and homologous structures, functions between these complexes are not completely similar: Whereas the DREAM- complex in mammals is known to repress genes in G0 phase, some of its components also regulate expression of these and other genes

during the G1/S phase of the cell cycle by a switch of the MuvB subunit to B-MYB and FOXM1 (Fig. 3c and 3d). The DRM- complex in *C. elegans* has so far only been found to function as a transcriptional repressor of germline development (65). Furthermore, a homolog to B-MYB or FOXM1 has so far not been identified in *C. elegans* and has not been purified or co-precipitated as a component of the DRM- complex (58).

2.4 Modulation of DRM- complex components in *C. elegans* reveal cellular functions beyond cell cycle regulation

RNAi mediated knock-down of DRM- complex genes lead to expression of germline- related genes such as *pgl-1* in the somatic cells (66). However, this observation is not limited to the DRM- complex but also to other regulators of synMuvB such as *lin-15B*. The upregulation of typical germline- related genes can also be increased by elevating the environmental temperature from 20°C to 26°C. However, these effects are not consistent for all DRM-complex mutants (67). This increase of environmental temperature is also linked to larval arrest in L1 stage in most of the DRM- complex mutants (67). However, this phenotype is not observed in mutants for *lin-52* and *lin*-53. Interestingly, the levels of germline- related gene expression in somatic cells increase also in mutants of these two genes with higher temperatures. This study also shows that even though all genes are related to the DRM-complex, they are not supposed to show similar behavior when mutated. Furthermore, it has been shown that LIN-53 in *C. elegans* acts together with other proteins such as HDA-1 (68) and LET-418 (69) in a nucleosome remodeling and histone deacetylase complex (NuRD) to repress vulva development genes (70). This complex shows different and distinct functions from the DRM- complex (58), even though LIN-53 is part of both complexes.

2.5 Transcriptional repression by the DRM- complex in *C. elegans*

The mechanism of transcriptional repression by the DRM- complex in *C. elegans* is not well understood yet and part of current biomedical research.

ChIP- seq of *lin-35* null mutants revealed a decrease of chromatin occupancy by the other components of the DRM- complex. However, many target genes are still repressed under these conditions. This suggests a collaboration between LIN-35 and the other components of the DRM- complex for a successful target gene repression. Furthermore, a knock-down of MuvB- core complex genes but not *efl-1* or *dpl-1* in the *lin-35* knock-out model resulted in upregulation of genes which were still repressed in the single *lin-35* knock-out mutant (64). Thus, it was proposed that MuvB can also directly repress target genes by

mechanisms not involving the transcription regulators EFL-1 and DPL-1 (64). In the DREAM- complex LIN54 represses and activates genes over a CHR- binding motif (71). Investigations in *C. elegans* on this cellular function are still missing and part of current biomedical research.

Recent studies suggest histone modifications as a mechanism for the DRM- complex to regulate gene expression (72). One of these studies supposed H3K9 methylation as a mechanism for germline- related gene regulation by members of the DRM- complex and synMuvB (72). In this study, H3K9me2 promoter enrichment is especially reduced in *lin-15B* and at a lower degree also in DRM- complex mutants. This reduction is predominant in promoter regions of genes which are normally expressed in the germline and repressed by the synMuvB genes in somatic tissue (72). Furthermore, increased levels of H3K4me3 at promoter sites of germline- related genes, which corresponds to active gene expression (73), were detected in DRM- complex mutants and *lin-15B* mutants when compared to wildtype. Interestingly, a subset of genes was identified which exhibit elevated levels of H3K4me3 levels but not decreased levels of H3K9me2 in DRM- complex mutants but not *lin-15B* mutants (72).

The previous described temperature sensitivity of these mutants could also be readjusted by the knock-down of *set-25* and *met-2* which are both important genes for H3K9 methylation (72). This study points to a link between the DRM- complex, LIN-15B and H3K9me2 for repression of germline- related genes.

Another study showed that genes which are repressed by the DRM- complex have an enrichment of HTZ-1/H2A.Z within gene body regions. This could be an additional mechanism for transcriptional repression (74). The same study also showed that upregulation of genes in DRM- complex mutants is similar when *hzt-1* is knocked- down using RNAi (74).

Therefore, it is possible that transcriptional regulation of genes repressed by the DRM-complex is achieved via promoter but also gene body regulation.

In summary, these studies show that the nematode *C. elegans* is a useful model for biomedical research in the field of transcriptional processes during cell cycle regulation and DNA repair. This organism exhibits common DNA repair pathways such as the NER and also cell cycle regulators such as the DRM- complex which exist in similar format in mammals. These requirements are ideal for its use as a model for studying the relation of both mechanisms in the same context. Comprehending how the cell cycle regulation affects the DNA damage response and repair could also help to understand cancer development and resistance to chemotherapies or irradiation.

2.6 Central question and personal aim in this thesis

The central aim of my thesis was to characterize the role of the DRM- complex in DNA-repair in *C. elegans*. For this purpose, different mutant models of the NER and the DRM-complex were subjected to DNA damage in order to investigate their individual phenotypes in DDR. UV-B irradiation was used because it is established as a common strategy to induce DNA damage and subsequently DDR by the NER in *C. elegans*. Readouts for these experiments were survival and developmental delay. As a further control, health span was tested by counting the pharyngeal motion of the worms (92).

In my thesis I concentrated especially on the development of *C. elegans* larvae after UV-B treatment at L1 stage. L1 worms consist almost completely of well-characterized somatic cells and four gonad precursor cells (50). Thus, this feature makes it perfect to study DNA repair. Wildtype L1 worms exhibit a delay in development after UV-B induced DNA damage (57). This delay is prolonged to a larval arrest or germline defect when mutants of the NER are subjected to the same type of DNA damage. With this approach, by studying larval development after UV-B exposure, I investigated additional mutants for components of the DRM- complex. The phenotype of these mutants was compared to wildtype and mutants of different DNA repair pathways, in order to learn more about the relations between DNA repair and cell cycle regulation. Furthermore, *in-vivo* investigations with fluorescent protein markers and *in-vitro* investigations using qRT-PCR or western blot analyses were used for further characterization of the mechanisms underlying the developmental phenotype in this study, and in previously described experiments. These investigations in *C. elegans* could be also relevant for other organisms. The goal of these experiments was to obtain new insights into the relation of cell cycle and DNA repair. This could be further relevant for future biomedical research and therapy development in the cancer field.

3. Material and Methods

3.1 Condition for cultivation of nematodes

If not described otherwise in the results section, strains were maintained on nematode growth media (NGM) agar plates at 20 degrees Celsius (°C) containing the *Escherichia coli* strain OP50 according to the protocol of Brenner (75). The often used M9 buffer is also described in this protocol. All cultivation procedures were carried out according to this protocol, therefore these procedures are not described in further detail.

Small (S)-plates with a diameter of 35 mm, medium (M)-plates with a diameter of 60 mm and large (L)-plates with a diameter of 100 mm were used in this work. Usually L-NGM plates were seeded with 700 µl of OP50 and incubated overnight at 37°C, to allow the bacteria to grow. If not described otherwise M- NGM plates usually contained an amount of 200 µl OP50, whereas the S- NGM plates only had been seeded with 50 µl bacterial suspension.

M9-plates (76) which are used in the 5-Ethynyl-2´Deoxyuridin (EdU)-Assay contain 1.2 % agar and 0.6% agarose diluted in M9 buffer solution. Before plates were poured, a final concentration of 1 mg/ml ampicillin was added.

3.2 Buffer solutions

The Phosphate Buffered Saline Tween (PBST) buffer contains an addition of 0.1% Tween 20 (Roth, 9127.1). The 1x PBS buffer contains the following ingredients as written in table 1.

1xPBS pH 7.4, adjusted with 0.1 M NaOH	**Amount for 1 l**
Na_2HPO_4	1.44 g
KH_2PO_4	0.24 g
NaCl	8 g
KCl	0.2 g
ddH_2O	up to 1 l

Table 1: Contents for one litre of 1x PBS.

The fixing buffer solution used for the EdU assay contains the following ingredients (table 2). The ingredients of the 3-(N-Morpholino)propanesulfonic acid, 4-Morpholinepropanesulfonic (MOPS) buffer and lysis buffer used for the western blot analyses were adapted from the protocol of Springhorn et al (77) (table 3 and 4).

Ingredients	**Amount for 500 µl in [µl]**
10x Egg Buffer	55
Tween 20	5
16% Paraformaldehyde	95
ddH_2O	345

Table 2: Contents for 500 µl of fixing buffer solution.

Ingredients	**Amount for 1 l**
MOPS (Sigma, SLBQ6089V)	10.46 g
TRIS Base	6.05 g
EDTA 0.5 M	2 ml
20% SDS (Roth, 1057.1)	5 ml
ddH_2O	up to 1 l

Table 3: Contents for 1 litre of MOPS buffer solution.

Ingredients	**Amount for 20 ml**
1 M Tris HCL	0.5 ml
1.5 M NaCl	2 ml
1 mM EDTA	40 µl
1% Triton x-100 (Roth, 3051.2)	2 ml
1% SDS	1 ml
1% Sodium deoxycholate (Sigma, BCBS5256V)	0.2 g
ddH_20	14.46 ml

Table 4: Contents for 20 ml of lysis buffer.

To genotype mutant strains after intercrossing, DNA was isolated using the single worm lysis buffer as shown in table 5.

Ingredients	Amount for 100 ml
1 M KCl	5 ml
1 M Tris (pH 8.3)	1 ml
1 M $MgCl_2$	0.25 ml
Tween 20	0.45 ml
1% SDS	1 ml
Gelatine (Sigma, G2500)	0.2 g
ddH_2O	Up to 100 ml

Table 5: Contents for 100 ml of single worm lysis buffer.

3.3 Lysogeny broth medium and agar

The lysogeny broth (LB) medium and LB agar contain the following ingredients as shown in table 6 and 7. The LB medium and LB agar was filled up with water and then autoclaved. If not described otherwise LB agar plates or LB media contain ampicillin at a final concentration of 100 mg/ml. Ampicillin was added to the LB agar at temperatures less than 56°C, to avoid denaturation.

LB Medium	Amount for 1 l
NaCl	10 g
Tryptone	10 g
Yeast Extract	5 g
ddH_2O	Up to 1 l

Table 6: Contents for 1 litre of LB medium.

LB Agar	Amount for 1 l
NaCl	10 g
Tryptone	10 g
Yeast Extract	5 g
Agar	18 g
ddH_2O	Up to 1 l

Table 7: Contents for one litre of LB-agar.

3.4 Strains

All strains were cultured according to standard conditions (75). I used following strains for my experiments: N2 (wildtype), *lin-52(n771), lin-35(n745), efl-1(se1), dpl-1(2994), lin-53(n833), lin-54(n2331), lin-9(n112), lin-37(n758), xpc-1(tm3886), lin-52(n771); xpc-1(tm3886), xpa-1(ok698), xpa-1(ok698); sbjIn27[pBS128(xpa-1::GFP) + pBS174(myo-2::tdTomato)], lin-52(n771); xpa-1(ok698), lin-52(n771); xpa-1(ok698); sbjIn27 [pBS128(xpa-1::GFP) + pBS174(myo-2::tdTomato)], csb-1(ok2335), lin-52(n771); csb-1(ok2335), csa-1(tm4539), lin-52(n771); csa-1(tm4539), exo-3(ok3559), lin-52(n771); exo-3(ok3559), parp-1(ok988), lin-52(n771); parp-1(ok988)*, *atm-1(gk186), lin-52(n771); atm-1(gk186), hpl-2(tm1489), lin-13(n770), lin-15B(n765), let-418(n3536), hda-1(e1795), polh-1(lf31), lin-52(n771); polh-1(lf31), brc-1(tm1145), lin-52(n771); brc-1(tm1145)*, *efl-1(se1); brc-1(tm1145)*.

The single mutants were obtained from the Caenorhabditis Genetics Center of the University of Minnesota, USA.

The strain *xpa-1(ok698); sbjIn27[pBS128(xpa-1::GFP) + pBS174(myo-2::tdTomato)]* was established and obtained from Dr. Matthias Rieckher at our institute (CECAD) in Cologne.

The double mutants *lin-52(n771); xpc-1(tm3886)*, *lin-52(n771); xpc-1(tm3886); csb-1(ok2335)*, *lin-52(n771); csa-1(tm4539)*, *lin-52(n771); atm-1*(gk186), *lin-52(n771); polh-1(lf31), lin-52(n771); brc-1(tm1145)* and *lin-52; csb-1(ok2335)* were crossed and obtained from Arturo Bujarrabal at our institute.

The following double mutants for this project were crossed by myself: *lin-52(n771); exo-3(ok3559), lin-52(n771); parp-1(ok988), lin-52(n771); xpa-1(ok698)* and *lin-52(n771); xpa-1(ok698); sbjIn27[pBS128(xpa-1::GFP) + pBS174(myo-2::tdTomato)]*.

The strain *xpa-1(syb788)[CR(xpa-1::V5+TEV+linker+Ypet)]* was generated by SunyBiotech, the double mutant *lin-52(n771);xpa-1(syb788)[CR(xpa-1::V5+TEV+linker+Ypet)]* was crossed by myself.

3.5 Genotyping and crossing

For genotyping the worms, the Mango-Taq-polymerase kit from Bioline (BIO-21083) was used. The standard protocol is shown in table 8. If not described otherwise, the Biometra TAdvanced Thermocycler by Analytic Jena (846-x-070-211) was used. Deletions could be easily determined by gel electrophoresis with the amplificated sequences. The gel contained 1% agarose dissolved in 1x TAE buffer (40 mM Tris-acetate, 1 mM EDTA) and 0.004% ethidium bromide (Roth, 2218.1).

Ingredient	Amount [µl] for one reaction
5x Mango Taq reaction buffer	4
100 mM dNTP	0.5
50 mM $MgCl_2$	1
forward primer 100 µM	1
reverse primer 100 µM	1
ddH_2O	11.3
Mango Taq	0.2
Sample DNA	1

Table 8: Contents for one PCR reaction using the Mango-Taq-polymerase by Bioline.

Crossing of two different mutant strains can be easily done with the nematode *C. elegans*. Beyond hermaphrodites' nematodes also exist as male worms at low percentages. For intercrossing experiments, five male worms of one mutant strain were put together with two hermaphrodite L4 worms of the other strain on a S- NGM plate with 5 µl of OP50. Ten L4 worms of the following F1 generation were then separated on two M-plates. Worms could lay eggs and the following F2 generation was grown until they reached the L4 stage. 40 worms of this stage and generation were then transferred as single worms to S- plates. On

the next day, these worms reached the adult stage and laid eggs. As soon as these worms laid eggs, they could be used to isolate their DNA for genotyping, as their progeny is supposed to have the identical genotype. For this purpose, the worms were transferred to a mixture of 0.6 µl of proteinase K at a concentration of 50 µg/µl (Thermo Scientific, EO0492) with 5.4 µl of single worm lysis buffer (table 5). This worm lysis solution was then heated up using a PCR machine with following protocol, as shown in table 9.

Time	Temperature in Celsius
65 minutes	65
15 minutes	95
∞	10

Table 9: PCR program for worm lysis.

3.5.1 *lin-52(n771)* mutant strain

The *lin-52(n771)* mutant strain carries a cytosine to thymidine point mutation in exon one on chromosome III (78). To genotype this mutation, DNA fragments from this locus were amplified using PCR and the primers described below. Amplified samples were cleaned- up using the NucleoSpin Gel and PCR Clean-up kit (Macherey-Nagel, 740609.50) and afterwards were subjected to Sanger sequencing which had been done by GATC/Eurowings, in order to identify this base exchange. The following primer pair was used, which were not designed by myself:

Forward primer: 5-CACAGCATCTTCCTTGAGAAACG-3

Reverse primer: 5-ATTTGTAAAGTACCCACCGGCTAG-3

3.5.2 *exo-3(ok3559)* mutant strain

The *exo-3(ok3559)* mutant strain (79) with a deletion of around 600 base pairs, was identified by using PCR and a gel electrophoresis. The following primes were used for genotyping this mutation:

Forward primer external: 5-CGAAAAGCAGAAGAAGCACC-3

Reverse primer external: 5-TGAAAAATTTCAATTCCCCG-3

Forward primer internal: 5-CTCGCCTCGATCTTCACAA-3

Reverse primer internal: 5-CAGCTTCCAGACGAGACCTT-3

In table 10 the PCR program for this mutation can be seen:

Program	Time	Temperature in Celsius
1.Heat denaturation	3 minutes	94
2.Denaturation	45 seconds	94
3.Annealing	30 seconds	53
4.Elongation	3 minutes	72
5.Go to number 2, 35x cycles		
6.Final elongation	7 minutes	72
7.End	∞	10

Table 10: PCR program for genotyping the *exo-3(ok3559)* mutant strain.

3.5.3 *parp-1(ok988)* mutant strain

The *parp-1(ok988)* mutant strain (79) exhibits a deletion of around 1000bp. This can be easily genotyped by performing a PCR and a gel electrophoresis. The following primers which were not designed by myself were used:

Forward primer external: 5-ACCTATCGGCTTCAAATGTACC-3

Reverse primer external.: 5-TCATTTTTGGGGGATTTCAG-3

Forward primer internal.: 5-TCCCAGAGAAGATCGGATTG-3

Reverse primer internal.: 5-AAAGAATCGAATCGCAAAGC-3

The following PCR program was used which is shown in table 11:

Program	Time	Temperature in Celsius
1.Heat denaturation	3 minutes	94
2.Denaturation	45 seconds	94
3.Annealing	30 seconds	56
4.Elongation	3 minutes	72
5.Go to number 2, 35x cycles		
6.Final elongation	7 minutes	72
7.End	∞	10

Table 11: PCR program for genotyping the *parp-1*(ok988) mutant strain.

3.5.4 *xpa-1(ok698)* mutant strain

The *xpa-1(ok698)* mutant strain (79) contains a deletion of around 900bp which was also genotyped by PCR and a gel electrophoresis, using the following primers which were not designed by myself.

Forward primer external: 5-TCTGTGATGACGACGATGAGG-3

Reverse primer external: 5-CTGGAGCCAATCCAACTGATG-3

Forward primer internal: 5-GATTGCGATCTGGATCTGCGCAAACC-3

Reverse primer internal: 5-GAGCCAATCCAACTGATGCTGATCGAAG-3

The following PCR program which was used to genotype this mutation can be seen in table 12:

Program	Time in minutes	Temperature in Celsius
1.Heat denaturation	3	94
2.Denaturation	1	94
3.Annealing	1	55 (external primer pair) 58 (internal primer pair)
4.Elongation	1	72
5.Go to number 2, 35x cycles		
6.Final elongation	7	72
7.End	∞	10

Table 12: PCR program for genotyping the *xpa-1*(ok698) mutant strain.

3.5.5 *xpa-1(syb788)[CR(xpa-1::V5+TEV+linker+Ypet)]* mutant strain

The *xpa-1(syb788)[CR(xpa-1::V5+TEV+linker+Ypet)]* mutant strain was obtained by SunyBiotech, carrying an insert of 792bp. This insertion contains, Ypet as a fluorescent protein, and a V5 tag which was used for western blot analysis. This strain was genotyped by doing a PCR and a gel electrophoresis, using the following primers which were not designed by myself:

Forward primer external: 5- CGAGGAGAAAGAGAGCGAC-3

Forward primer internal: 5-GTTAGTCCGTGTACTCCACTC-3

Reverse primer: 5- ACAGAATCCGCCACCAAG-3

The following PCR program which is shown in table 13 was used to characterize this mutation:

Program	Time in minutes	Temperature in Celsius
1.Heat denaturation	3	94
2.Denaturation	45 seconds	94
3.Annealing	30 seconds	62
4.Elongation	2	72
5.Go to number 2, 35x cycles		
6.Final elongation	10	72
7.End	∞	10

Table 13: Table showing the PCR program for genotyping the *xpa-1(syb788)[CR(xpa-1::V5+TEV+linker+Ypet)]* mutant.

3.5.6 *brc-1(tm1145)* mutant strain

The *brc-1(tm1145)* mutant strain (79) carries a deletion of 617bp. Furthermore, this mutant strain is also carrying the *brd-1(dw1)* deletion allele. Both proteins form, under normal conditions, a heterodimer to coordinate homologous recombination (80). Therefore, this mutant worm is a good knock-out model. The *brc-1(tm1145)* mutant strain was identified by using a PCR and a gel electrophoresis. The following primers which identify this mutation were not designed by me:

Forward primer external: 5-TCGATTCGCTGGTTTCTCTG-3

Reverse primer external: 5-ATGAATACGTTCAAGTCACTGC-3

Forward primer internal: 5-TGGCTGGTTCTGGCGGTTC-3

The following PCR program was used which is shown in table 14:

Program	Time in minutes	Temperature in Celsius
1.Heat denaturation	3	94
2.Denaturation	45 seconds	94
3.Annealing	30 seconds	56
4.Elongation	3	72
5.Go to number 2, 35x cycles		
6.Final elongation	7	72
7.End	∞	10

Table 14: PCR program for genotyping the *brc-1(tm1145)* mutant strain.

3.5.7 *efl-1(se1)* mutant strain

For intercross experiments with the *efl-1(se-1)* mutant strain the temperature sensitive phenotype was used to genotype this loss of function mutation. Worms with this mutation are sterile when early larval stages were maintained at 26°C (81). Therefore, I maintained eggs of the F2 progeny on S- plates at 26°C until adulthood was reached. Subsequently, the plates were checked for progeny. Plates with no progeny and adult worms were claimed as sterile worms, carrying the *efl-1(se1)* mutation.

3.6 Bleach synchronization

The protocol was taken over and modified from the methods described by Porta-de-la-Riva et al (82). Worms which had been grown to adult stage and were laying eggs, were washed from the plates using 4 ml of M9 buffer. To obtain the eggs, the worms were bleached using 1 ml of a fresh alkaline bleach solution (5% sodium hypochlorite solution, 5 M NaOH mixed in a ratio of 2:1). Immediately after adding the alkaline solution, worms were vortexed for 5 minutes. Afterwards the worms were centrifuged at 1251 relative centrifugal force (RCF) for

2 minutes. This step was followed by three washing steps, using 5 ml of M9 buffer per round and tube. To allow the eggs to hatch, the strains were maintained for 18 hours in 10 ml of M9 buffer on a roller (CAT Roller RM10W-80V) at 20°C. The L1 stage was selected by filtering the hatched L1 worms through a 11 µm hydrophilic filter (Millipore, NY1104700). The average number of worms was calculated by counting the number of L1 worms in three 10 µl drops and estimating the mean from these numbers.

3.7 Analysis of development

In order to investigate how DNA damage influences differentiation and growth of the worms according to different stages, they were subjected to different forms of DNA damage. The different larval stages were determined by eye using a stereomicroscope. Today the morphology in the different stages is a likely criterion to rate the variable larval stages. As described previously, L4 staged worm can be easily seen by the invagination of the vulva cells (49), which appears in a round spot in the middle of the worm. Other larval stages were classified according to differences in length (44) and other anatomical features. In figure 2a and 2b examples of different larval stages in *C. elegans* are given. The worms hatch normally after 10-12 hours and are subsequently named as L1 worms. Whereas the L1 worms need 12-16 hours to reach the following L2 stage, the mean time in higher larval stages is a bit shorter with 8-12 hours (figure 2c).

3.7.1 Analysis of development after UV-B irradiation

UV-B irradiation on L1 worms and the subsequent analysis of the worms´ development was used as a basic technique for DNA damage, following the protocol described by Rieckher et al (57).

The worms were first bleached, as described above, and about 50 worms per strain and condition were plated in three separate S- NGM plates (three biological replicates). The plates were allowed to dry before the L1 worms were irradiated with different doses. Usually 40 mJ/cm² or 60 mJ/cm² of UV-B 310 nm irradiation were applied, using a broadband PL-L 36W/UVB (Waldmann, 451436623-00005077) with a UV6 Phillips irradiation bulb.

Subsequently, 50 µl of OP50 was added to each plate and the worms were maintained at 20°C for 48 hours to develop. Afterwards, the different larval stages were determined by eye using a stereomicroscope.

During the course of the experiments, it was generally observed that the phenotype of wildtype and most mutant worms, DRM- complex mutant worms being an exception, showed a similar phenotype at 60 mJ/cm^2 UV-B irradiation. This is consistent with similar previous studies (57) and was interpreted as a consequence to the fact that this dose was very high so that DNA damage was beyond its cellular response capacity.

3.7.2 Analysis of development using methyl- methanesulphonate

Worms were bleached and filtered as described above. 100 L1 worms per strain and condition were used. This experiment was also performed with three biological replicates. The worms were incubated for one hour on a shaker at room temperature with 0 mg/ml, 0.5 mg/ml, 0.75 mg/ml and 1 mg/ml of methyl- methanesulphonate (MMS) diluted in M9 buffer in a final volume of 200 µl per sample. Following three washing steps were performed using 500 µl of M9 buffer for each step. The treated strains were then plated on S-NGM plates and incubated for 48 hours at 20°C. The different larval stages were then determined by eye using a stereomicroscope.

3.7.3 Analysis of development using Trioxsalen and UV-A irradiation

For this assay Trioxsalen (Sigma, SLBB7588V) in combination with UV-A irradiation was used, to induce DNA damage, described previously by David M. Wilson et al (83). 2 mg/ml Trioxsalen was dissolved in Dimethylsulfoxid (DMSO, Thermofisher 20688) at 50°C on a bench shaker for 30 minutes. The dissolved Trioxsalen was then diluted with M9 buffer to obtain a final concentration of 50 µg/ml Trioxsalen per treated sample. Worms were bleached and filtered as described before. 70 worms were treated with Trioxsalen in biological replicates for each condition in a final volume of 400 µl per sample. Subsequently, the tubes were incubated for 2 hours on a rotator (Stuart SB3/1) in the dark. The worms were transferred to 24-well plates and irradiated for 4 (~ 200 mJ/cm^2) or 6 (~300 mJ/cm^2) minutes with UV-A using a Benchtop 3UV Transilluminator (UVP, LTF00207). Afterwards the worms were washed three times with M9 buffer and transferred to S- NGM plates. The plates were stored at 20°C for 48 hours before the different larval stages were determined by eye using a stereomicroscope.

3.7.4 Analysis of egg hatching using ionizing radiation

Worms were bleached and filtered as described before. 200 L1 worms were plated on L-NGM plates and incubated at 20°C for 72 hours to reach the adult stage. At this point, five adult staged worms were transferred to a S- NGM plate. These worms were left to lay eggs for two hours before the worms were removed. Per condition and strain three independent plates (biological replicate) were prepared. The eggs were left untreated or gamma-irradiated with 20 Gy or 40 Gy, using the BIOBEAM 8000 by Eckert & Ziegler containing Caesium137 as a radionucleotide with an activity of 81.4 TBq +/- 20%. To determine the hatching ratio upon the different doses of gamma-irradiation, the eggs were incubated at 20°C for 24 hours. Afterwards, the number of hatched eggs was counted and compared to the amount of unhatched eggs.

3.8 Detection of DNA synthesis using the Click-it 5-Ethynyl-2´Deoxyuridin (EdU) Alexa Fluor 488 Imaging Kit

To image and quantify cell proliferation in larval worms during development, the Click-it EdU Alexa Fluor 488 Imaging Kit by Thermofisher (C10337) and the thymidine-deficient *E.coli* strain MG1693 was used. It was necessary to use thymidine deficient bacteria, because this assay is based on the integration of the thymidine nucleoside analog EdU into the DNA during the cell division. The MG1693 bacteria was grown overnight in the dark at 37°C in M9 buffer containing 1% Glucose, 1 mM $MgSO_4$, 1.25 µg/ml thiamine, 0.5 µM thymidine and 20 µM EdU (76).

Worms were bleached as described above and 10.000 worms per timepoint and condition were plated on L- NGM plates, containing no food. This condition was used to avoid irradiation of the light sensible EdU plates seeded with MG1693, which could lead to a change of this experimental setup. Furthermore, the bacterial layer may shield the worms from being irradiated. Thus, the chosen condition may provide a higher level of standardization that is necessary to compare different groups of genetically altered worms. After UV irradiation, treated and unirradiated-control worms were washed from the NGM plates and transferred to the EdU plates, containing 200 µl of 5:1 concentrated MG1693. The worms were maintained on these plates at 20°C in the dark for different timepoints (0, 6, 12, 24 hours). For each timepoint worms were washed from the plate using 5 ml of M9 buffer followed by three washing rounds using 5 ml of M9 buffer per round and sample. Afterwards, the supernatant of M9 buffer was discarded and 5 µl of the left worm pellet was

transferred into 5 µl of fixing buffer solution (table 2). 5 µl of this resuspension was transferred to a HistoBond + adhesive microscope slides (Marienfeld, 0810401) and a 24x24mm coverslip was attached. After two minutes of drying at room temperature, slides were put onto dry ice. 10 minutes later, freeze cracking was performed by removing quickly the coverslip. The microscope slides were incubated in methanol at -20°C for 10 minutes, followed by three washing steps in 1x PBST buffer. The Click-it EdU Alexa Fluor 488 Imaging Kit (Thermofisher, C10337) was used, according to the manufacturer's instructions, except for using only 70 µl of EdU staining mix per slide and including an additional DAPI staining for counterstaining of cell nuclei. After the staining, the slides were allowed to dry for 24 hours at room temperature in the dark. Microscopic analysis was done using the Zeiss LSM710 confocal microscope.

3.9 GFP rating of different larval stages using the Multi-Range Large Particle Flow Cytometer (BioSorter)

The strains *xpa-1(ok698); sbjIn27[pBS128(xpa-1::GFP) + pBS174(myo-2::tdTomato)]* and its intercross with the *lin-52(n771)* mutant were bleached and filtered as described before, and about 1000 L1 worms were transferred to two separate L-NGM plates. The plates were stored for either 24 hours (L3 stage), 48 hours (L4 stage) or 72 hours (adult stage) at 20°C. Using 5 ml of M9 buffer, the worms were collected from the plates and washed once using 10 ml of M9 buffer to reduce the leftover of OP50 in the liquid and in the worms themselves, which can lead to increased autofluorescence. Directly afterwards, the green fluorescent protein (GFP) levels were measured by using the Multi-Range Large Particle Flow Cytometer (BioSorter) by Union Biometrica. N2 wildtype worms were used as a negative control, because they do not express a fluorescent protein compared to the *xpa-1(ok698); sbjIn27[pBS128(xpa-1::GFP) + pBS174(myo-2::tdTomato)]* strain or its intercross. The analysis regarding to this strain was altered to reduce the influence of autofluorescence effects in the worms.

To confirm the specific worm stages and avoid outliers at different stages, worms were isolated according to the criteria as shown in table 15. The gain of the green laser had to be changed between the different worm stages to include all the events in the measurable limits of the BioSorter. Reaching the limits of the laser at a green peak height of 65000 Arbitrary Units (AU), the gain of the green laser needed to be lowered from 2.0 to 1.8 AU for L3 worms, 2.0 to 1.7 AU and 700 to 650 PMT volts for L4 worms and from 2.0 to 1.0 AU and 700 to 600 PMT volts for day 1 adult worms. This is the reason for the lower green peak height rates in the figure 17, compared to the L1 and L3 stage.

Worm Stage	Extinction Rate [AU]	Red Peak Height [AU]	Autofluorescence/ Green peak height [AU]
L1 except wildtype	8-34	10^4-10^5	
L1 (wildtype)	8-34	100-1000	< 5000
L3 except wildtype	32.5-100	10^4-10^5	
L3 (wildtype)	32.5-100	100-1000	< 7000
L4 except wildtype	82-254	10^4-10^5	
L4 (wildtype)	82-254	100-1000	< 7000
Adult except wildtype	350-800	10^4-10^5	
Adult (wildtype)	350-800	100-1000	< 7000

Table 15: Analytic procedure for determining and sorting of different larval stages which were detected by Multi-Range Large Particle Flow Cytometer.

3.10 Western blot analysis

For western blot analysis, the protocol of Springhorn et al (77) was used with minor modifications. For *C. elegans,* an anti-XPA-1-antibody doesn´t exist. Therefore the strain *xpa-1(syb788)[CR(xpa-1::V5+TEV+linker+Ypet)]* was used, carrying a V5-tag, which could be detected by western blot analysis to identify the XPA-1 protein. The full size of the “new” fusion protein is around 60 kDa.

The worms were collected at L1 or L4 stage. The L1 worms were taken 18 hours after bleaching, applying no food to prevent larval development and false elevated XPA-1 protein levels. About 1000 bleached L1 worms were transferred to L-NGM plates and incubated for 48 hours at 20°C, to collect L4 worms later. The L4 worms were washed from the plate using 5 ml of M9 buffer and transferred to a tube, followed by three washes with 5 ml of M9 buffer. The L1 worms appeared free of OP50 bacteria after being bleached, therefore a washing step could be skipped. To isolate the worm pellet, worms were spun down at 200 RCF for two minutes and the supernatant liquid was removed. L1 or L4 worms were then transferred with 1 ml of cold lysis buffer into a fresh tube. Worms were spun down shortly at 3381 RCF with a table centrifuge and again the supernatant was removed. Then the same amount of lysis buffer was added as the volume of the remaining worm pellet in the bottom of the tube.

The samples were incubated for five minutes at 95°C, followed by a shock-freeze step in liquid nitrogen. Afterwards, the samples were sonicated at 4°C using the Bioruptor Pico sonication device (Diagneode, B01060010), followed by another shock-freeze in liquid nitrogen and subsequent, incubation for five minutes at 95°C and another shock-freeze in liquid nitrogen. The samples were thawed at room temperature before being spun down for 10 minutes at 18407 RCF at 4°C. The clear lysate was transferred into a fresh tube, which could then be stored at -80°C.

To quantify the amount of protein in each sample, the Pierce 660nm Protein Assay Kit (ThermoFisher, 22662) was used, following the instructor's manual. The quantification was done with the EnSpire Multimodal Plate Reader by PerkinElmer. To standardize each sample to the same amount of protein, 13 µg of protein of each sample was used and if needed diluted with ddH_2O to a final volume of 20 µl. To dissolve disulfide pairs, 5 µl of 5x Laemmli buffer were added to each tube and the samples were incubated for 5 minutes at 96°C.

Afterwards the samples were loaded on a NuPAGE 4-12% Bi-Tris Protein Gel, 1.5 mm, 10-well (Invitrogen, NP0335BOX). As a reference, the PageRuler Prestained Protein ladder (ThermoFisher, 26616) mixed with 5 µl of 1x Laemmli buffer was added in the first and last well. The gel was run with the MOPS buffer for 85 minutes at 150 volts. The gel was then transferred to a nitrocellulose membrane using the Trans-Blot Turbo Transfer Pack (Bio-Rad, 64263110) and the Trans-Blot Turbo Transfer System (Bio-Rad, 1704150).

Before the membrane was blocked with 5% milk powder (Roth, T145.3) in 1x PBS for one hour, a ponceau staining was performed, to control the loading, followed by three additional washes using ddH_2O. Afterwards, the membrane was cut between 25 and 35 kDa to allow differential antibody staining. The control protein was histone H3, stained with a polyclonal rabbit anti- histone H3-antibody by Abcam (ab1791). The XPA-1 staining was performed via a V5-tag, using the strain *xpa-1(syb788)[CR(xpa-1::V5+TEV+linker+Ypet)]* as explained above. Therefore, the monoclonal mouse anti-V5 tag-antibody by AbD Serotec (MCA1360) was used. The rabbit anti- histone H3-antibody was diluted 1:10.000 and the mouse anti-V5 tag-antibody was diluted 1:3000, each in 1% milk powder dissolved in 1x PBS. The cut membrane was incubated separately at 4°C overnight.

On the following day, the cut membrane was washed three times with 1xPBST before the second antibody was added. For the rabbit anti- histone H3-antibody a 680 CW donkey anti-rabbit-antibody by Licor (926-32223) and for the mouse anti-V5 tag-antibody a 800 CW donkey anti-mouse-antibody by Licor (926-32212) was used. Both antibodies were diluted 1:10.000 in 10x Roti-Block solution (Roth, A151.4), diluted with 1x PBS in ratio 1:10. The cut membrane was incubated for two hours at room temperature.

Afterwards, the membrane was washed again three times with 1x PBST, followed by one wash with 1x PBS. The cut membrane was assembled and imaged using the Odyssey Clx by Licor. Quantification of the band intensities was done using the Image Studio 5.2 for Odyssey Clx. The statistical analysis was done according the paper of Sean C. Taylor et al (84).

3.11 Quantitative real- time PCR

For quantitative real- time PCR (qRT-PCR) analysis the number of worms was chosen individually for both experiments, but the following experimental procedure was performed similarly for all experiments.

For the measurement of *xpa-1* transcript levels in *lin-52(n771)* mutant worms at different larval stages 10.000 L1 and 1000 L4 worms were used for each biological replicate. L1 worms were used 18 hours after bleaching, L4 worms were collected 48 hours after transferring bleached L1 worms to L-NGM plates and maintaining them at 20°C. For the L4 stage, worms were collected from the plates using 5 ml of M9 buffer and transferred to tubes, followed by three washes with 10 ml of M9 buffer, to minimize the bacteria load in the worm fraction.

For the qRT-PCR analysis in UV-B irradiated worms, 5000 L1 worms per strain were used in biological replicates. Worms were transferred to M-NGM plates and the treated group was then irradiated with 60 mJ/cm^2 of UV-B irradiation. Afterwards worms were kept under standard conditions for different timepoints (1 hour and 3 hours after treatment). At each timepoint the worms were washed from the M-NGM plates using 5 ml of M9 buffer, followed by three washes with 10 ml of M9 buffer.

To isolate the worm pellet, worms were spun down at 200 RCF for two minutes. The supernatant liquid was then removed. Using 1 ml of TRIZol (Ambion, 15596018) the worm pellets were transferred to precellys vials (VWR, 432-0351), filled with a 0.5 cm layer of 1 mm beads (Roth, 11079110z). Samples were then frozen at -80°C.

To homogenize the samples, the Peqlab Precellys machine (VWR,432-3750) was used, shaking the samples twice at 5000 rpm for 30 seconds. The samples then were incubated for 5 minutes at room temperature, 100 µl of bromchloropropane were then added, followed by 15 seconds of vortexing and another incubation for two minutes at room temperature. To collect a clear phase, samples were centrifuged for 15 minutes at 12000 RCF at 4°C. The clear phase was transferred to a tube and 350 µl of 70% absolute ethanol was added.

The RNA extraction was then performed, using the RNeasy Mini Kit (Qiagen, 74104) following the instructor´s manual. The sample was eluted in 30 µl of RNAse free water. The concentration of the samples was measured using the NanoDrop 8000 by ThermoScientific (ND-8000-GL).

For the reverse transcription into cDNA, the measured RNA levels were standardized, using ddH_2O to dilute samples if needed, to obtain a final volume of 11.5 µl for each sample. The first step of the PCR program (table 16) was then started with the diluted sample cDNA, using the S1000 Thermal cycler by BioRad (1852196). After the first PCR step was finished, samples were quickly removed from the PCR machine and 8.5 µl of master mix (table 17) was added to each tube, using the SuperScript III reverse transcriptase enzyme kit (Invitrogen, 18080044). The PCR program was then continued. The resulting samples of cDNA were then diluted using 50µl of ddH_2O.

The quantitative real- time (qRT) PCR was done in biological replicates in a 96- well plate with 2.5 µl of the sample cDNA and 22,5 µl of the master mix (table 18) per well.

Time in minutes	Temperature in °C
2	70
90	42
5	92

Table 16: cDNA PCR program

Ingredients	Company (Cat. number)	Volume in µl
5x fs buffer	Invitrogen (18080044)	4
0.1 mM DTT	Invitrogen (18080044)	2
dNTP 10 mM	Invitrogen (10297018)	1
Oligo $(dT)_{20}$	Invitrogen (18418020)	1
SuperScript III reverse transcriptase enzyme	Invitrogen (18080044)	0.5

Table 17: Contents for one reverse transcriptase reaction.

Ingredients	Company (Cat. number)	Volume in µl
ddH_2O		15.575
10x PCR buffer	Invitrogen (10966018)	2.5
$MgCl_2$ 50 mM	Invitrogen (10966018)	1.25
dNTP 10 mM	Invitrogen (10297018)	0.5
Platinum SYBR Green diluted 1:400	Invitrogen (11744500)	0.075
Platinum taq polymerase	Invitrogen (10966018)	0.1
Forward primer		1.25
Reverse primer		1.25

Table 18: Table showing the contents for one qRT- PCR master mix reaction.

Gene Name	Primer
tbg-1	Forward: 5-CAATGTGCCCATCAATTCGG-3 Reverse: 5-AACAAGAAGCGAGTGACGTC-3
eif-3.c	Forward: 5-ACACTTGACGAGCCCACCGAC-3 Reverse: 5-TGCCGCTCGTTCCTTCCTGG-3
Y45F10D.4	Forward: 5-CGAGAACCCGCGAAATGTCGGA-3 Reverse: 5-CGGTTGCCAGGGAAGATGAGGC-3
vha-6	Forward: 5-ATATCGGAAACCGATCTGTCGT-3 Reverse: 5-CGAAGCTTGCATCTCTGCTC-3
lmn-1	Forward: 5- CATCTCHTAAAGGTACTCGTAG-3 Reverse: 5-GTTGAGCCAAATGAATCGTC-3
xpa-1	Forward: 5-AAAGGTTTGATGGACAGTTGG-3 Reverse: 5-TGTTTCAATCTGGCACTTCAG-3
xpc-1	Forward: 5-GGAAGATGAATGGGAAGAAATGG-3 Reverse: 5-AGCAGAGAAGATGTACCTTATGAG-3
csb-1	Forward: 5-ATAGTGGAAAGGTGGAAATGAC-3 Reverse: 5-ACGCATTTGATTCCCTTCTC-3
csa-1	Forward: 5-AAGAACAACAAGTTTCACGG-3 Reverse: 5-CAAATAGTAGCATTTGGTCACC-3

Table 19: Primer pairs used in the qPCR assay.

The primers used for the qRT-PCR, were designed by different members of the lab. They are listed in table 19. As housekeeping genes for comparative analyses, the following genes were used: *tbg-1*, *eif-3.c* and *Y45F10D.4*. For qRT-PCR analysis with the *csb-1(ok2335)* and *lin-52(n771); csb-1(ok2335)* mutant strains, I used different housekeeping genes which revealed better standardized conditions. The housekeeping genes were: *vha-6*, *Y45F10D.4* and *lmn-1*.

For the qRT- PCR the CFX96 Real Timer PCR Detection System by BioRad (185-5096) was used. The program is described in table 20. The determination of the threshold cycle (C_t) was done with the CFX- Manager Software (BioRad, 184-5001). The statistical analysis was estimate as described previously by Schmittgen et al (85).

Step	Time in seconds	Temperature in Celsius
1	180	95
2	30	95
3	30	58
4	20	72
5 Signal acquisition, then go to number 2 39x		
6 Signal acquisition	5	65
7	5	95

Table 20: Program for quantitative real- time PCR.

3.12 Statistical analysis

The statistical analysis for developmental assays was done in two ways. The Fisher´s exact test examines independency of two characteristic parameters in a contingency table. This test was used for comparison of all four stages together in developmental assay. The Fisher´s exact test reveals overall differences between stages but does not show a difference in a single stage. For the Fisher´s exact test analysis a 4x2 contingency table was created using the statistics program RStudio.

To compare single stages with each other, the two-tailed t-test was used, which examines the mean of two groups but can´t prove the overall difference. The t-test statistic was done with Microsoft Excel.

The data from the BioSorter were first transformed into a logarithmic function. To test for possible significant differences an one-way Anova was performed, comparing the single and double mutant worms for each larval stage. Subsequently, a Tukey test was applied to compare two different groups from one larval stage with each other.

The Cohen´s d with pooled standard deviation was used, which examines the difference of two means, expressed in standard deviations. Having fixed limits of effect size, this

statistical analysis makes it possible to compare the size of difference also between different stages or different strains. The original fixed intervals of Cohen were used for this analysis (86).

3.13 Cell culture

Mouse embryonic stem cells (mESC) were maintained on tissue culture (TC) dishes with a diameter of 100x17mm (Sarstedt, 83.3902) at 37°C with 5% CO_2. The dishes were incubated with 0.1% gelatine at 37°C with 5% CO_2 for a minimum of 30 minutes before the mESC were added. The ingredients for the mESC media are shown in table 21.

Cells were split by performing a washing step with DPBS (Gibco,14190250) followed by 2 ml of 0.05% Trypsin-EDTA (Gibco, 25300062), if a TC dish 100 was used. For 96- well plate I used 30 µl, for a 24-well plate 0.1 ml and for a 6-well-plate 0.25 ml of 0.05% Trypsin-EDTA. Subsequently cells were incubated for five minutes at 37°C before a fourfold volume of mESC media was added to the trypsin-EDTA to stop the reaction. The cell suspension was spun down at 200 RCF for five minutes to produce a cell pellet. The supernatant media was discarded, and fresh media was added to the cells. Cells could be then seeded again on new TC dishes or well-plates.

mESC media	**Company (Cat. number)**	**Amount [ml] for 50 ml final volume**
Knock-out DMEM	Gibco (10829018)	41
MEM Non-Essential Amino Acids Solution 100X	Gibco (11140050)	0.5
L-Glutamin 200mM	Gibco (25030081)	0.5
Penicillin + Streptomycin 10000 U/ml	Gibco (15140122)	0.5
B-Mercapthoethanol 100 mM	Gibco (21985023)	0.05
Fetal Bovine Serum (FBS)	HyClone (SH3070.03)	7.5
Leukemia inhibitory factor (LIF) 0.1 mg/ml	Gibco (PMC9484)	0.005

Table 21: Ingredients for 50 ml of mESC media.

3.13.1 CRISPR- Cas9 approach in E14 mouse embryonic stem cells

The *E. coli* bacteria strain TOP10 and the plasmid px330A was a gift by Sara de la Cruz Molina, ZMMK, Cologne. The plasmid px330A is derived from the plasmid px330 but carries an additional puromycin resistance gene, which allows to select the cells not only by GFP positivity, but also by puromycin resistance.

With the CRISPR- Cas9 approach it was intended to knock-out the gene *Lin52* in mESC. As described before, the phosphorylation at serine 28 in LIN52 (exon two in *Lin52*) by DYRK1A plays a key role for DREAM complex assembling (31). Thus, a defect in this area of the gene and corresponding protein provides good knock-out conditions for my experiments. Two oligo pairs were designed to cut out a 4350bp large sequence, eliminating exon two, three and four in *Lin52*. The oligo nucleotide sequence is shown in table 22.

Oligo	gRNA with enzyme sequence	On-target locus
LIN52 (5')	5-caccGATTACATCATGCCCCAAT-3	chr12: +85797038
LIN52 (3')	5-caccGAAAGGGGCCTCGACGCAC-3	chr12: -85801388

Table 22: gRNA sequences used in the CRISPR- Cas9 approach.

3.13.1.1 Transformation

To insert the plasmid px330A into the TOP10 bacterial strain, 30 µl of bacterial suspension were mixed with 1 µl of this plasmid in a tube and incubated for one minute on ice. Subsequently, a heat shock at 37°C for one minute was done followed by another incubation on ice for one minute. 900 µl of LB media was added before the sample was again incubated at 37°C for one hour on a table shaker with 34 RCF. To concentrate the bacteria pellet, the sample was spun down at 3381 rpm for two minutes and the supernatant media except of 50 µl was discarded. The leftover was then incubated on a LB plate with ampicillin for overnight at 37°C.

3.13.1.2 Mini culture

To prepare a single colony culture, one colony from the incubated LB plate was picked and transferred to 5 ml of LB media with ampicillin (1:1000). Samples were then stored at 37°C for overnight.

3.13.1.3 Plasmid isolation

For plasmid isolation, the NucleoSpin Plasmid Kit by Macherey – Nagel (740588.50) was used. In the last step of this kit the sample was eluted in 30 µl of RNAse free water. The concentration of the plasmid was measured using the NanoDrop 8000.

3.13.1.4 Digestion of vector

Restriction digestion was done with following ingredients at 37°C for 30 minutes, shown in table 23.

Ingredients	**Company (Order number)**	**Amount**
extracted vector		1 µg
Fast Digest BbIL	ThermoScientific (FD1014)	1 µl
10x Fast Digest Buffer	ThermoScientific (B64)	2 µl
ddH_2O		Up to 20 µl

Table 23: Ingredients for restriction digestion.

Subsequently, to purify the digested vector, the NucleoSpin Gel and PCR Clean-up kit by Macherey - Nagel (740609.50) was used.

The annealing of the complementary oligos was done by using 1 µl of a 100 µM oligo stock, 7 µl of ddH_2O and 1 µl of 10xT4 Ligation buffer by New England Biolabs (B0202S).

The samples were incubated at 95°C for five minutes followed by cooling down to 25°C with a cooling rate of 5°C/min.

3.13.1.5 Ligation

The ligation of the annealed oligos into the digested vector was done by incubation the ingredients at 16°C overnight (table 24).

To clone the created vector, transformation, mini culture and plasmid isolation was done as described before. To confirm the plasmid sequence, the isolated plasmid was analyzed by sanger sequencing done by GATC/Eurofins.

For sequencing the plasmid, the following sequence as primer was used:

5-GGAAAGTCCCTATTGGCGTT-3

Ingredients	**Company (order number)**	**Amount**
Annealed Oligo 1:200 diluted		1 µl
Digested vector		50 ng
10xT4 Ligation Buffer	New England Biolabs (B0202S)	1 µl
T4 Ligase	New England Biolabs (M0202S)	1 µl
ddH_2O		Up to 11 µl

Table 24: Ingredients for ligation the oligos to the plasmid.

3.13.1.6 Transfection

For transfection, the Lipofectamine3000 Transfection Reagent by Invitrogen (L3000001) was used according to the manufacturer's instructions. The mESC were transfected with either 3.75 µl or 7.5 µl of Lipofectamine 3000 reagent with an amount of 50.000 or 100.000 cells in a 6- well plate (Sarstedt, 83.3920).

After 24 hours at 37°C the GFP signal in the cells was detected under a fluorescent microscope. Subsequently, a concentration of 2 µg/ml puromycin was added to the cells to obtain only these cells which carry the plasmid with the puromycin resistance. The following day the puromycin was replaced to normal mESC media again. Five days after transfection, the cells were split again and were diluted up to a single cell in a volume of 100 µl of mESC media, to create a single cell culture. This cell dilution was then transferred to a 96-well plate (VWR, 734-2328) using 100 µl per well. Upon colony growth, the cell clones were transferred to 24-well plates (Sarstedt, 83.3922) and further on to 6-well plates. Half of the amount was then frozen at -80°C using FBS with DMSO (ITW reagents, A3672,0050) in a ratio 10:1, whereas the other half was used to extract DNA to genotype the cell colonies.

3.13.1.7 Genotyping

The DNA was extracted using the Puregene Core Cell Kit by Qiagen (158745), following the instructor´s manual.

Genotyping was done by performing a PCR using the Q5 high fidelity DNA- Polymerase by NEB (M0491). In table 25 the components and in table 26 the PCR program setup can be seen.

The following primers were used:

Forward primer external: 5-GCTGCGGATTGAACATAGGAC-3

Reverse primer external: 5-AACCTGAGATGCCTTGAGAC-3

Forward primer internal: 5-TGCCTCCTTTCCTGTCTTTG-3

Sanger sequencing performed by GATC/Eurofins was used to determine the area around the CRISPR- Cas9 induced deletion, to avoid undetected new mutations, as a result of CRISPR- Cas9 approach.

Ingredient	Amount [µl] for one reaction
5x Q5 reaction buffer	10
100 mM dNTP	1
forward primer 10 µM	2.5
reverse primer 10 µM	2.5
ddH_2O	33.5
Q5 high-fidelity DNA polymerase	0.5

Table 25: Ingredients for one PCR reaction using the Q5 high fidelity DNA- Polymerase.

Program	Time in minutes	Temperature in Celsius
1.Heat denaturation	0:30	98
2.Denaturation	0:10	98
3.Annealing	0:30	60
4.Elongation	3:30	72
5.Go to number 2, 35x cycles		
6.Final elongation	2	72
7.End	∞	4

Table 26: PCR program for genotyping transfected mESC.

4. Results

4.1 Effects of UV-B irradiation on larval development in *C. elegans*

UV-B irradiation is a well-established model to induce DNA damage in cultured cells and organisms. In the nematode *C. elegans*, UV-B irradiation induces specific forms of DNA damage such as cyclobutane pyrimidine dimers (CPDs) or pyrimidine (6-4) pyrimidone photoproducts (6-4 PPs). These are primarily repaired by nucleotide excision repair (NER) (13). Mutants which lack genes encoding for components of the NER machinery exhibit different phenotypes when irradiated, depending on the affected part of the NER (53,54). UV-C irradiation may cause similar effects in *C. elegans* but is described in the literature to cause less reproducible effects between experiments (54). As described in the introduction, wildtype worms go through a typical larval development, classified in four larval stages until adulthood is reached (Fig. 2). Typical differences between larval stages are anatomical structure or length (44). Upon UV-B irradiation of L1 worms, a delay in standard larval development can be seen. This delay can be explained as a result of the DNA damage response (DDR), which includes DNA repair and cell cycle inhibition. A loss of DNA repair capacity can result in a stronger larval delay than in control wildtype worms. This can be seen e.g. in *xpa*-1 mutant worms, which exhibit a larval arrest after UV-B irradiation at the L1 stage. This indicates that the rate of larval development after UV-B treatment of worms at the L1 stage can be used to classify the efficiency of DNA repair, even though other variables such as faster cell division also have to be considered. The developmental assay, a central experimental setup used in my thesis, is based on this method. It is used for testing mutant worms in order to define the relevance of various gene defects for DNA repair.

Under standard conditions (20°C), wildtype worms usually reach the L4 stage after 48 hours when L1 worms are fed (Fig. 4a). Prominent alterations in larval development were detectable when L1 worms were subjected to UV-B irradiation. Upon 40 mJ/cm^2 of UV-B irradiation, wildtype worms were still able to enter L3 (Fig. 4b). However, the percentage of worms that have not reached to L4 stage at 48 hours is markedly higher than in non-irradiated worms. Furthermore, also wildtype worms in L2 or even L1 stage were detected at the same irradiation conditions, verifying the effect of developmental delay by DNA damage. The percentage of L1 and L2 wildtype worms increased markedly when UV-B irradiation was applied at a dose of 60 mJ/cm^2 to the worms (Fig. 4c). Under this condition, only few worms were able to reach the L3 stage, in comparison to standard conditions and the lower UV-B irradiation dose (Fig. 4b).

This observation is consistent with the literature (57) and shows the susceptibility of wildtype larvae to UV-B induced DNA damage.

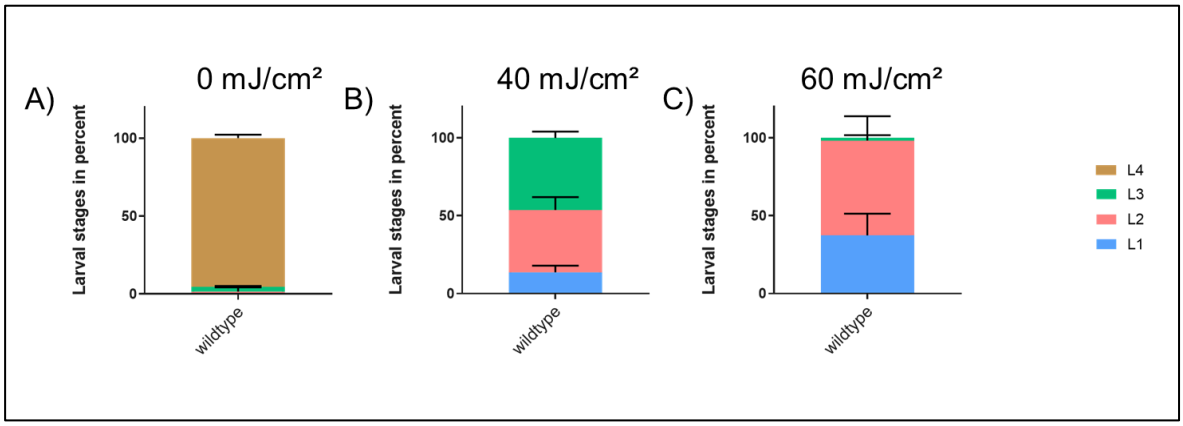

Figure 4. **Development of wildtype worms following UV-B irradiation.**

The developmental assay shows the different larval stages in percent of wildtype worms. Starved L1 worms were irradiated with UV-B and fed for 48 hours under standard conditions before different larval stages were determined. 4a) Larval development of wildtype under standard conditions. 4b) and 4c) Larval development of wildtype after 40 mJ/cm² or 60 mJ/cm² of UV-B irradiation. This experiment was performed in biological replicates. Error bars represent standard deviation.

At this point it is important to mention that the effects of larval development after UV-B irradiation were variable from experiment to experiment. Therefore, wildtype controls were included in all subsequent experiments and the effects in genetically altered worms were always judged in relation to wildtype in all experiments.

4.2 DRM- complex mutants exhibit less larval arrest than wildtype controls after UV-B irradiation

In all organisms, cell cycle regulation is an important mechanism of the DDR to prevent uncontrolled cell division after DNA damage, which can lead to cancer. The DRM- complex is a central cell cycle regulator in *C. elegans,* as described in further detail in the introduction. To study the role of cell cycle regulation after UV-B irradiation, I used different mutant strains for the DRM- complex: The *dpl-1(n2994)* mutant exhibits a splice- acceptor mutation in front of the fifth exon and is supposed to be a loss of function mutation for the *dpl-1* gene (63). The *efl-1(se1)* mutation is supposed to affect the heterodimer binding domain of EFL-1 (81) whereas the *lin-35(n745)* mutation carries a nonsense mutation (62) and is thought to affect the pocket protein in DRM- complex in *C. elegans* (64,81). The other mutations putatively affect subunits of the MuvB core unit: The *lin-9(n112)* mutation carries a missense mutation in the *lin-9* gene (58), the *lin-37(n758)* mutant model affects a splice

region and is supposed to be a null mutant for the corresponding gene product (58). The *lin-52(n771)* mutant model contains a glutamine-to-lysine missense mutation (78) and the *lin-54(n2231)* mutant model carries a glycine-to-glutamic missense mutation (87). Both worm models are predicted to have a loss of function mutation (78,87) which does not affect the binding of other DRM-complex partners (58). The *lin-53(n833)* mutation is a leucine-to-phenylalanine missense mutation and has been characterized as a “dominant- negative-mutation” for the corresponding gene product (62).

As a first step in studying DDR in DRM- complex mutants, I wanted to investigate the alterations in larval development in these mutant strains, to determine if defects in the DRM-complex may result in a special phenotype. Furthermore, UV-B irradiation was used at different doses to induce DNA damage and to study the DDR in these mutants. For this purpose, I used the developmental assay.

In Figure 5a the normal development of DRM- complex mutants under standard conditions can be seen, 48 hours after starved L1 worms were fed. However, some DRM-complex mutants, e.g. the *lin-9(n112), lin-35(n745)* and *lin-37(n758)* mutants exhibited a delay in larval development. This becomes apparent by the much higher percentage of worms reaching only the L3 stage in comparison to L4 stage. It is important to notice, that these mutants show a delay but still can reach L4 and adult stage and even can produce eggs at later time points (data not shown). This relative increase in the proportion of L3 stage worms was not observed in the *dpl-1(n2994), efl-1(se1), lin-52(n771), lin-53(n833)* and *lin-54(n2231)* mutant strains.

Surprisingly, irradiating the DRM-complex mutants with UV-B irradiation let to a less arrested development when compared to wildtype (Fig. 5b and 5c). Figure 5b shows the effect of UV-B irradiation at a dose of 40 mJ/cm^2 in mutant worms. All DRM- complex mutants reveal a faster development than wildtype. This difference was statistically significant (p- value < 0.05) when analyzed with the Fisher´s exact test (supplemental table 1).

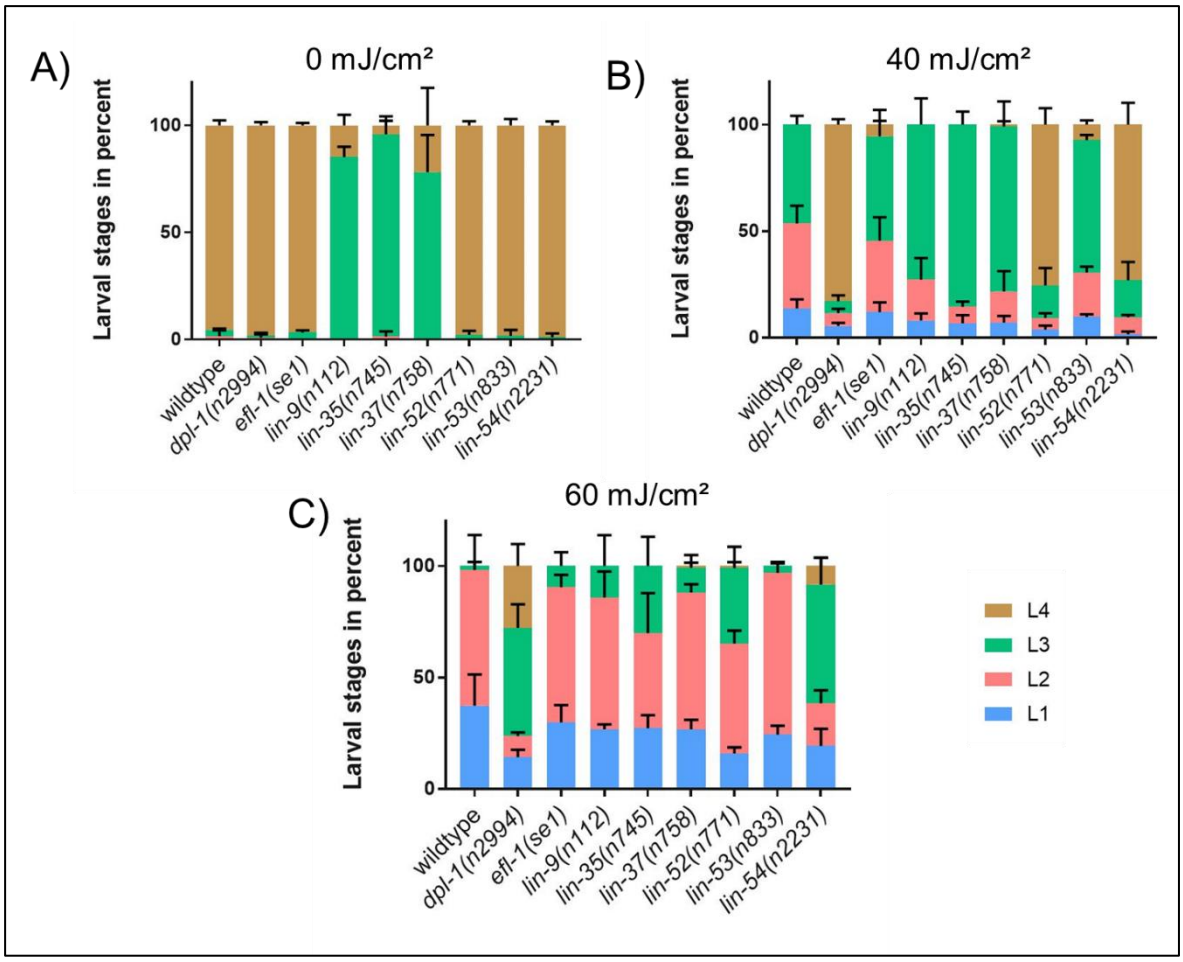

Figure 5. **Development of DRM- complex mutant strains following UV-B irradiation.**

The developmental assay shows the different larval stages in percent of mutant and wildtype worms. Starved L1 worms were irradiated with UV-B and fed for 48 hours under standard conditions before different larval stages were determined. 5a) Development of DRM- complex mutant worms and wildtype under standard conditions. 5b) and 5c) Development of DRM- complex mutant worms and wildtype after 40 mJ/cm² or 60 mJ/cm² of UV-B irradiation. DRM- complex mutant worms show a faster development than wildtype after UV- B irradiation. This experiment was performed in biological replicates. Error bars represent standard deviation. Statistical analysis can be found in the supplemental table 1.

Under irradiating conditions, the DRM- complex mutants react in three different ways in their larval development compared to normal standard conditions: The *dpl-1(n2994), lin-54(n2231)* and *lin-52(n771)* mutants only show a small difference in comparison to unirradiated worms. At 40 mJ/cm^2 of UV-B irradiation, up to 80% of these mutant worms reach the L4 stage. As described above, the *lin-9(n112), lin-35(n745)* and *lin-37(n758)* mutant strains exhibit a slower development under normal conditions. Surprisingly, after irradiation, these mutants reveal a significantly less delayed development compared to wildtype at this condition. Even though these mutants also fail to enter the L4 stage at 40 mJ/cm^2, the fraction of L3 worms is significantly (p- value < 0.05) higher than in wildtype when analyzed with the two- tailed t- test (supplemental table 1). The percentage of L3 worms in this group of mutants stays almost stable under irradiation conditions at

40 mJ/cm^2, similar as under standard unirradiated conditions. The *efl-1(se1)* and *lin-53(n833)* mutant strains still show a small percentage of L4 stage worms at 40 mJ/cm^2, but this is markedly reduced in comparison to the same mutant worms kept under standard conditions. In fact, the percentage of L3 worms increases in these mutants at 40 mJ/cm^2 compared to control. The percentage of L3 worms at 40 mJ/cm^2 only appears significantly different in the two- tailed t- test for the *lin-53(n833)* mutant strain compared to wildtype (supplemental table 1), whereas the *efl-1(se1)* mutant doesn´t. The Fisher´s exact test revealed a significant difference for both mutant strains when compared to wildtype (p-value < 0.05, supplemental table 1).

Elevating the dose of UV-B irradiation levels to 60 mJ/cm^2 did not allow most wildtype worms to reach the L3 stage 48 hours later. Under the same condition, all DRM- complex mutants reached the L3 stage at variable degree (Fig. 5c). The overall difference in larval development was statistically analyzed with the Fisher´s exact test. This confirmed the statistical significance of the effect (p- value < 0.05, supplemental table 1), with one exception. The strain *lin-53(n833)* does not show a significant difference compared to wildtype worms but does reveal a trend to significance having a p- value of 0.08 in the Fisher´s exact test (supplemental table 1).

The strong difference in development of *dpl-1(n2994), lin-54(n2231) and lin-52(n771)* mutants compared to wildtype persists at 60 mJ/cm^2. These mutants are still able to reach the L4 stage, even though the percentage decreases prominently when compared to the lower dose (Fig. 5b and 5c). This decrease can be also seen at the L3 stage, but not as strong as in wildtype worms. The percentage of L3 worms in these mutant strains shows a significant difference compared to wildtype worms, when analyzed with a two- tailed t-test. (p- value < 0.01, supplemental table 1). The *lin-9(n112), lin-35(n745)* and *lin-37(n758)* mutant worms show reduced percentage of L3 worms in comparison to the same worms treated with 40 mJ/cm^2, but still more than the percentage of wildtype worms at 60 mJ/cm^2. Statistical significance for the L3 stage at 60 mJ/cm^2 compared to wildtype did not become apparent for each of these mutants (p- value < 0.05, two-tailed t-test, supplemental table 1) but showed a trend towards significance. Supplemental figure 1 shows representative pictures of DRM- complex mutants and wildtype worms from this experiment. Furthermore, examples for the classification of the different larval stages are demonstrated in the same figure.

The different intensities of UV-B irradiation revealed that the *lin-52(n771)* mutant worms always showed a marked faster development than wildtype worms. Therefore, subsequent experiments were performed mainly using this mutant.

In summary, this experiment revealed that worms with mutations in different components of the DRM- complex exhibit a different phenotype compared to wildtype. Under standard conditions some mutant strains show a delay in development compared to wildtype. Surprisingly, after UV-B irradiation, DRM- complex mutants could overcome the DNA-damage- induced developmental delay at variable degrees in comparison to wildtype. This could indicate that the DNA repair is more efficient or alternatively, that these mutants do not sense DNA damage adequately, resulting in faster cell cycle progression. Before addressing this question, it needs to be determined whether these phenotypes are DRM-complex specific. Therefore, a comparative analysis was made with mutants for associated complexes such as the nucleosome remodeling and histone deacetylase (NuRD)-complex and other genes encoding members of the class B synthetic multivulva group. This could give insights if the newly discovered phenotype in DRM- complex mutants is restricted to mutants for this complex or can be further found in close- by complexes.

4.3 Developmental analysis of other synMuvB mutants after UV-B irradiation

The synMuvB group can be separated in different complexes: The DRM- complex, the NuRD- complex and as another group, genes apart from these complexes such as *hpl-2* (62), *lin-13* (60) or *lin-15B* (60,88). To investigate the behavior of related complexes according to the DRM- complex phenotype, I tested the *hpl-2(tm1489)*, *lin-13(n770)* and *lin-15B(n765)* mutant strains with the developmental assay.

All mutant strains exhibit similar behavior as wildtype under standard conditions (Fig. 6a). At 40 mJ/cm^2 of UV- B irradiation, the *lin-15B(n765)* mutant worms show a similar developmental delay as wildtype worms (Fig. 6b). Furthermore, the *hpl-2(tm1489)* and *lin-13(n770)* mutant strains exhibit even an increased developmental delay than wildtype (Fig. 6b). This difference is also significant (p- value < 0.05) in the Fisher´s exact test (Fig. 6b, supplemental table 2). At 60 mJ/cm^2 of UV-B irradiation, similar behavior in the development of all mutant strains in comparison to wildtype can be seen (Fig. 6c). This was statistically confirmed by the Fisher´s exact test, which showed no significant difference (p- value > 0.05, Fig. 6c).

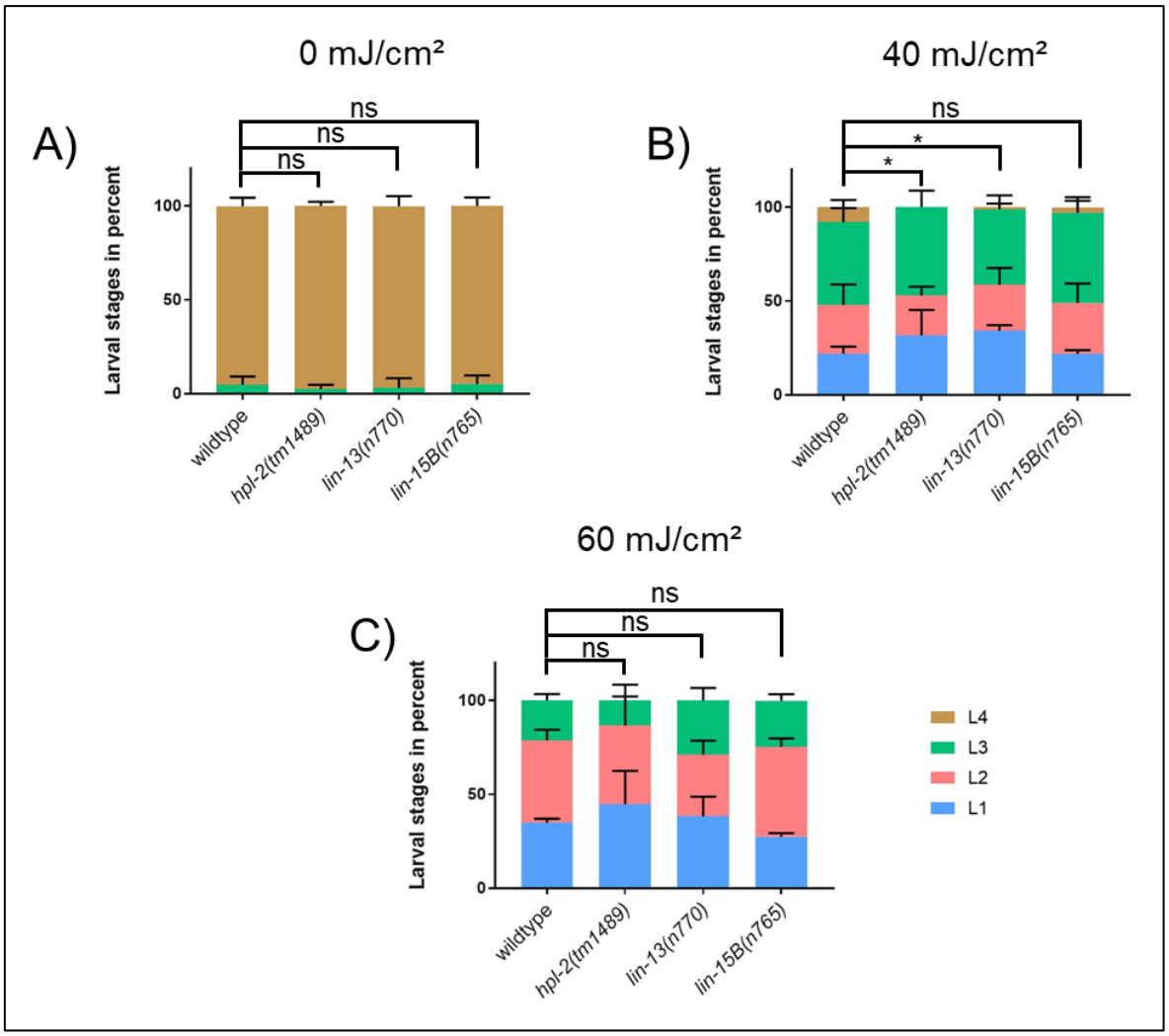

Figure 6. **Development of synMuvB mutant strains following UV-B irradiation.**

The developmental assay shows the different larval stages in percent of mutant and wildtype worms. Starved L1 worms were irradiated with UV-B and fed for 48 hours under standard conditions before different larval stages were determined. 6a) Development of synMuvB mutant worms and wildtype under standard conditions. 6b) and 6c) Development of synMuvB mutant worms and wildtype after 40 mJ/cm² or 60 mJ/cm² of UV-B irradiation. SynMuvB mutant worms show similar behavior as wildtype after UV-B irradiation. Experiment was performed in biological replicates. Error bars represent standard deviation. Asterisks indicate significance in the Fisher´s exact test, $p > 0.05$ =ns, $p<0.05$ = *, $p<0.01$ = **, $p<0.001$ = ***. Further statistical results can be found in supplemental table 2.

In summary, these results show that the *hpl-2(tm1489)*, *lin-13(n770)* and *lin-15B(n765)* mutant strains behave similarly as wildtype worms after UV-B irradiation. Thus, this indicates that the phenotype which was discovered in the preceding experiment in DRM-complex mutants is independent from other mutants of the class B synthetic multivulva group.

4.4 Developmental analysis of mutants for the nucleosome remodeling and histone deacetylase complex after UV-B irradiation

The NuRD- complex in *C. elegans* consists of proteins which are also classified as class B synthetic multivulva gene products, such as LIN-53, LET-418 (69) and HDA-1 (68,70). For this reason, the NuRD-complex mutant worms were investigated in the developmental assay. LIN-53, LET-418 and HDA-1 are all established homologs of the mammalian NuRD-complex (69). This complex is supposed to have a repressing function in vulva development in *C. elegans* (62,70). In this experiment, the *let-418(n3536)* and the heterozygote balanced *hda-1(e1795)* mutant strains were used. Mutant worms with the homozygous mutation in *hda-1* exhibited a high larval arrest after UV- treatment and under standard conditions (data not shown) for which reason the balanced heterozygote worms were used in this developmental assay.

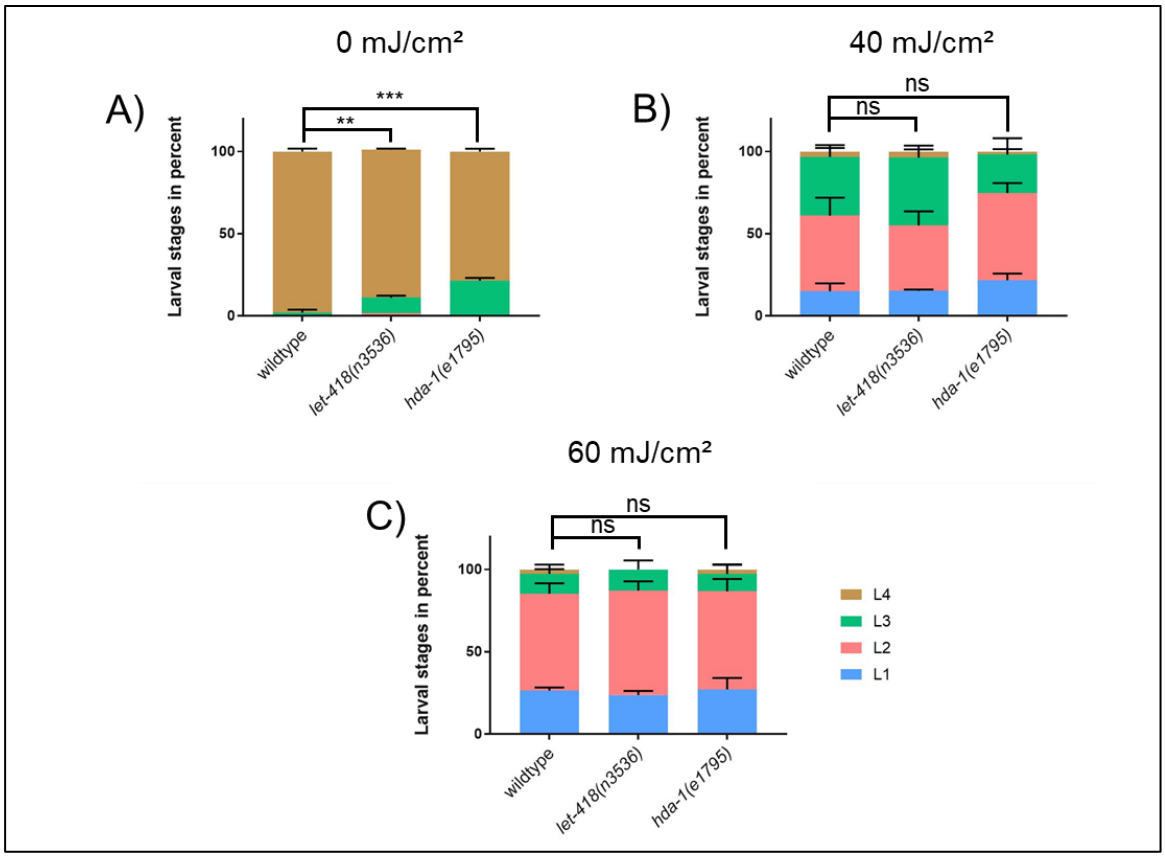

Figure 7. **Development of NuRD- complex mutant strains following UV-B irradiation.**

The developmental assay shows the different larval stages in percent of mutant strains and wildtype. Starved L1 worms were irradiated with UV-B and fed for 48 hours under standard conditions before different larval stages were determined. 7a) Development of NuRD- complex mutant worms and wildtype under standard conditions 7b) and 7c) Development of NuRD- complex mutant worms and wildtype after 40 mJ/cm² or 60 mJ/cm² of UV-B irradiation. NuRD- complex mutant worms show similar behavior as wildtype after UV-B irradiation. Experiment was performed in biological replicates. Error bars represent standard deviation. Asterisks indicate significance in the Fisher´s exact test, $p > 0.05$ =ns, $p < 0.05$ = *, $p < 0.01$ = **, $p < 0.001$ = ***. Further statistical results can be found in supplemental table 3.

The *let-418(n3536)* and *hda-1(e1795)* mutant worms show a higher percentage of worms at L3 stage in comparison to wildtype under standard conditions (Fig. 7a). In figure 7b and 7c these mutants were treated with different doses of UV-B irradiation. Both mutant strains exhibit a similar developmental delay as wildtype. The statistical analysis of these mutants compared to wildtype did not indicate any significance (p- value > 0.05, Fisher´s exact test, Fig. 7b and 7b, supplemental table 3).

In summary, the developmental phenotype observed in DRM- complex mutants was specific, since it appeared independent from other class B synthetic multivulva genes and the NuRD complex.

4.5 DRM- complex mutants do not exhibit faster cell cycle progression

The phenotype observed in the DRM- complex mutants after UV-B irradiation could be explained in several ways. This includes a more efficient or faster DNA repair, inefficiently regulated cell cycle or an insufficient induction of DNA damage response. In order to differentiate between these possibilities, cell cycle progression in these mutants under standard and UV- irradiated conditions was investigated.

In mammalian cells, a central function of the DREAM- complex is the regulation of gene expression during the cell cycle (89). It is also involved in mediating cell cycle arrest when DNA damage is detected (37,38). Previous studies have shown that deletion of genes for the DREAM- complex leads to mitotic defects, nuclear abnormalities and inefficient cell cycle progression in cultured mouse cells (90,91). These results may indicate that the previously described phenotype in DRM- complex mutants in *C. elegans* can be explained by disturbed or inefficiently regulated cell cycle.

To prove that the less arrested development after UV- irradiation is not a consequence of defective cell cycle regulation, an EdU assay was performed. This experimental approach allows the quantification of new divided cells in the worms. Under normal conditions, the *lin-52(n771)* mutants exhibit a comparable number of dividing cells than wildtype worms at different timepoints, indicating that a faster cell division is unlikely (Fig. 8a). Furthermore, the *lin-52(n771)* mutant worms revealed no difference to wildtype in the first 12 hours after irradiation (Fig. 8b). At 24 hours after UV-B irradiation, a significantly higher number of new cells could be seen in the *lin-52(n771)* mutant strain compared to wildtype (Fig. 8b and 8c). This finding supports submitted data (92), which revealed that *lin-52(n771)* mutant worms show a reduced level of CPDs at 24 hours after irradiation. This may indicate that in *lin-52(n771)* mutant worms, a faster repair of DNA damage enables faster cell cycle entry and therefore accelerated larval development. Representative pictures of the EdU assay for *lin-52(n771)* mutant and wildtype worms are shown in figure 8c and supplemental figure 2a and 2b.

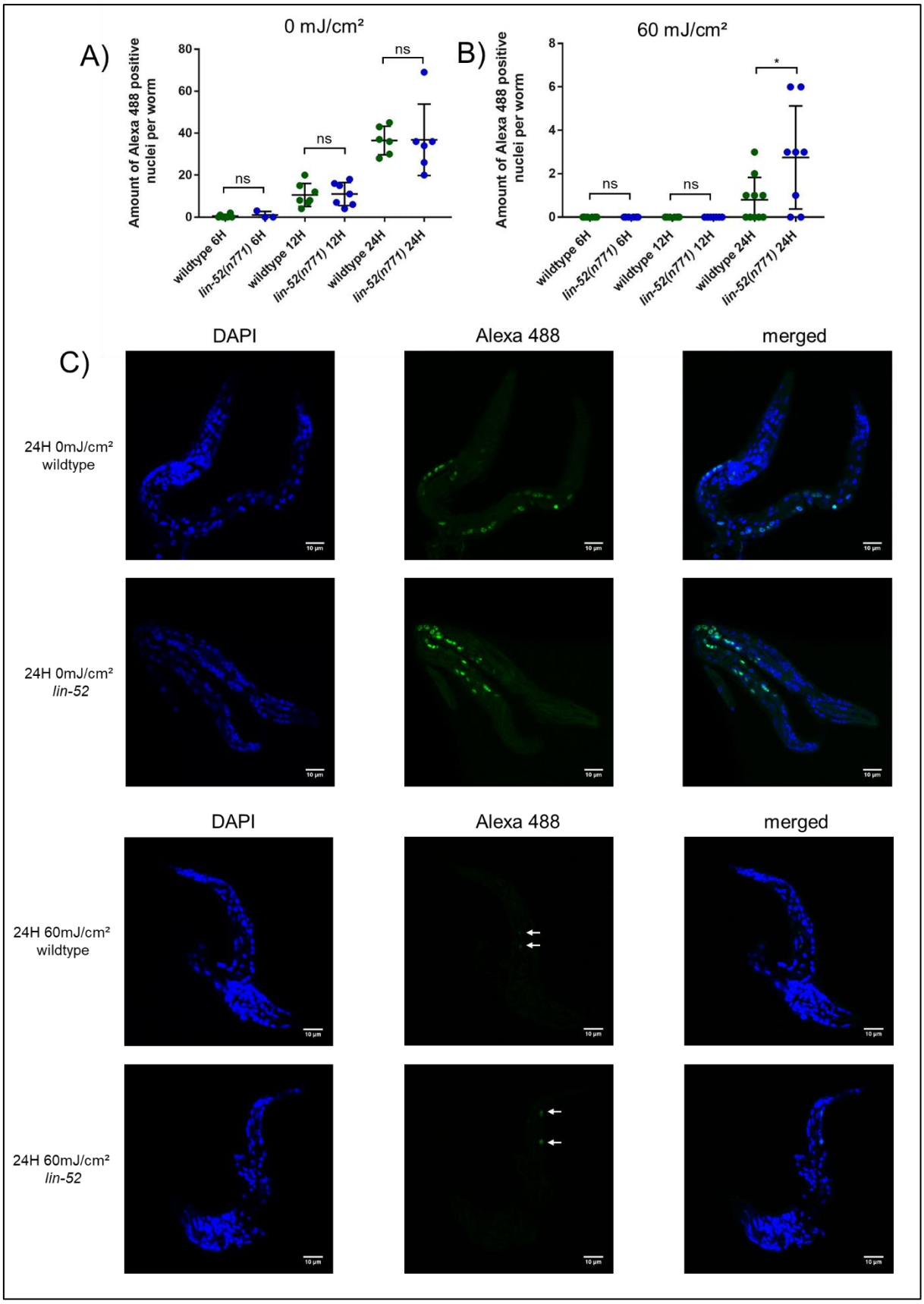
A)
0 mJ/cm²
Amount of Alexa 488 positive nuclei per worm
ns
ns
ns
wildtype 6H
lin-52(n771) 6H
wildtype 12H
lin-52(n771) 12H
wildtype 24H
lin-52(n771) 24H
B)
60 mJ/cm²
Amount of Alexa 488 positive nuclei per worm
ns
ns
*
C)
DAPI
Alexa 488
merged
24H 0mJ/cm² wildtype
24H 0mJ/cm² lin-52
24H 60mJ/cm² wildtype
24H 60mJ/cm² lin-52

Figure 8. **Cell cycle progression and DNA damage response in DRM- complex mutants and wildtype**

8a) Amount of Alexa 488 positive nuclei per worm at different timepoints under standard conditions. Timepoints indicate time after starved L1 worms were fed. The *lin-52(n771)* mutant worms exhibit equal behavior as wildtype. 8b) Amount of Alexa 488 positive nuclei per worm at different timepoints. Timepoints indicate time after L1 worms were irradiated with 60mJ/cm² of UV-B. The *lin-52(n771)* mutant worms show similar behavior as wildtype up to 24 hours after UV-B irradiation. Each point in these graphs indicates one individual worm. Error bars represent standard deviation. Asterisks indicate significance in the unpaired parametric two- tailed t-test, $p > 0.05$ =ns, $p < 0.05$ = *, $p < 0.01$ = **, $p < 0.001$ = ***. 8c) Representative pictures of wildtype and *lin-52(n771)* mutant worms in an EdU Alexa Fluor 488 assay. Nuclei were stained with DAPI, new divided cells were labeled with Alexa 488. Pictures show 24 hours timepoint after UV-B irradiation and control. All pictures were done with the same magnification. Overall magnification 630x. Arrows indicate Alexa 488 positive cells, scale bar showing length of 10 µm.

In summary, these data indicate, that the faster development of DRM- complex mutants after UV-B irradiation is not caused by accelerated cell cycle. On the basis of these data and submitted data showing faster removal of CPDs in DRM- complex mutants after UV-B irradiation (92), it is possible that these mutants can repair DNA damage more efficiently and therefore develop faster than wildtype. Investigating the underlying DNA repair mechanism or mechanisms in DRM- complex mutants could explain the detected phenotype.

4.6 Analysis of target genes involved in the DNA damage response in DRM- complex mutants

In order to identify potential modifying genes for the DRM- mutants phenotype, RNAseq analysis by Arturo Bujarrabal were used. In this analysis, transcript levels of UV-B irradiated and non- irradiated L1 *lin-52(n771)* mutant worms were compared to wildtype worms. The results of this analysis were available for my study. The goal was to explain the phenotype why DRM- complex mutants apparently exhibit faster DNA repair. Therefore, I focused on gene candidates which were upregulated in this RNAseq analysis and which are known to function in DNA repair mechanisms.

4.6.1 Analysis of DNA damage response checkpoint genes in DRM- complex mutants

Central regulators for DDR- mediated germ cell apoptosis and cell cycle arrest in *C. elegans* are ATM-1 and ATL-1 (93). It is possible, that these regulators react in a different manner

in DRM- complex mutants which results in the observed phenotype after UV-B irradiation. Furthermore, it was shown that transcript levels of *atm-1* appeared upregulated in the above mentioned RNAseq analysis. For this purpose, *lin-52(n771)* mutant worms were crossed with the *atm-1(gk186)* mutant strain, to study possible effects by lowering the DNA damage response. Previous studies have shown, that ATL-1 is more involved in UV induced damage response (93) in comparison to ATM-1. However, during my practical work for this thesis it was not possible to cross an appropriate *atl-1* mutant model with DRM- complex mutants.

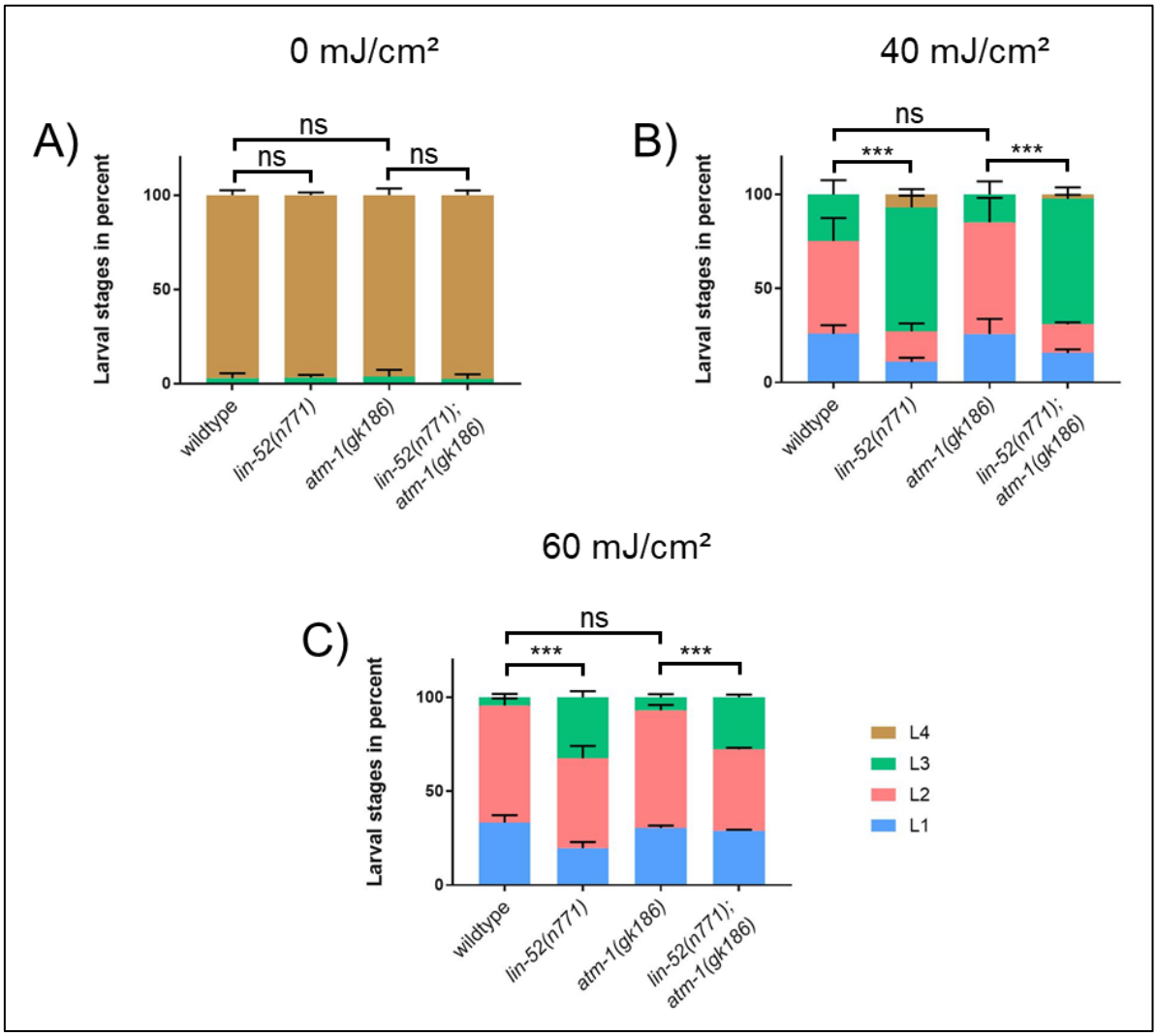

Figure 9. **DRM- complex and *atm-1* deficient mutants following UV-B irradiation**

Developmental assay which shows the different larval stages in percent of mutant and wildtype worms. Starved L1 worms were irradiated with UV-B and fed for 48 hours under standard conditions before different larval stages were determined. 9a) Development of mutant strains and wildtype under standard conditions. No significant difference. 9b) and 9c) The *atm-1(gk186)* worms show similar behavior as wildtype. The *lin-52(n771); atm-1(gk186)* double mutant shows significant faster development than wildtype and *atm-1(gk186)* single mutant. This experiment was performed in biological replicates. Error bars represent standard deviation. Asterisks indicate significance in the Fisher´s exact test, $p > 0.05$ =ns, $p<0.05$ = *, $p<0.01$ = **, $p<0.001$ = ***. Further statistical analysis can be found in supplemental table 4.

The *atm-1(gk186)* single mutant worms exhibit similar development as wildtype under standard conditions, but also after UV-B irradiation (Fig. 9a, 9b and 9c). The *lin-52(n771); atm-1(gk186)* intercrossed mutants also reveal similar development under standard conditions (Fig. 9a). Surprisingly, after UV-B irradiation of L1 worms, these intercrossed mutants show a faster development than wildtype or *atm-1(gk186)* single mutant strains (Fig. 9b and 9c). This was statistically significant (p- value < 0.001) when analyzed by the Fisher´s exact test (supplemental table 4). The *lin-52(n771); atm-1(gk186)* mutant strain reveals even significantly higher percentage of L3 worms and significantly lower percentage of L2 worms at 40 mJ/cm^2 and 60 mJ/cm^2 compared to wildtype or the *atm-1(gk186)* mutant strain, in a two- tailed t-test (Fig. 9b and 9c, supplemental table 4). Furthermore, the *lin-52(n771); atm-1(gk186)* intercrossed mutant strain equals the *lin-52(n771)* single mutant strain. Because the *atm-1(gk186)* mutation did not change cell cycle progression in wildtype worms, the lack of effect in *lin-52(n771)* mutants does not allow a conclusion about altered cell cycle progression after DNA damage. In order to draw this conclusion, it would have been necessary to cross the *lin-52(n771)* mutant also with an *atm-1/atl-1* double mutant line, as ATL-1 seems to be more involved in UV induced damage response (93). Unfortunately, the attempt to achieve this goal by RNAi technologies was not successful (data not shown) and another attempt to intercross *atm*-1/*atl-1* double mutants with the *lin-52(n771)* mutant strain did also not work with classical intercross experiments.

4.6.2 Analysis of EXO-3 activity in DRM- complex mutants

Among these candidates, *exo-3* appeared as an interesting candidate gene. EXO-3 is a hydrolytic apurinic/ apyrimidinic exonuclease that normally is involved in base excision repair in *C. elegans* (94,95). A previous study by Andreas Schlotterer et al (96) showed that RNAi mediated knock-down of *exo-3* results in decreased longevity, increase of mitochondrial deletions, limited motility and increased reactive oxygen species formation in *C. elegans*. Thus, these characteristics made it interesting to test the *exo-3(ok3559)* mutant strain in the developmental assay.

The *exo-3(ok3559)* mutant strain shows a small delay in development under standard conditions (Fig. 10a). This difference became more prominent when this mutant was irradiated with 40 mJ/cm^2 and 60 mJ/cm^2. *Exo-3(ok3559)* mutants exhibit a stronger sensitivity to UV-B irradiation than wildtype worms (Fig. 10b and 10c). This is also significantly different (p- value < 0.001, Fisher´s exact test). Under both irradiating conditions, the *exo-3(ok3559)* shows higher percentages of L1 worms than wildtype, indicative of a more accentuated developmental arrest in these mutants.

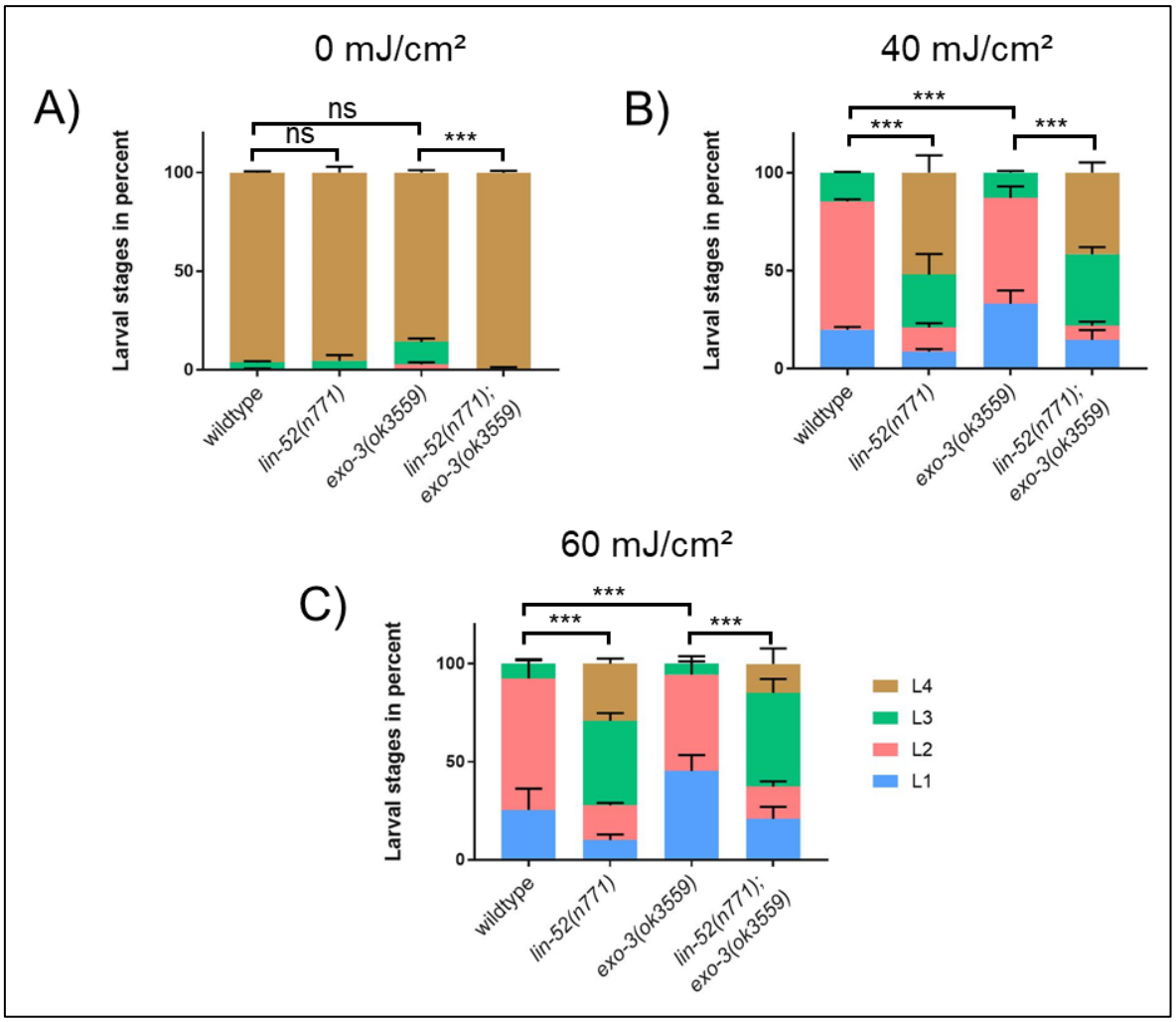

Figure 10. **DRM- complex and *exo-3* deficient mutants following UV-B irradiation**.

Developmental assay which shows the different larval stages in percent of mutant and wildtype worms. Starved L1 worms were irradiated with UV-B and fed for 48 hours under standard conditions before different larval stages were determined. 10a) Development of mutant strains and wildtype under standard conditions. 10b) and 10c) Mutant strains and wildtype were irradiated with 40 mJ/cm² or 60 mJ/cm² of UV-B. The UV-B irradiation sensitive phenotype of *exo-3(ok3559)* mutant worms can be partial rescued by intercross with the *lin-52(n771)* mutant. Experiment was performed in biological replicates and repeated three times. Error bars represent standard deviation. Asterisks indicate significance in the Fisher´s exact test, p> 0.05 =ns, p<0.05 = *, p<0.01 = **, p<0.001 = ***. Further statistical analysis can be found in supplemental table 5.

Surprisingly, the developmental arrest of *exo-3(ok3559)* mutant worms improves by intercross with the *lin-52(n771)* mutant strain. Figure 10b shows that the double mutant accomplishes a high percentage of L4 and L3 worms at 40 mJ/cm^2 irradiation, whereas single *exo-3(ok3559)* mutants are almost unable to enter the L3 stage under the same conditions. This difference is highly significant (p- value < 0.001, Fisher´s exact test, Fig. 10b). Furthermore, the two- tailed t-test shows a significant difference (p- value < 0.01) for the percentage of L3 worms with this mutation at 40 mJ/cm^2 irradiation (supplemental table 5). At 60 mJ/cm^2 of irradiation the double mutants show a decrease in the percentage of L4 worms and increased percentage of L3 worms. Under the same conditions the

exo-3(ok3559) mutant worms almost fail to enter the L3 stage. In parallel, the percentage of L1 and L2 worms increases markedly. This developmental rescue of the arrested *exo-3(ok3559)* single mutant by the *lin-52(n771); exo-3(ok3559)* intercross appears highly significant (p- value < 0.001) in the Fisher´s exact test. The two- tailed t-test for these mutants also shows a significant difference for each larval stage (p- value < 0.05, supplemental table 5).

The upregulated transcription levels of *exo-3* in the *lin-52(n771)* mutant originally suggested that this gene could mediate the effect of apparently faster DNA repair. If this is true, then the intercrossed mutant should not exhibit a less delayed development anymore. Surprisingly, the intercrossed mutant is able to restore the *exo-3(ok3559)* phenotype. These double mutant worms show almost similar development as the *lin-52(n771)* single mutants under irradiating conditions, indicating that the upregulation of *exo-3* cannot explain the developmental phenotype of the DRM- complex mutants. At 40 mJ/cm^2 of UV-B irradiations the intercrossed mutant shows smaller percentage of L4 worms and higher percentage of L3 worms than the *lin-52(n771)* mutant worms. Both stages exhibit no significant difference (p- value > 0.05) in the two- tailed t-test, even though the overall difference for all stages is significant (p- value < 0.05, Fisher´s exact test, supplemental table 5). Figure 10c shows a higher percentage of L1 worms and a smaller percentage of L4 worms in the intercrossed mutants compared to the *lin-52(n771)* single mutant strain. This is significantly different (p-value < 0.05), using the two- tailed t- test (supplemental table 5). Analysis of overall development of both groups under these conditions exhibited also a significant difference (p- value < 0.01, Fisher´s exact test, supplemental table 5).

In summary the *exo-3(ok355)* single mutants show a developmental delay which indicates enhanced sensitivity to UV-B irradiation. This delay is significantly stronger than in wildtype which is consistent with literature (96). This developmental arrest can be restored by an intercross with the *lin-52(n771)* mutant strain. A similar development as in *lin-52(n771)* could not be reached. Thus, a possible impact by the loss of the *exo-3* gene cannot be excluded but may be unlikely.

4.6.3 Analysis of PARP-1 activity in DRM- complex mutants

In humans, the PARP1 gene functions in DNA excision repair (97). The corresponding protein is activated by DNA single strand breaks (98) and is supposed to be a modulator for early DNA damage signaling (99). There is also evidence that this gene is involved in the UV-B damage response (100). These functions point to an important role as a target for tumor therapies. PARP inhibitors are used in BRCA deficient cells to induce cell cycle arrest and apoptosis in these cells (101,102).

In *C. elegans*, a homolog to the human PARP1 has been identified (103), which is also known as *pme-1*. PARP inhibitors in combination with IR lead to reduced embryonic survival in *C. elegans* (104).

This gene also appears upregulated in the RNAseq analysis. Thus, it appears as another interesting candidate for further analysis by intercross with DRM- complex mutants. In the following developmental assay, the *parp-1(ok988)* mutant strain was used as a knock-out model.

The *parp-1(ok988)* mutant strain exhibits a small reduction of L4 worms and higher percentage of L3 worms compared to wildtype under standard conditions (Fig. 11a). This difference is significant (p- value < 0.05) in a two- tailed t-test (supplemental table 6). At 40 mJ/cm^2 of UV-B irradiation the *parp-1(ok988)* mutant strain shows a stronger developmental delay compared to wildtype. The mutant worms are almost unable to reach the L4 stage, showing higher percentages in the lower larval stages (Fig. 11b). The Fisher´s exact test revealed a significant difference between wildtype and the *parp-1(ok988)* mutant strain (p- value < 0.001). Figure 11b shows that wildtype worms are able to reach the L4 stage, even though they are irradiated with 40 mJ/cm^2. At this point it should be remembered that the effect of UV-B irradiation can vary between experiments. Therefore, genetically altered worms are always judged in relation to wildtype. At 60 mJ/cm^2 of UV-B irradiation the *parp-1(ok988)* mutant worms and wildtype behave similarly (Fig. 11c). The Fisher´s exact test as well as the two- tailed t- test for each larval stage reveal no significantly difference (p- value > 0.05, fig. 11c, supplemental table 6).

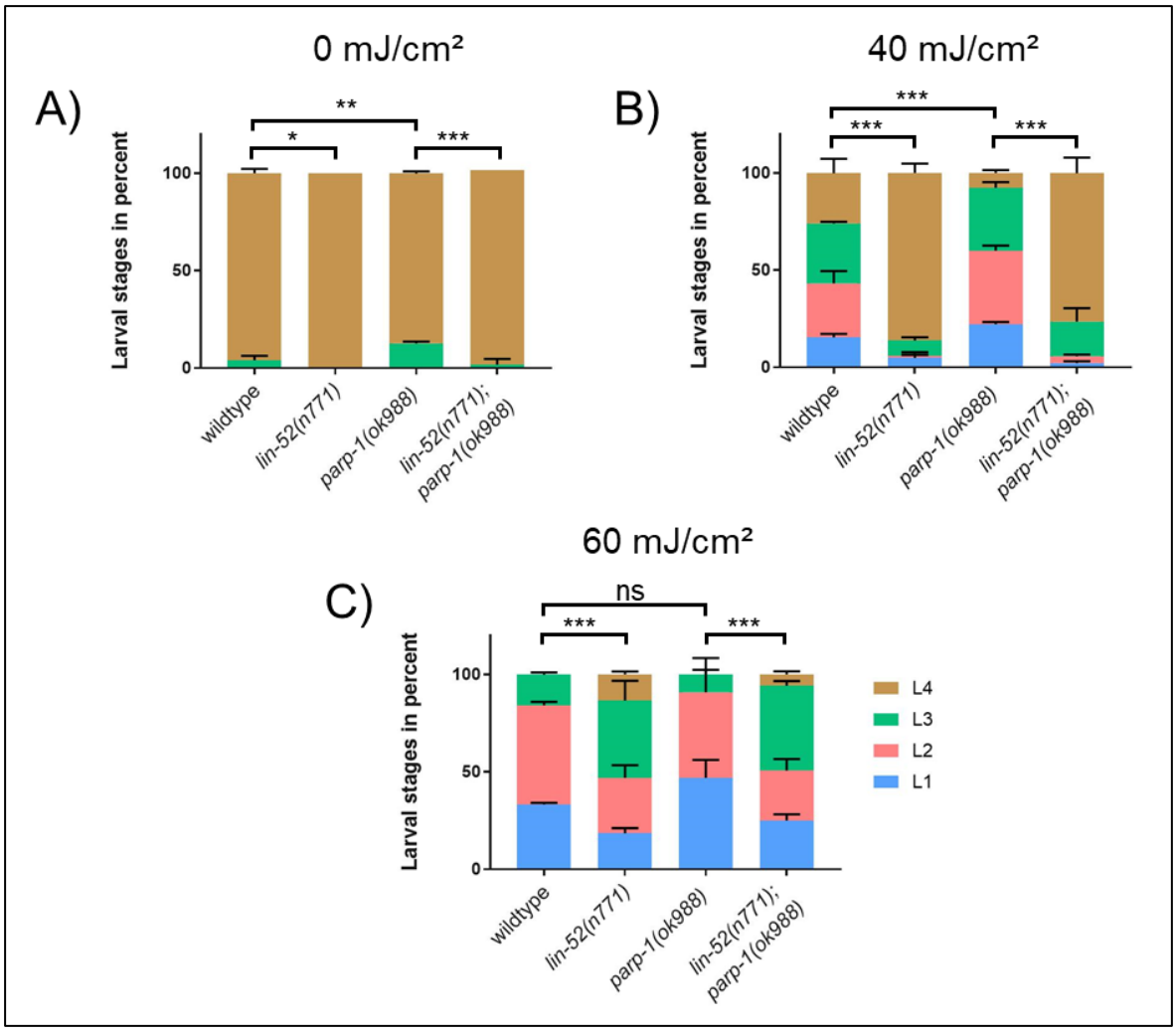

Figure 11. **DRM- complex and *parp-1* deficient mutants following UV-B irradiation**.

Developmental assay which shows the different larval stages in percent of mutant and wildtype worms. Starved L1 worms were irradiated with UV-B and fed for 48 hours under standard conditions before different larval stages were determined. 11a) Development of mutant strains and wildtype under standard conditions. 11b) and 11c) Mutant strains and wildtype were irradiated with 40 mJ/cm² or 60 mJ/cm² of UV-B. The double mutant can rescue partially the *parp-1(ok988)* mutant strain. Experiment was performed in biological replicates and repeated three times. Error bars represent standard deviation. Asterisks indicate significance in the Fisher´s exact test, p> 0.05 =ns, p<0.05 = *, p<0.01 = **, p<0.001 = ***. Further statistical analysis can be found in supplemental table 6.

The *parp-1(ok988)* single mutant was crossed with *lin-52(n771)* to investigate a possible impact of PARP-1 in the DRM- complex mutant´s phenotype. Under standard conditions the intercrossed mutant shows a lower percentage of L3 worms than the *parp-1(ok988)* single mutant. This difference also appears significant (p- value < 0.01) in a two- tailed t-test (supplemental table 6). Irradiating conditions for the intercrossed mutant lead to a higher percentage of L4 worms than in *parp-1(ok988)* mutants and also higher than in wildtype, with lower percentage of L3 worms (Fig. 11b). The percentage of worms in these two larval stages are significantly different (p- value < 0.05) in a two- tailed t- test (supplemental table 6). The difference in overall development appears also highly

significant (p- value < 0.001) in the Fisher´s exact test (Fig. 11b). At 60 mJ/cm^2 of UV-B irradiation some double mutant worms are still able to enter the L4 stage, whereas wildtype and the *parp-1(ok988)* single mutants are not (Fig. 11c). The percentage of L3 worms increases in comparison to the latter dose and is also higher than in wildtype and *parp-1(ok988)* single mutant at the same dose. The percentage of L3 worms for *parp-1(ok988)* single mutant and the intercrossed mutants is significantly different (p- value < 0.01) in the two- tailed t- test (supplemental table 6). Furthermore, both strains show significant differences (p- value < 0.001) in the Fisher´s exact test at the same dose (Fig. 11c). This result was unexpected because *parp-1* appeared as a candidate which could be mediating the effects of the *lin-52(n771)* mutation and other mutations related to the DRM- complex in the developmental assay under UV-B irradiation. Surprisingly, the intercrossed mutant and the *lin-52(n771)* single mutant do not differ under standard or even irradiating conditions. A statistical difference with the Fisher´s exact test or the two- tailed t- test could not be observed, with one exception: The percentage of L4 worms at 60 mJ/cm^2 irradiation is significantly higher in *lin-52(n771)* single mutants than in the intercrossed strain. This statistical difference however did not appear consistent when the experiment was repeated. Thus, the effect needs to be interpreted with caution. However, it is unlikely that the improved response to UV-B irradiation in DRM- complex mutant worms is caused by enhanced PARP-1 activity.

The results shown in figure 10 and 11 indicate that despite the upregulation of *exo*-3 and *parp-1* transcript levels in *lin-52(n771)* mutant worms, these genes apparently do not explain the preserved phenotype in DRM- complex mutants. The developmental arrest of *exo-3(ok3559)* mutant strain was partial rescued by an intercross with the *lin-52(n771)* mutant. Furthermore, the *parp-1(ok988)* mutant, which behaves similar as wildtype after irradiation, can be fully rescued by an intercross with *lin-52(n771)* up to a DRM- complex mutant phenotype. Thus, the *lin-52(n771)* phenotype can even occur in the absence of single DNA repair genes such as *parp-1* and *exo-3*.

4.7 The role of the nucleotide excision repair in DRM- complex mutants

The above described findings indicate that tested DNA repair genes that are upregulated at transcript level in *lin-52(n771)* mutants cannot explain the phenotype of DRM- complex mutants. Therefore, I decided to investigate the nucleotide excision repair (NER) in this context. The NER appeared as an interesting target because this type of repair mechanism usually repairs UV-B induced DNA damage. As described in the introduction, the NER in *C. elegans* can be divided into two different branches: Transcription-Coupled (TC) repair which repairs damage of the transcribed strand and Global- Genome (GG) NER which repairs defects in the whole genome (13). Interestingly, these two repair pathways are differently prevalent at different larval stages and different tissues. Whereas the TC-NER is more relevant in somatic tissue, the GG-NER is more active in the germ and early embryonic cells (53,54).

By intercrossing DRM- complex mutants with knock-out models of the NER pathway, possible effects on the preserved phenotype can be studied. If the hypothesis is correct that the NER has an impact on the DRM- complex mutants' phenotype, then an additional knock-out of NER candidates should cause further arrest to larval development. Therefore, the same developmental assay as described above was used in the following experiment. These analyses were started first by investigating the impact of genes relevant for TC-NER in the developmental assay after crossing them with DRM- complex mutants.

4.7.1 Impact of the transcription- coupled- nucleotide excision repair in DRM- complex mutants after UV-B irradiation

In the following experiments I used two knock-out models for genes which are involved in the TC-NER: The *csa-1(tm4539)* and the *csb-1(ok2335)* mutants. Both mutants are expected to be null mutants and hypersensitive to UV-B irradiation (54,55). Thus, the UV-B irradiation dose was lowered to 15 mJ/cm^2 and 30 mJ/cm^2 of UV-B irradiation in the following experiment.

The *csa-1(tm4539)* mutant strain behaves similar as wildtype under standard conditions in a developmental assay (Fig. 12a). At 15 mJ/cm^2 of UV- B irradiation this mutant shows a higher percentage of L3 worms with corresponding lower percentage of L4 worms than wildtype (Fig. 12b). The overall difference between these strains is significant at this dose (p- value < 0.01, Fisher´s exact test, Fig. 12b). Figure 12c exhibits that the *csa-1(tm4539)* mutant worms are almost unable to reach the L4 or even L3 stage after 30 mJ/cm^2 of UV-

B irradiation. Thus, they show a high percentage of L1 and L2 stage worms in comparison to wildtype. At the same dose the control worms were still able to reach the L4 stage at high percentages. These differences are also significant (p- value < 0.05) in the two- tailed t-test (supplemental table 7) and the Fisher´s exact test (Fig. 12c). The phenotype of *csa-1(tm4539)* mutants was investigated further in combination with a DRM- complex mutant by performing an intercross with the *lin-52(n771)* mutant. This intercrossed mutant showed a normal development under standard conditions in the developmental assay (Fig. 12a). At 15 mJ/cm^2 the intercrossed mutant did not show a significantly difference (p- value > 0.05) to wildtype or to the *csa-1(tm4539)* mutant in development (Fisher´s exact test, supplemental table 7). At 30 mJ/cm^2 the intercrossed mutant exhibits a higher percentage of L3 worms than in the *csa-1(tm4539)* single mutant (Fig. 12c). In particular, the percentage of L3 stage worms in comparison to L2 worms was enhanced in the intercrossed mutant in comparison to *csa-1(tm4539)* single mutants. The difference between the L3 stage for these mutants appeared significant (p- value < 0.05, two- tailed t-test, supplemental table 7) as well as the Fisher´s exact test result (p- value < 0.01) for these mutants (Fig. 12c). At the same dose the percentage for L1 and L2 worms shows statistically no difference between these mutants (p- value > 0.05, two -tailed t- test, supplemental table 7). This experiment was done in order to determine the phenotype of the DRM- complex mutants under conditions of a reduced TC-NER. Indeed, this experiment showed that the intercrossed mutant is more sensitive to UV-B irradiation than wildtype or *lin-52(n771)* single mutants, especially at 30 mJ/cm^2. At this dose the intercrossed mutant exhibits a significant difference (p- value < 0.001) in developmental delay in comparison to wildtype or the *lin-52(n771)* single mutant (Fisher´s exact test, supplemental table 7).

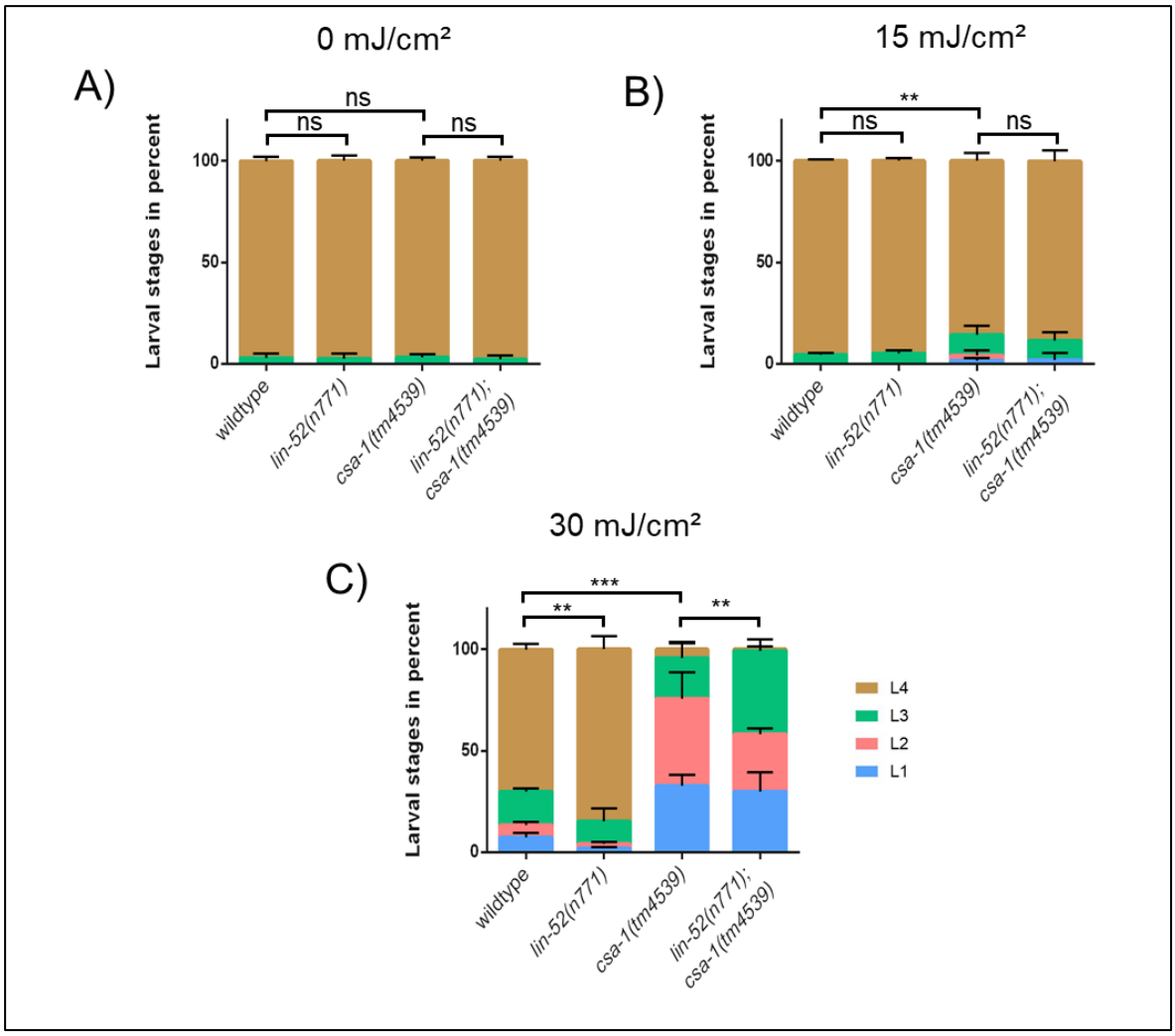
A)
0 mJ/cm²
ns
ns
ns
Larval stages in percent
100
50
0
wildtype
lin-52(n771)
csa-1(tm4539)
lin-52(n771); csa-1(tm4539)
B)
15 mJ/cm²
**
ns
ns
Larval stages in percent
100
50
0
wildtype
lin-52(n771)
csa-1(tm4539)
lin-52(n771); csa-1(tm4539)
C)
30 mJ/cm²
***
**
**
Larval stages in percent
100
50
0
wildtype
lin-52(n771)
csa-1(tm4539)
lin-52(n771); csa-1(tm4539)
L4
L3
L2
L1

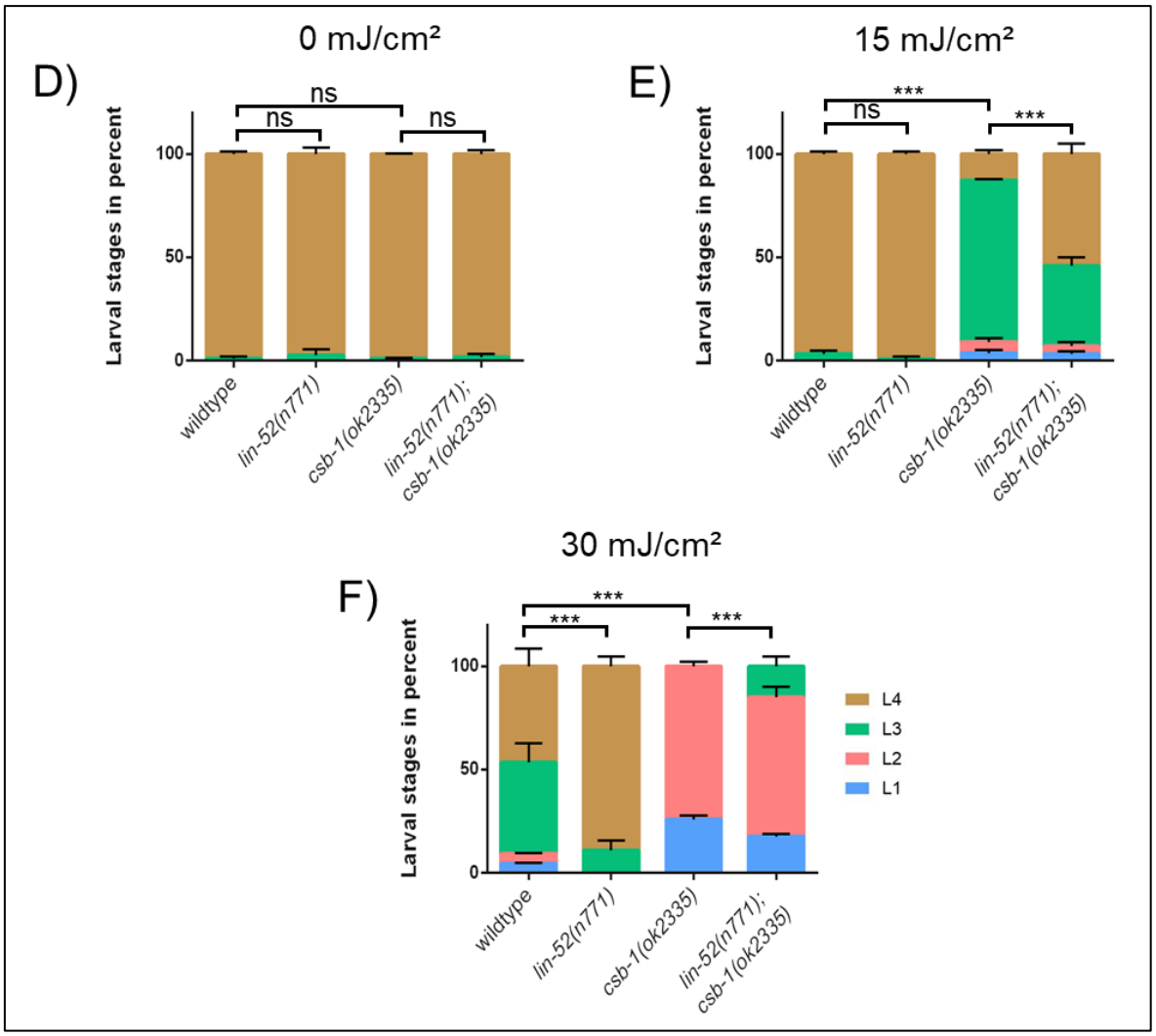

Figure 12. **TC-NER deficiency in DRM- complex mutant worms following UV-B irradiation.**

Developmental assay which shows the different larval stages in percent of mutant and wildtype worms. Starved L1 worms were irradiated with UV-B and fed for 48 hours under standard conditions before different larval stages were determined 12a) and 12d) Development of mutant worms and wildtype under standard conditions. 12b) and 12e) Mutant worms and wildtype were irradiated with 15 mJ/cm² of UV-B. 12c) and 12f) Mutant worms and wildtype were irradiated with 30 mJ/cm² of UV-B. The phenotype of single TC-NER deficient mutant worms is rescued partial by intercross with the *lin-52(n771)* mutant. Both experiments were performed in biological replicates and repeated three times. Error bars represent standard deviation. Asterisks indicate significance in the Fisher´s exact test, p> 0.05 =ns, p<0.05 = *, p<0.01 = **, p<0.001 = ***. Further statistical analysis can be found in the supplemental table 7 and 8.

To further study whether the observed DNA damage resistance in DRM- complex mutants is dependent on TC-NER activity, the *csb-1(ok2335)* mutant strain was used. This single mutant behaves similarly as wildtype in the developmental assay under standard conditions (Fig. 12d). At 15 mJ/cm^2 the percentage of L4 worms is reduced markedly in this mutant with higher levels of L3 worms compared to wildtype (Fig.12e). This difference is significant (p- value < 0.01) in the two- tailed t- test in all stages (supplemental table 8) and also appears significant in the Fisher´s exact test (p- value < 0.001, Fig. 12e). This effect

becomes more prominent at 30 mJ/cm^2 of UV-B irradiation where the *csb-1(ok2335)* single mutant arrests in the L2 stage, whereas the wildtype still reaches the L4 stage (Fig. 12f). This obviously hypersensitive mutant strain was intercrossed with the *lin-52(n771)* mutant. The *lin-52(n771); csb-1(ok2335)* intercrossed mutant strain shows a normal development, similar as wildtype, under standard conditions (Fig. 12d). At 15 mJ/cm^2 the intercrossed mutant shows higher percentage rates of L4 worms with lowered levels of L3 worms than the *csb-1(ok2335)* single mutant (Fig. 12e). This difference appeared significantly different (p- value < 0.001) in the two- tailed t- test when these mutant strains were compared (supplemental table 8). The Fisher´s exact test also exhibits a significantly difference (p-value < 0.001, Fig. 12e). Figure 12f shows that the double mutants could enter the L3 stage in comparison to the *csb-1(ok2335)* single mutants. The percentage of L1 worms is significantly reduced (p- value < 0.01, two- tailed t- test, supplemental table 8) in the intercrossed mutants in comparison to *csb-1(ok2335)* single mutants. The overall difference between both strains also appeared significant (p- value < 0.001, Fisher´s exact test, Fig. 12f). Interestingly, the intercrossed mutant is not able to reach similar development as wildtype or *lin-52(n771)* single mutants under irradiating conditions. This difference is also highly significant (p- value < 0.001) in the Fisher´s exact test for both irradiated groups (supplemental table 8). Indeed, this experiment confirms previous results with the *lin-52(n771); csa-1(tm4539)* mutants. The *lin-52(n771); csb-1(ok2335)* double mutant can accomplish higher developmental stages than the *csb-1(ok2335)* single mutant under irradiating conditions but does not reveal similar development as wildtype or the classical phenotype of DRM- complex mutants.

These results indicate that the TC-NER could be partially involved as a candidate mechanism explaining the phenotype of DRM- complex mutants under UV-B irradiation. However, due to the partial rescue of the TC-NER mutants sensitivity in *lin-52(n771)*, it is possible that other DNA repair mechanisms beyond TC-NER are responsible for the improved DNA repair in DRM- complex mutants.

As described previously, TC-NER mutants exhibit a developmental arrest whereas GG-NER exhibit a lack in germ cell development but reveal less defective somatic tissue after UV-B irradiation of L1 worms (53,54). These experiments have shown that *lin-52(n771); csb-1(ok2335)* intercrossed mutants reveal significantly lower levels of L1 stage worms than *csb-1(ok2335)* single mutants, and that they are still able to enter the L3 stage at 30 mJ/cm^2 of UV-B irradiation. This finding could support the hypothesis that the GG-NER is more active in these double-crossed mutants which could explain the partial rescue. Furthermore, it should be kept in mind, that synMuvB mutant worms exhibit upregulated levels of germline related genes in somatic tissue (67) which could also explain improved GG-NER in DRM-complex and TC-NER deficient mutants. Before this could be tested in a complete knock-

out for the NER in a DRM- complex mutant background, it is important to control if GG-NER deficient mutants exhibit also a partial rescue when intercrossed with DRM- complex mutants.

4.7.2 Impact of the global- genome- nucleotide excision repair in DRM- complex mutants after UV-B irradiation

The second NER sub-branch is the GG-NER. Mutants for the GG-NER were tested in the same setup as TC-NER mutants before, to study the impact of GG-NER in the development of DRM- complex mutants after UV-B exposure. For this purpose, I used the *xpc-1(tm3886)* mutant strain which produces a shortened form of the XPC-1 protein (54).

Under standard conditions, this mutant behaves similar as wildtype in the developmental assay (Fig. 13a). Figure 13b shows that after 40 mJ/cm^2 of UV- B irradiation the *xpc-1(tm3886)* mutant worms fail to enter the L4 stage and reach the L3 stage at only a small percentage. Compared to wildtype, these stages were reached at significantly lower percentages (p- value < 0.01, two-tailed t- test, supplemental table 9) in these mutants. At 60 mJ/cm^2 the *xpc-1(tm3886)* single mutant arrests in the L2 stage. Surprisingly, wildtype worms show similar behavior to this single mutant strain at this dose. The statistical analysis reveals no significant differences (p- value > 0.05) between these strains in both tests (two-tailed t- test, Fisher´s exact test, supplemental table 9). This result is reasoned on condition that 60 mJ/cm^2 is a high irradiation dose for L1 worms which leads to difficult conditions to distinguish between sensitive strains. However, strains which are partial resistant to UV-B irradiation exhibit stronger results in comparison to sensitive strains at this dose. Otherwise, it is also possible that with 60 mJ/cm^2 of UV-B irradiation the TC-NER and other DNA repair mechanism are upregulated in the *xpc-1(tm3886)* mutant because of a higher DNA damage response. As described before, the GG-NER is also known to play a minor role in DNA damage repair in somatic tissue (54).

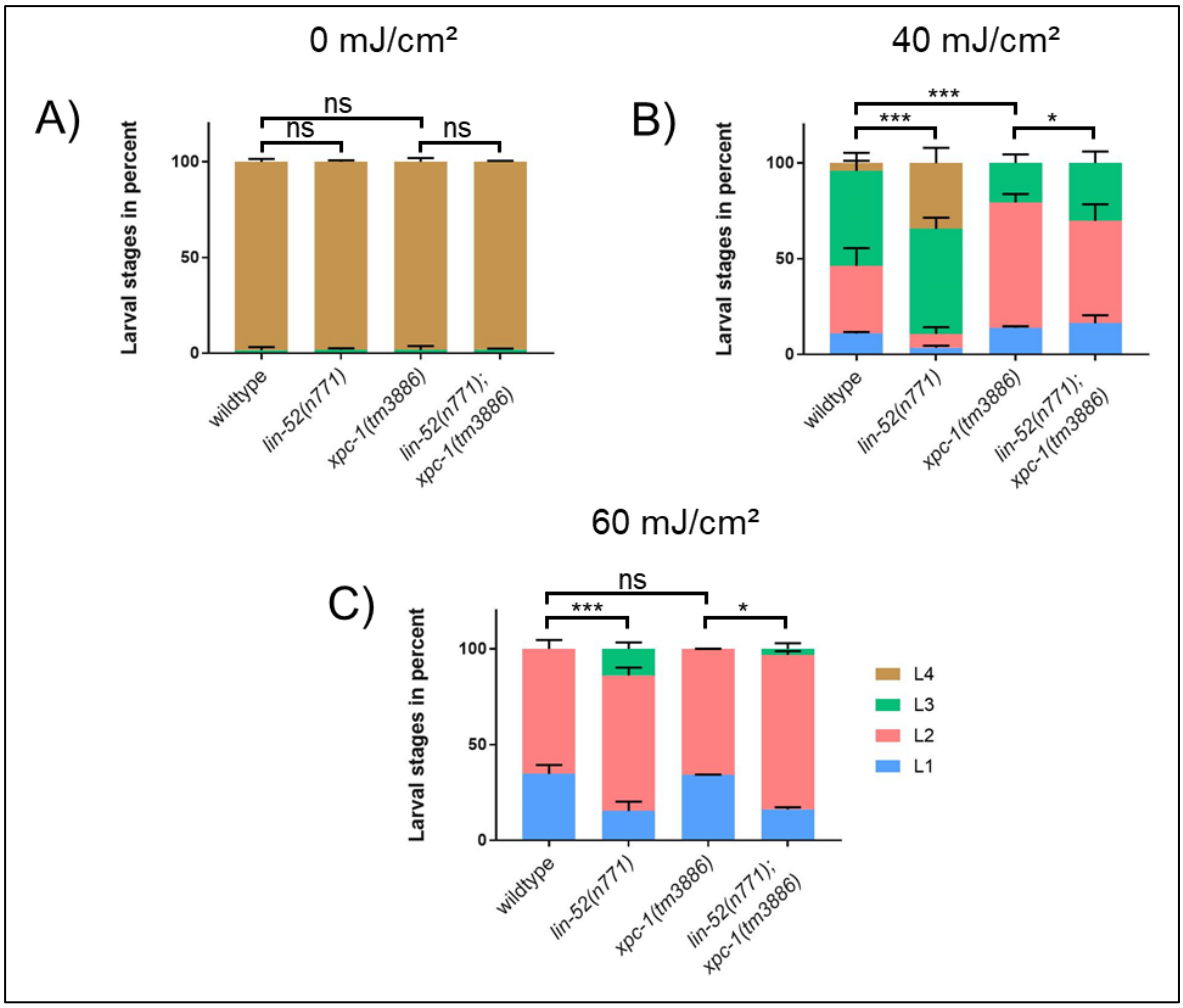

Figure 13. **Development of DRM- complex mutant worms after UV-B irradiation in a GG-NER deficient background.**

Developmental assay which shows the different larval stages in percent of mutant and wildtype worms. Starved L1 worms were irradiated with UV-B and fed for 48 hours under standard conditions before different larval stages were determined. 13a) Development of mutant worms and wildtype under standard conditions. 13b) and 13c) Mutant and wildtype worms were irradiated with 40 mJ/cm² or 60 mJ/cm² of UV-B. The *lin-52(n771); xpc-1(tm3886)* intercrossed mutant worms rescue partially the phenotype of the single GG-NER deficient strain. Experiment was performed in biological replicates and repeated three times. Error bars represent standard deviation. Asterisks indicate significance in the Fisher´s exact test, p> 0.05 =ns, p<0.05 = *, p<0.01 = **, p<0.001 = ***. Further statistical analysis can be found in supplemental table 9.

To investigate this phenotype in a DRM- complex mutant, the *xpc-1(tm3886)* single mutant strain was used for intercross with the *lin-52(n771)* mutant strain. Under standard conditions the *lin-52(n771); xpc-1(tm3886)* mutant behaves similar to wildtype, almost all worms reach the L4 stage, 48 hours after L1 worms were fed. At 40 mJ/cm^2 the intercrossed mutants fail to enter the L4 stage but seem to show a higher percentage of L3 worms than the *xpc-1(tm3886)* single mutants (Fig. 13b). Using a threshold of 0.05 this difference did not appear significant in a two- tailed t-test but shows a trend with a p- value of 0.09 (supplemental table 9). The overall difference between these mutants is significant (p- value < 0.05, Fisher´s exact test, Fig. 13b). Interestingly, at 60 mJ/cm^2 the intercrossed mutant shows a

higher percentage of L2 worms and lower levels of arrested L1 worms than the *xpc-1(tm3886)* single mutant and wildtype. The higher percentage of L2 worms in the *lin-52(n771); xpc-1(tm3886)* double mutants is also significantly different (p- value < 0.001) in the two- tailed t-test when compared to wildtype or *xpc-1(tm3886)* single mutant (supplemental table 9). Furthermore, the Fisher´s exact test reveals significant differences (p- value < 0.05) between the intercrossed mutant and the *xpc-1(tm3886)* single mutant. However, the development of this double mutant worms is not similar to the *lin-52(n771)* single mutant after UV-B irradiation which also appears significantly different (p- value < 0.001, Fisher´s exact test, supplemental table 9).

In summary these data demonstrate that TC- and GG-NER deficient mutants reveal sensitivity to UV-B irradiation, leading to an arrest in larval development. This arrest can be partially reduced in a double- cross with the *lin-52(n771)* mutant. It is therefore possible that if one branch of the NER is diminished by a knock-out, the other branch can replace the disturbed function and that this could be enhanced in a DRM- complex mutant background. To test this hypothesis, knock-out models for genes such as *xpa-1*, which are working in the downstream common pathway of both NER sub-branches, can be used for further analysis.

4.7.3 Deficiency of the nucleotide excision repair in DRM- complex mutants leads to larval arrest after UV- B irradiation

To investigate the combined loss of the GG- and TC-NER in a DRM- complex mutant background, the *xpa-1(ok698)* mutant strain was used. This mutant strain is known in literature to be hypersensitive to small doses of UV- B irradiations (56). Thus, the wildtype strain may appear similar in the irradiated group than under standard conditions, because of the low irradiation doses used.

The *xpa-1(ok698)* mutant strain shows a larval development similar to wildtype under standard conditions in the developmental assay (Fig. 14a). UV-B irradiation with 5 mJ/cm^2 already leads to a strong developmental arrest in these mutants (Fig. 14b). More than 30% of the *xpa-1(ok698)* mutant worms arrest at the L1 stage, whereas the rest reaches the L2 stage. At 10 mJ/cm^2 of UV- B irradiations almost 80% of these mutant worms' arrest at the L1 stage (Fig. 14c). Surprisingly, an intercross of this mutant with the *lin-52(n771)* mutant strain reveals a similar developmental delay as in the *xpa-1(ok698)* single mutant after UV-B irradiation (Fig. 14b and 14c). The Fisher´s exact test as well as the two- tailed t- test showed no statistical difference (p- value > 0.05) between these two strains (supplemental

table 10). Similar results can be seen in a developmental assay with the *lin-52(n771); csb-1(ok2335); xpc-1(tm3886)* mutant strain compared to the *csb-1(ok2335); xpc-1(tm3886)* double mutant (supplemental figure 3).

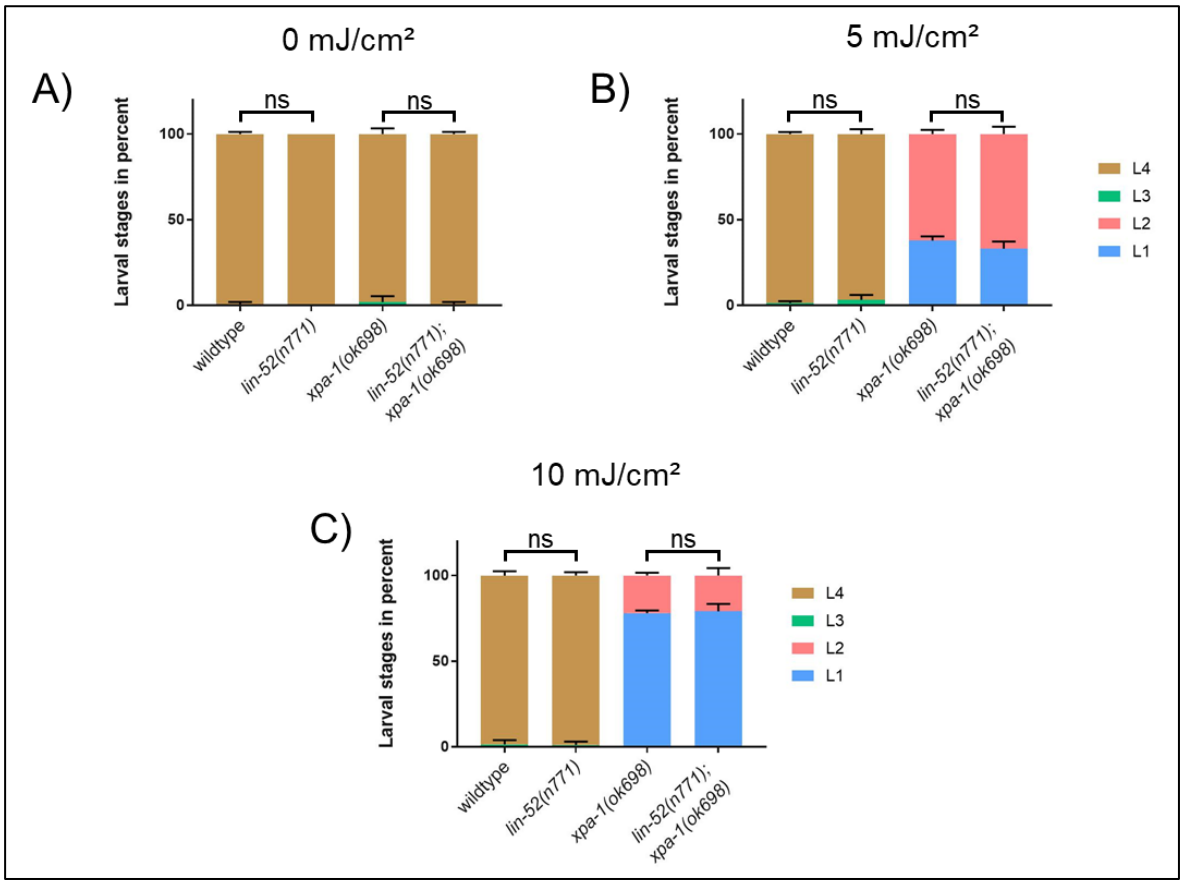

Figure 14. **Development of DRM- complex mutant worms after UV-B irradiation in NER deficient background.**

Developmental assay which shows the different larval stages in percent of mutant and wildtype worms. Starved L1 worms were irradiated with UV-B and fed for 48 hours under standard conditions before different larval stages were determined. 14a) Development of mutant worms and wildtype under standard conditions. 14b) and 14c) Mutant and wildtype worms were irradiated with 5 mJ/cm² or 10 mJ/cm² of UV-B. The *lin-52(n771); xpa-1(698)* mutant worms behaves similar as the *xpa-1(ok698)* single mutant worms. Experiment was performed in biological replicates and repeated three times. Error bars represent standard deviation. Asterisks indicate significance in the Fisher´s exact test, p> 0.05 =ns, p<0.05 = *, p<0.01 = **, p<0.001 = ***. Further statistical analysis can be found in supplemental table 10.

This finding indicates that an absence of one NER sub-branch in DRM- complex mutants leads to partial but not full rescue of the larval arrest. However, this rescue is abolished when *xpa-1* is diminished in *lin-52(n771)* mutant worms. Thus, this indicates that DRM-complex mutant worms require both, the TC- and GG-NER, to achieve DNA damage resistance leading to less delayed larval development. However, the exact regulation of the NER in DRM- complex mutants remains unclear. RNAseq analysis revealed upregulated transcript levels for *csa-1* in the *lin-52(n771)* mutants at six hours after UV-B irradiation of L1 worms, but further upregulated expressions of other typical genes involved in the NER could not be observed. Apart from regulation on the transcript level, differences in protein levels that could, for example, be due to altered translational control or altered protein stability are also possible. In order to test these hypothesis, *in-vitro* studies by western blot analysis or *in- vivo* studies by flow cytometry with fluorescent proteins are suited experimental procedures.

4.8 *In-vivo* and *in-vitro* analysis in DRM- complex mutants after UV-B irradiation

4.8.1 qRT-PCR analysis in *lin-52(n771)* mutant worms after UV-B irradiation

The RNAseq analysis exhibited the transcription levels of *lin-52(n771)* mutant worms compared to wildtype at six hours after 60 mJ/cm^2 of UV-B irradiation. In this analysis, upregulated transcript levels of *csa-1* in the mutant strain appeared minor. However, no further upregulation of other typical NER genes was apparent in this RNAseq data set. Thus, it is possible that if in *lin-52(n771)* mutant worms the NER is more effective than in wildtype, transcript levels of NER genes may appear upregulated at earlier time points. For this reason, transcript levels for such candidates were measured in L1 *lin-52(n771)* mutant worms at one and three hours after 60 mJ/cm^2 of UV-B irradiation and under standard conditions. The results were compared to wildtype.

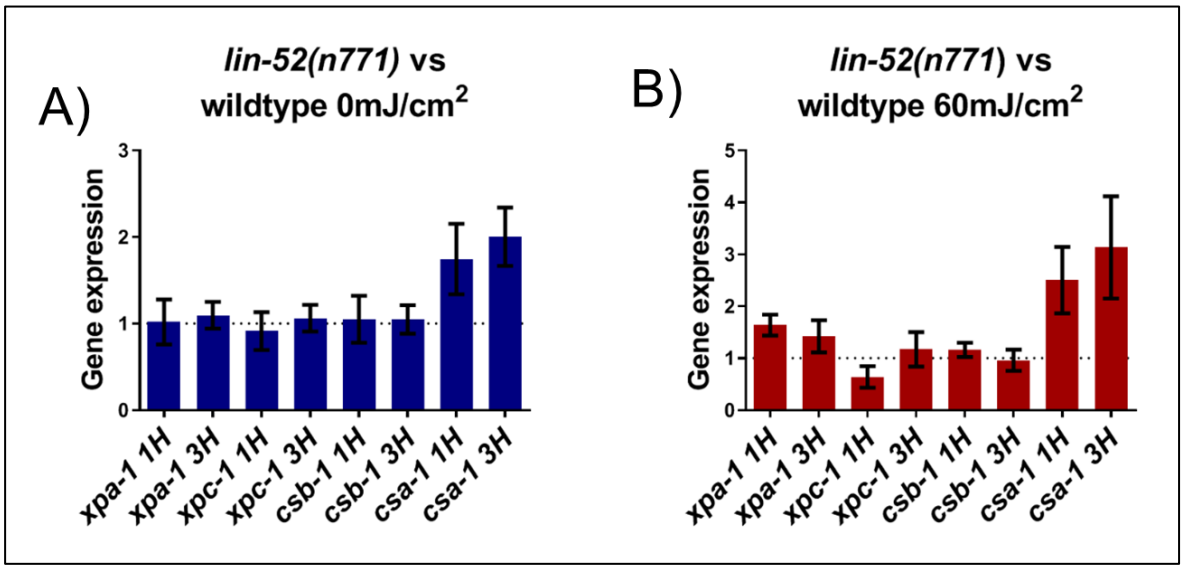

Figure 15. **qRT-PCR analysis in *lin-52(n771)* mutant worms after UV-B irradiation**

L1 worms were fed with OP50, treated with 60 mJ/cm² of UV-B irradiation and collected one or three hours after treatment. The unirradiated control was only fed with OP50 and maintained under standard conditions like the UV-B irradiated group until the timepoint was reached. *Lmn-1, vha-6* and *Y45F10D.4* were used as housekeeping genes. Error bars indicate standard deviation. Experiment was performed in biological replicates. 15a) Relative expression ratios of typical NER genes measured by qRT-PCR in *lin-52(n771)* mutant worms compared to wildtype under standard conditions. Upregulated transcript levels of *csa-1* can be seen in the *lin-52(n771)* mutant worms.15b) Relative expression ratios of typical NER genes measured by qRT-PCR in *lin-52(n771)* mutant worms compared to wildtype after 60 mJ/cm² of UV-B irradiation. Upregulated transcript levels of *csa-1* can be seen in the *lin-52(n771)* mutant worms.

Surprisingly, at both time points, the ratio of NER genes such as *xpa-1, csb-1* and *xpc-1* after UV-B irradiation or even at standard conditions are similar when compared to wildtype (Fig. 15a and 15b). The ratio of altered gene expression are in a range of 1 which indicates that there is no important impact on transcript regulation. Contrary to this, transcript levels of *csa-1* are higher in the *lin-52(n771)* mutant strain compared to wildtype after UV-B irradiation but also under standard conditions. Under standard conditions the ratios are in a range between 1.5 and 2.0 (Fig. 15a). The relative expression ratio even increases with 60 mJ/cm^2 of UV-B irradiation, with a ratio of 2.5 at the one-hour timepoint and 3.13 at the three- hour time point (Fig. 15b). These results are also consistent with the RNAseq analysis which confirmed upregulation with a fold change of 1.58 at six hours after UV-B irradiation.

The upregulation of *csa-1* is most likely not a consequence of UV-B irradiation but of the *lin-52(n771)* mutation because transcript levels of *csa-1* appear upregulated also under standard conditions in *lin-52(n771)* worms compared to wildtype. The experiments performed in this study show that the developmental delay of *csa-1(4539)* mutant worms can be partially rescued by an intercross with the *lin-52(n771)* mutant (Fig.12b and 12c). This indicates that even though *csa-1* expression appears upregulated at transcript levels in a DRM- complex mutant, the phenotype of DRM- complex mutants after UV-B irradiation cannot entirely be explained as a result of this.

In summary this qRT-PCR data demonstrates no apparent upregulation of NER genes, except *csa-1,* in *lin-52(n771)* mutant worms at early timepoints which is consistent with the RNAseq analysis. Even though altered transcript levels cannot explain the phenotype, other regulatory processes that affect the protein levels for components of the DNA repair machinery are still possible.

4.8.2 Enrichment of the GG-NER in TC-NER and DRM- complex mutant worms after UV-B irradiation

The experiments shown in figure 12 and 13 reveal that double mutants with mutations in the GG- or TC-NER and the DRM- complex exhibit a partial developmental rescue in comparison to single GG- or TC-NER deficient mutants. For this reason, I followed the hypothesis that an insufficiency of one NER sub-branch can be replaced by the other in DRM- complex mutant worms.

This hypothesis was further investigated by measuring transcript levels of NER gene products by qRT-PCR in the *lin-52(n771); csb-1(ok2335)* intercrossed mutant strain after UV-B irradiation. A matter of special importance in this experiment are the transcript levels of GG-NER genes in *lin-52(n771); csb-1(ok2335)* mutant worms compared to *lin-52(n771)* single mutant worms. Upregulated transcript levels of GG-NER genes in a *lin-52(n771); csb-1(ok2335)* when compared to a *csb-1(ok2335)* single mutant could explain the supporting role of the GG-NER in the double mutant. This experiment was carried out together with the preceding qRT-PCR approach.

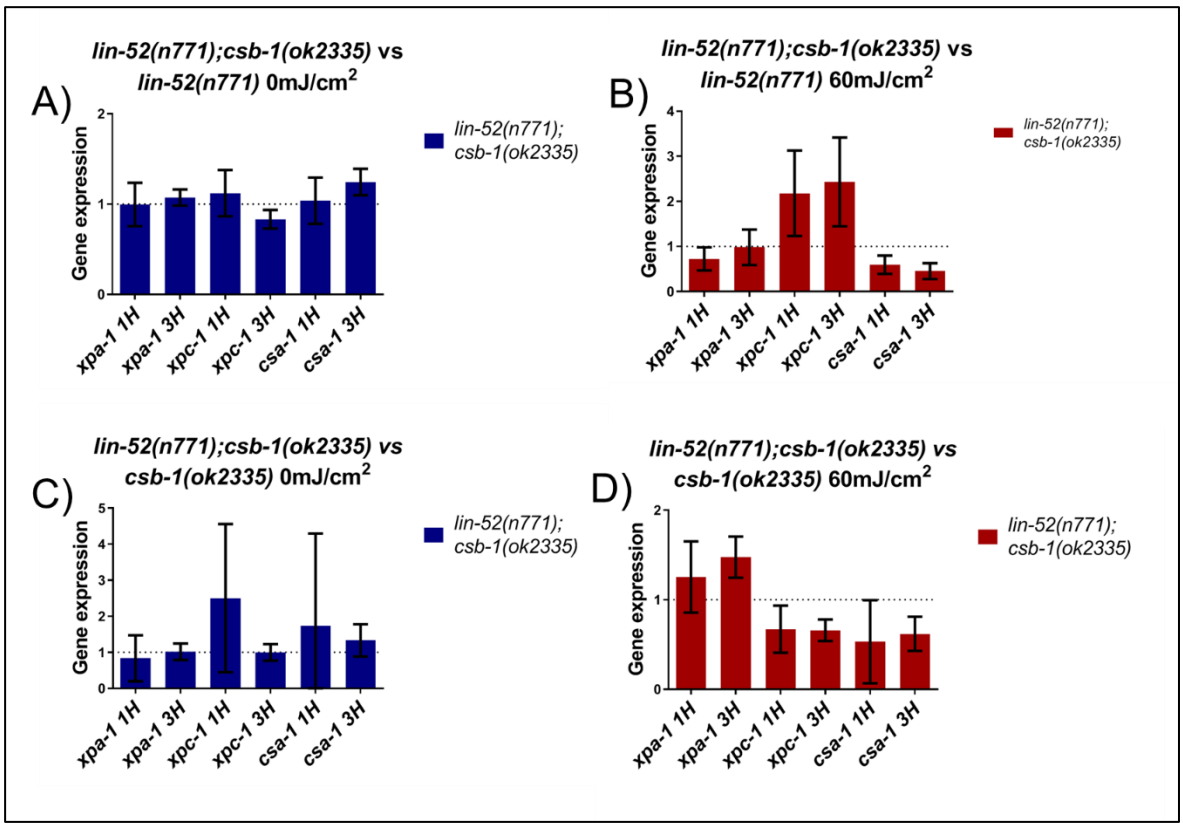

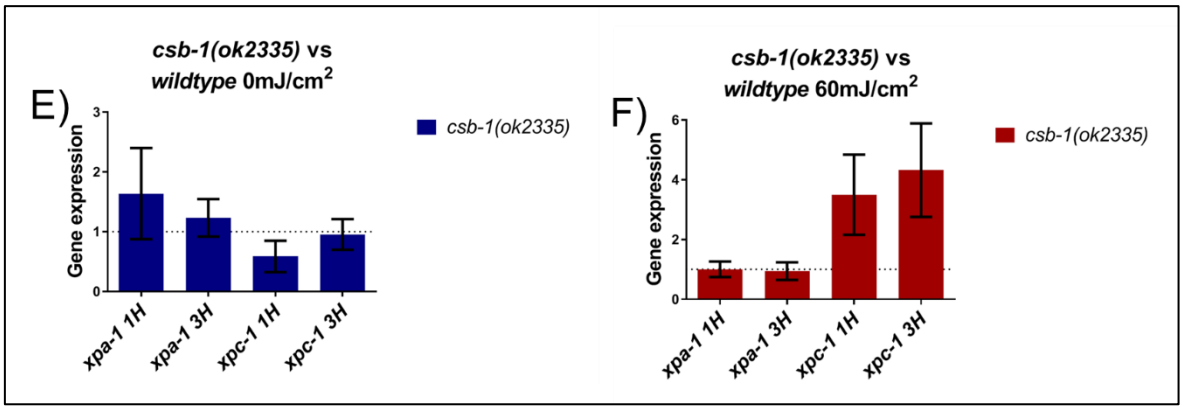

Figure 16. **qRT-PCR analysis in *csb-1(ok2335)* and *lin-52(n771)* mutant worms after UV-B irradiation**

L1 worms were fed with OP50, treated with 60 mJ/cm² of UV-B irradiation and collected one or three hours after treatment. The unirradiated control was only fed with OP50 and maintained under standard conditions like the UV-B irradiated group until the timepoint was reached. *Lmn-1, vha-6* and *Y45F10D.4* were used as housekeeping genes. Error bars indicate standard deviation. Experiment was performed in biological replicates. 16a) Relative expression ratios of typical NER genes measured by qRT-PCR in *lin-52(n771);csb-1(ok2335)* mutant worms compared to single *lin-52(n771)* mutant worms under standard conditions. 16b) Relative expression ratios of typical NER genes measured by qRT-PCR in *lin-52(n771);csb-1(ok2335)* mutant worms compared to single *lin-52(n771)* mutant worms after 60 mJ/cm² of UV-B irradiation. Upregulated transcript levels of *xpc-1* can be seen in the *lin-52(n771);csb-1(ok2335)* mutant worms. 16c) Relative expression ratios of typical NER genes measured by qRT-PCR in *lin-52(n771);csb-1(ok2335)* mutant worms compared to single *csb-1(ok2335)* mutant worms under standard conditions. 16d) Relative expression ratios of typical NER genes measured by qRT-PCR in *lin-52(n771);csb-1(ok2335)* mutant worms compared to single *csb-1(ok2335)* mutant worms after 60 mJ/cm² of UV-B irradiation. 16e) Relative expression ratios of *xpa-1* and *xpc-1* measured by qRT-PCR in *csb-1(ok2335)* mutant worms compared to wildtype under standard conditions. 16f) Relative expression ratios of *xpa-1* and *xpc-1* measured by qRT-PCR in *csb-1(ok2335)* mutant worms compared to wildtype after 60 mJ/cm² of UV-B irradiation.

Under standard conditions, the transcript levels for typical NER genes are similar between both mutant worms with a ratio around 1 (Fig. 16a). After UV-B irradiation the *csa-1* expression levels appear downregulated in this double mutant compared to the *lin-52(n771)* single mutant (Fig. 16b). Interestingly, *xpc-1* expression levels appear upregulated in *lin-52(n771); csb-1(ok2335)* intercrossed mutant worms compared to the *lin-52(n771)* single mutant with ratios of 2.17 at one hour and 2.43 at three hours after UV-B irradiation (Fig. 16b). This indicates that TC-NER and DRM- complex double mutant worms induce the GG-NER more strongly than DRM- complex single mutants after UV-B irradiation. At this point it is important to prove if this switch to the GG-NER is a result of the mutation in the DRM-complex or the TC-NER. Therefore *csb-1(ok2335)* single mutant worms were compared to the *lin-52(n771); csb-1(ok2335)* intercrossed mutant in the same experimental setup. Under standard conditions, the transcript levels for these genes in the *lin-52(n771); csb-1(ok2335)* intercrossed mutant worms are similar to *csb-1(ok2335)* single mutant worms with ratios around 1 (Fig. 16c). The *xpc-1* and *csa-1* transcript levels may appear upregulated at the one-hour time point but exhibit high standard deviation. Thus, a reliable conclusion can´t be

drawn. After UV-B irradiation the *xpa-1* transcript levels slightly increase whereas the *csa-1* expression levels may even be downregulated in the *lin-52(n771); csb-1(ok2335)* double mutant compared to *csb-1(ok2335)* single mutant worms (Fig. 16d). At one hour after UV-B irradiation the ratio of *csa-1* shows a high standard deviation (SD= +/- 0.46). Therefore, this result should be interpreted with care and possibly does not reflect a real downregulation of *csa-1* expression.

Surprisingly, after UV-B irradiation the *xpc-1* expression level appears even slightly downregulated in *lin-52(n771); csb-1(ok2335)* intercrossed worms when compared to *csb-1(ok2335)* single mutant worms with a ratio of around 0.65 at both timepoints (Fig 16d).

In addition, the *csb-1(ok2335)* single mutant was compared to wildtype in the same experimental setup. Gene expression of *xpa-1* appears elevated after one hour under standard conditions but also exhibits a higher level of variation. The transcript level of *xpc-1* after one hour appears slightly downregulated in mutant worms compared to wildtype (Fig. 16e). Interestingly, after UV-B irradiation, the gene expression of *xpc-1* appears upregulated in the *csb-1 (ok2335)* mutant strain compared to wildtype with ratios of 3.5 at one hour and 4.32 at three hours after treatment (Fig. 16f).

This finding indicates that the upregulation of the GG-NER after UV-B irradiation in *lin-52(n771); csb-1(ok2335)* mutant worms may not be a consequence of a deficiency in the DRM- complex but as a response to the absence of the TC-NER. Thus, qRT-PCR transcript levels cannot explain the partial developmental rescue in TC- or GG-NER and DRM-complex double mutant worms.

However, transcript levels may not fully explain the DRM- complex phenotype. Investigations at protein level could give more insights into regulatory processes in DRM-complex mutants.

4.8.3 *In-vivo* fluorescence analysis of the nucleotide excision repair in DRM-complex mutants

DRM- complex mutants exhibit a larval arrest after UV-B irradiation when the NER is abolished by knock-out of *xpa-1*. However, the qRT- PCR studies were insufficient to explain this phenotype by altered transcription (Fig. 15). For this purpose, *in-vivo* investigations with fluorescence marked proteins could give insights in the regulatory processes in DRM- complex mutants that are responsible for altered larval development. The transgenic strain *xpa-1(ok698); sbjIn27[pBS128(xpa-1::GFP) + pBS174(myo-2::tdTomato)]* is a *xpa-1(ok698)* knock-out mutant model with an inserted *xpa-1*-GFP

transgene. Thus, it is suitable for further *in-vivo* investigations. This transgenic strain is in the following named in the abbreviated form *xpa-1(ok698);* sbjIn27. To quantify the GFP levels *in-vivo* in *C. elegans*, the BioSorter by UnionBiometrica was used for detection and quantification of GFP. The amount of XPA-1:: GFP levels was detected under standard conditions at different larval stages. To avoid the possibility of falsely positive elevated GFP intensity levels caused by multiple integrated copies of the transgene during the crossing with the *lin-52(n771)* mutant, two independent double mutants were used in this experiment. In case of such multiple copies, the double mutants could reveal different results. To distinguish possible autofluorescence effects, wildtype worms were used as a control in this experiment. This is important for the experiment as a confirmation that the transgenic model is properly expressed and that GFP is functional.

Figure 17 shows density plots of XPA-1:: GFP intensities in these transgenic strains. As expected, the *xpa-1(ok698)*; sbjIn27 transgenic strain exhibited at different larval stages (L1, L3, L4, adult day 1) higher intensities than wildtype (Fig. 17). Surprisingly, at all four stages the measured intensity for GFP was higher in both *lin-52(n771); xpa-1(698); sbjIn27* transgene strains, compared to the single mutant *xpa-1(698); sbjIn27* transgene strain (Fig. 17). This difference is highly significant (p- value < 0.001) in the Tukey´s test (supplemental tables 11-14). This indicates that *lin-52(n771)* can enhance the levels of XPA-1 protein under standard conditions during all four larval stages. In order to compare the effect size between all four stages, the Cohen´s d was determined. This statistical analysis revealed robustly a medium ($d \geq 0.5$) or even large ($d \geq 0.8$) effect size between the intercrossed mutants and the single transgenic strain (supplemental tables 11-14). The Tukey´s test also revealed a significant difference between the two double mutants at larval stages L1, L3 and at adult day 1 (supplemental tables 11-14). This significance can be interpreted as the result of big sample size ($312 < n < 600$) confirmed by the Cohen´s d which reveals only a small ($d \geq 0.2$) effect size when comparing these transgene intercrossed strains.

In summary, this experiment revealed that *lin-52(n771); xpa-1(ok698); sbjIn27* transgenic intercrossed mutants showed higher fluorescence intensities that represent high XPA-1::GFP levels than in the single transgenic strain during development under standard conditions. This finding may indicate that DRM- complex mutants can upregulate the NER by increasing the protein levels of XPA-1 and possibly also the levels of other proteins involved in NER. This could happen by enhanced protein synthesis, but also reduced protein degradation.

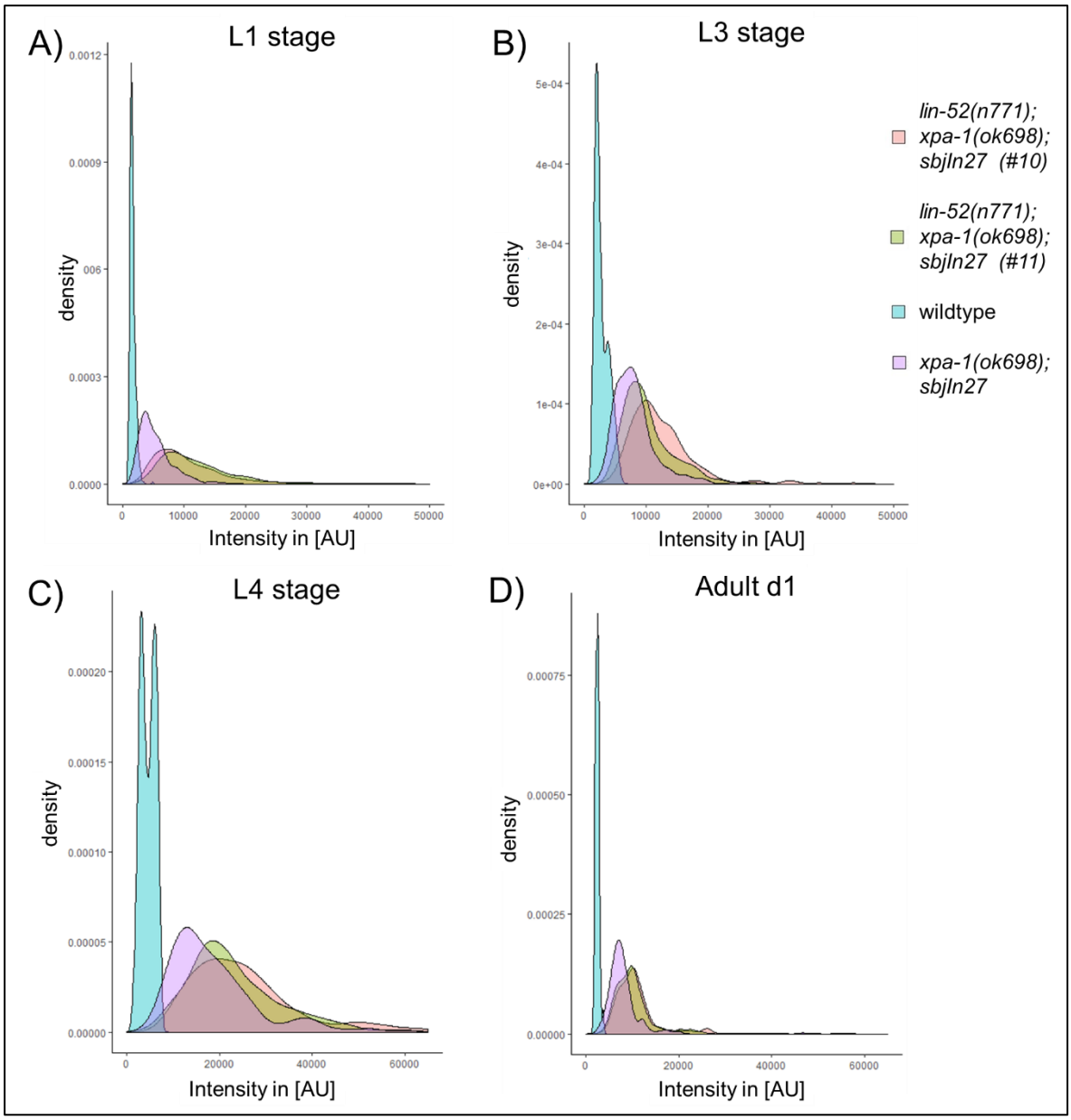

Figure 17. **Intensity of XPA-1::GFP levels in *xpa-1(ok698)* and DRM- complex mutant worms.**

Density blot showing the intensity of GFP levels, measured by Multi-Range Large Particle Flow Cytometer (BioSorter). Graphs were done with R studios using the ggplot packet. X- axis represents intensity of green peak height in AU. Y- axis represents the probability of density function for the kernel density estimation. Abbreviated forms of strain names are used in this figure: The *xpa-1(ok698); sbjIn27[pBS128(xpa-1::GFP) + pBS174(myo-2::tdTomato)]* transgene mutant strain was abbreviated as "*xpa-1(ok698); sbjIn27*". Numbers in brackets of the double mutant transgene strains indicate crossing number. GFP intensity was measured at different larval stages. 17a) L1 stage 17b) L3 stage 17c) L4 stage 17d) first day of adult stage. In all tested stages the intensity of GFP was higher in the intercrossed *lin-52(n771); xpa-1(ok698); sbjIn27* transgene mutant worms than in the *xpa-1(698); sbjIn27* single transgene mutant worms. Wildtype worms were used as control. Experiment was repeated three times. Statistical analysis can be found in supplemental tables 11-14.

4.8.4 Western blot analysis in DRM- complex mutants

At the time when the experiments with the transgenic strains were performed, the *xpa-1(syb788)[CR(xpa-1::V5+TEV+linker+Ypet)]* line was not yet available. This strain was generated by a CRISPR-Cas9 approach in order to label the XPA-1 protein with the fluorescent Ypet and a V5- tag. The advantage of this strain in comparison to the previous transgenic strain *xpa-1(ok698); sbjIn27* is the absence of extrachromosomal DNA that is inserted into the genome at a random position. However, *in-vivo* fluorescence analysis by using the BioSorter could not be repeated with this strain because this machine was not able to detect the Ypet fluorescence tracer. Thus, the characteristics of the V5-tag were used in order to measure the XPA-1 levels quantitatively by using a western blot approach. As described before, a XPA-1 antibody was yet not available for *C. elegans* during my experimental work for this thesis, but with the *xpa-1(syb788)[CR(xpa-1::V5+TEV+linker+Ypet)]* mutant strain the V5- tag could be detected with a V5 antibody. For this analysis the *xpa-1(syb788)[CR(xpa-1::V5+TEV+linker+Ypet)]* mutant strain was intercrossed with the *lin-52(n771)* strain. Measuring protein levels of XPA-1 in DRM-complex mutants by western blot analysis could confirm previous experiments *in-vivo* and give more insights in the protein regulation.

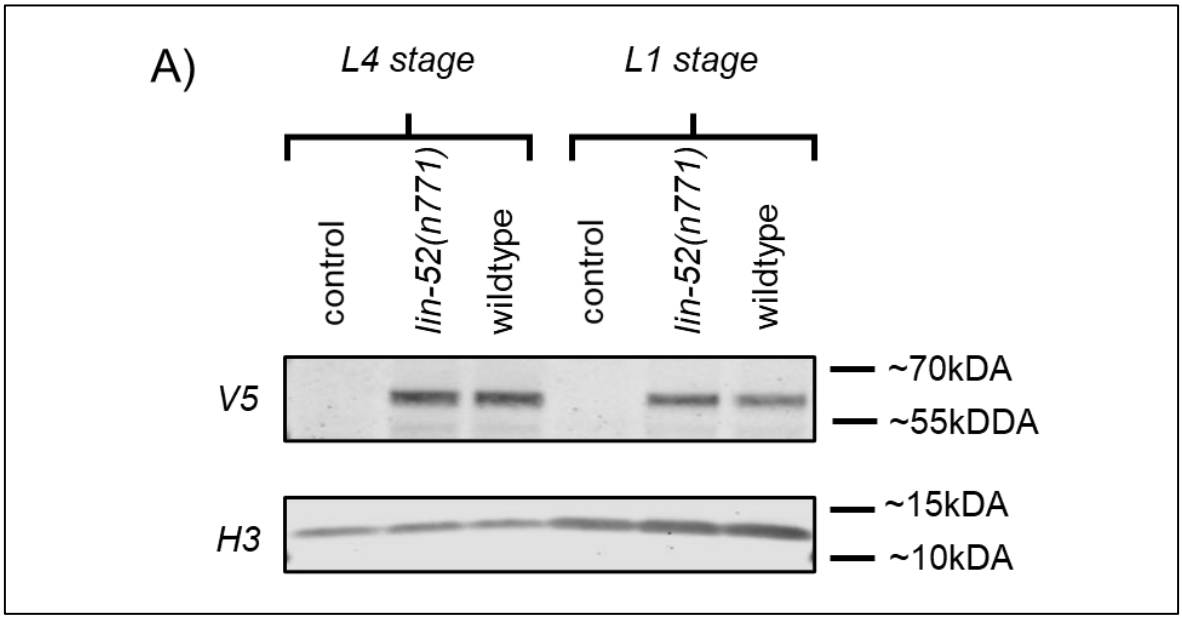

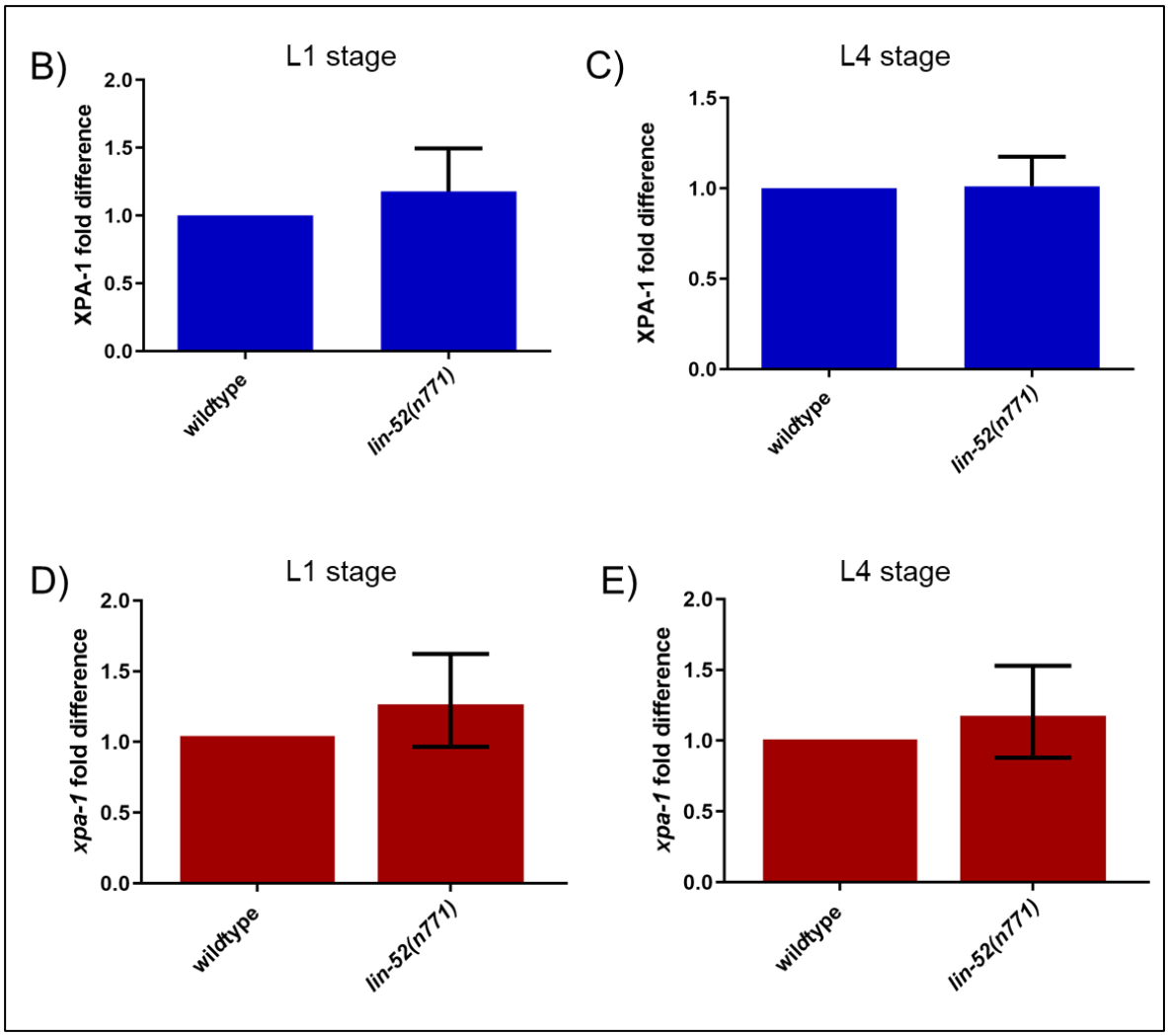

Figure 18. **Western blot and qRT-PCR analysis in *lin-52(n771)* mutant worms.**

18a) Western blot with the V5- tagged XPA-1 protein. H3 was used as a housekeeping protein. L1 and L4 worms were used in this experiment. Worms were maintained under standard conditions. Names are abbreviated: Wildtype worms were named “control”. The *xpa-1(syb788)[CR(xpa-1::V5+TEV+linker+Ypet)]* is named “wildtype”. “*Lin-52(n771)*” represents the intercross of *lin-52(n771)* with the *xpa-1(syb788)[CR(xpa-1::V5+TEV+linker+Ypet)]* mutant. 18b) and 18c) Quantification of the V5- tagged XPA-1 protein in the western blot in L1 and L4 worm stage. Abbreviated forms of strain names were used as explained before. The double mutant strain “*lin-52(n771)*” exhibits similar levels as “wildtype” in both tested larval stages. Graphs exhibit the mean of three independent western blot quantifications. Error bar indicates standard deviation. 18d) and 18e) mRNA transcript levels of *xpa-1* measured by qRT-PCR in wildtype and *lin-52(n771)* mutant worms at L1 and L4 stage. Worms were maintained under standard conditions. The *lin-52(n771)* mutant worms exhibit similar levels than wildtype in both tested larval stages. *Tbg-1, eif-3.c and Y45F10D.4* were used as housekeeping genes. Error bars indicate standard deviation. Experiment was performed in biological replicates.

Surprisingly, different levels of XPA-1 between this intercrossed mutant and the single mutant strain could not be detected at L1 and L4 stage (Fig. 18a, 18b and 18c). At the L1 stage the ratio of XPA-1 in *lin-52(n771); xpa-1(syb788)[CR(xpa-1::V5+TEV+linker+Ypet)]* mutant worms compared to *xpa-1(syb788)[CR(xpa-1::V5+TEV+linker+Ypet)]* worms is 1.17, at the L4 stage the ratio is 1.01. Therefore, I conclude that the double mutation does not have a different impact on XPA-1 protein levels when compared to the single mutant in this experiment. These results stand in contrast to the *in-vivo* investigations shown in figure 17. qRT-PCR analysis of L1 worms in the *lin-52(n771)* mutant already revealed similar levels of *xpa-1* than wildtype (Fig. 15). However, these transcript levels were measured in fed L1 worms. Therefore, transcript levels in starved L1 worms need to be tested to confirm previous results by western blot or *in-vivo* fluorescence analysis.

4.8.5 Quantification of *xpa-1* transcript levels using qRT- PCR in *lin-52(n771)* mutant worms

To confirm the data shown in figure 16 and 17 a qRT- PCR was performed in order to measure the expression levels of *xpa-1* in starved L1 worms, which corresponds to the condition at which the worms were used for the western blot analysis. Figure 18d and 18e show the quantification of the transcript levels of *xpa-1* in L1 and L4 worms in the *lin-52(n771)* mutant strain compared to wildtype. The *xpa-1* transcript levels were tested at the same developmental stages as used before for the western blot analysis, using qRT- PCR. At the L1 stage, the fold difference between the *lin-52(n771)* mutant strain and wildtype is 1.29 (Fig. 18d) and at the L4 stage 1.20 (Fig. 18e) which does not reflect a strong impact on the transcript regulation levels.

This result indicates that neither at transcript nor at protein level *xpa-1*/XPA-1 could be detected at increased amount in the *lin-52(n771)* mutant strain when compared to wildtype. It is possible that the NER in *lin-52(n771)* mutant worms is regulated differently beyond the detected transcript or protein levels. This could also explain elevated levels measured *in-vivo* and will be discussed later. Furthermore, knock-out of *xpa-1* in *lin-52(n771)* mutant worms results in similar development than that observed for *xpa-1* single mutants, when irradiated with UV-B. This indicates that the NER is of central importance in these mutants even though the exact regulative mechanism remains unclear.

4.9 Experiments with further DNA damage causing exposures in DRM-complex mutants

Previous experiments investigated the phenotype of DRM- complex mutants after UV-B irradiation. For further analysis it would also be interesting to know whether this new phenotype in DRM- mutants is limited to UV-B damage or if other types of DNA damage produce a similar outcome in the developmental assay. RNAseq analysis which were available for my studies revealed elevated transcript levels of gene products for different DNA damage repair pathways that are also activated by other forms of DNA damage than UV-B irradiation. Thus, it appears interesting to expand this study to other DNA repair mechanisms and damaging agents in order to test the potential impact of DRM- complex mutants on different responses to DNA repair. In the following experiments, DNA damage was applied to worms by using methyl methanesulphonate (MMS), UV- A irradiation in combination with trioxsalen treatment and ionizing radiation (IR).

4.9.1 UV-A irradiation and Trioxsalen treatment leads to developmental delay in mutants of the nucleotide excision repair and DRM- complex

Previous studies revealed a sensitivity for NER mutants to UV- A irradiation when worms were treated additionally with Trioxsalen (83). The combined treatment of UV-A and Trioxsalen induces interstrand cross links (ICL) as a special type of DNA damage (105). Thus, this treatment may be interesting to investigate DRM- complex mutants, in order to expand previous investigations with this phenotype upon UV-B damage. For this purpose, the experiment was established as a developmental assay similar to previous experiments, using the *xpa-1(ok698)* and the *lin-52(n771)* mutant strain (Fig. 14a, 14b and 14c). Treating worms only with Trioxsalen but not with UV-A irradiation lead to normal development of worms, similar to standard conditions (Fig. 19a). UV-A irradiation of worms without Trioxsalen treatment also resulted in normal development (data not shown). Only the combination of Trioxsalen with UV-A irradiation leads to developmental delay in worms. This delay is much weaker than in previous experiments with UV-B irradiation. Wildtype worms revealed a small reduction of L4 stage worms after 4 minutes of UV-A irradiation in combination with Trioxsalen treatment (Fig. 19b). This delay increased slightly with 6 minutes of UV-A irradiation (Fig. 19c). Surprisingly, the *lin-52(n771)* mutant worms reveal a faster development than wildtype under irradiating conditions (Fig. 19b and 19c). This difference is also significant in the Fisher´s exact test (p- value < 0.05). The *xpa-1(ok698)*

single mutant worms show a stronger developmental delay than wildtype under irradiating conditions, as expected and described before in literature (83). These mutants are not able to reach the L4 stage, whereas wildtype worms can reach this stage at a high percentage. After 4 minutes of UV-A irradiation, these mutants still exhibit a high percentage of worms that remain at L3 stage. The percentage of worms at this larval stage is reduced after 6 minutes of UV-A irradiation, with higher percentages remaining in the L1 and L2 stage. Surprisingly, the *lin-52(n771); xpa-1(ok698)* intercrossed mutant worms behave similar as the *xpa-1(ok698)* single mutant under irradiating conditions (Fig. 19b and 19c). The two-tailed t-test reveals no significantly difference (p- value > 0.05) after UV-A irradiation between all larval stages of these mutant strains (supplemental table 15).

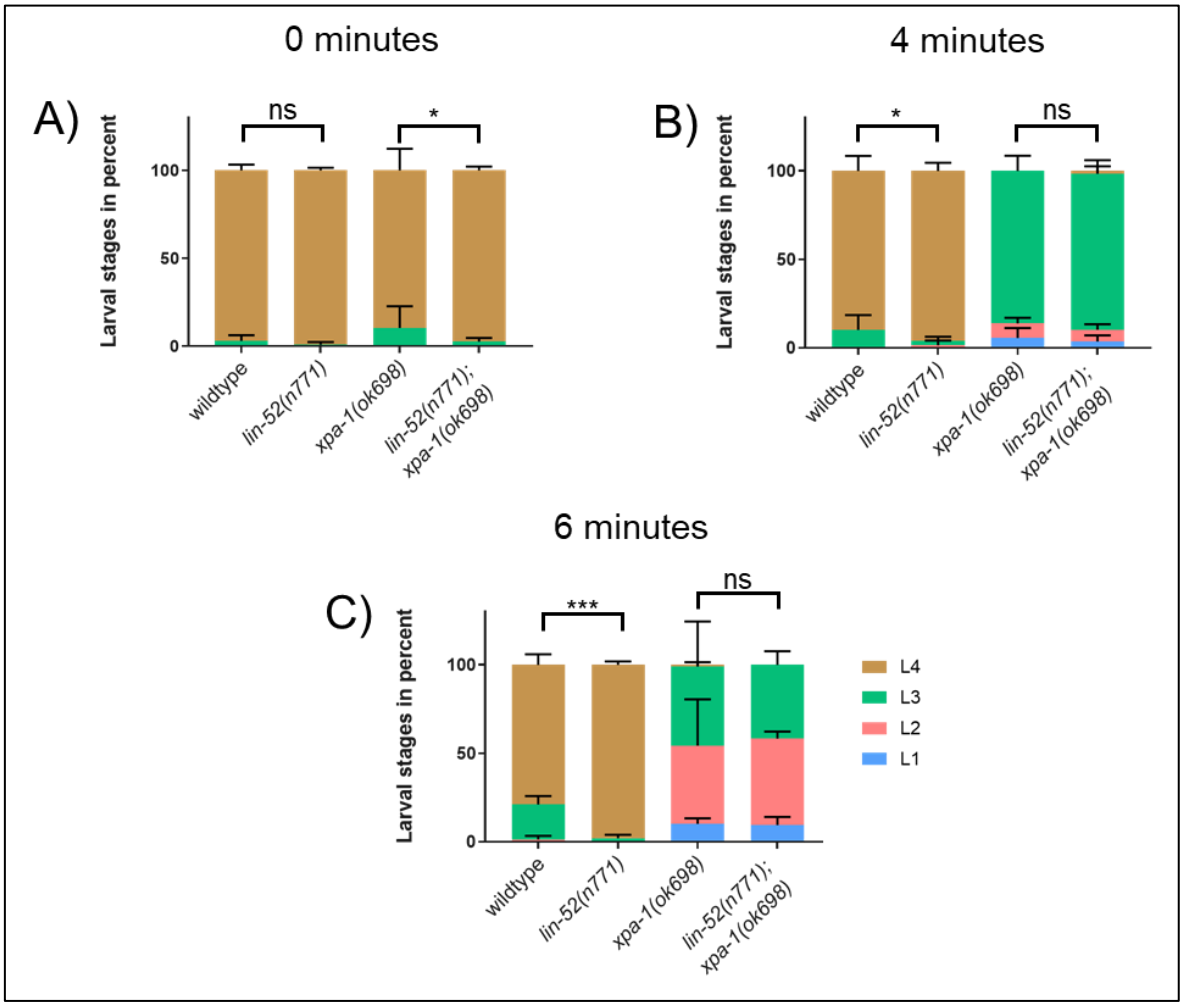

Figure 19. **Trioxsalen and UV-A treatment in DRM- complex and *xpa-1(ok698)* mutant strains.**

19a), 19b) and 19c) Developmental assay, showing worm stages in percent of different mutants and wildtype worms. L1 worms were treated with Trioxsalen and different time length of UV-A irradiation. The *lin-52(n771)* mutant worms show a faster development than wildtype after treatment. Error bars indicate standard deviation. Experiment was performed in biological replicates. Asterisks indicate significance in the Fisher´s exact test. p> 0.05 =ns, p<0.05 = *, p<0.01 = **, p<0.001 = ***. Further statistical analysis can be found in supplemental table 15.

This indicates that the *lin-52(n771)* mutant strain and possibly also other DRM- complex mutants reveal a decreased developmental delay after UV-A and Trioxsalen treatment compared to wildtype. Therefore, the DRM- complex mutants' phenotype is not limited to UV-B but becomes apparent also after UV-A and Trioxsalen exposure. Furthermore, the *lin-52(n771); xpa-1(ok698)* intercrossed mutant is not able to rescue the phenotype of the *xpa-1(ok698)* mutant strain after combined UV-A irradiation and Trioxsalen treatment. This confirms the role of the NER as the central DNA repair mechanism in DRM- complex mutants after UV-A irradiation and Trioxsalen treatment.

4.9.2 DRM- complex mutants show resistance to methyl- methanesulphonate treatment

It is known that the drug methyl- methanesulphonate (MMS) can block DNA synthesis by inducing alkylating lesions (106). In *C. elegans*, treatment of embryos with this drug leads to developmental delay (107). Furthermore, a loss of *polh-1*, which is involved in the repair of different types of DNA damage (108), results in a hypersensitive behavior to this drug (107,109). The RNAseq analysis also revealed upregulated transcript levels of *polh-1* in *lin-52(n771)* mutant worms. For this reason and to expand investigations with DRM- complex mutants, the *lin-52(n771)* mutant strain was crossed with the *polh-1(lf31)* (109). To compare results with previous data obtained after UV-B and UV-A + Trioxsalen exposure, this experiment was performed as a classical developmental assay. Instead of UV-B irradiation, L1 worms were exposed to different amounts of MMS for one hour.

All mutants showed a similar development as wildtype under standard conditions without MMS treatment (Fig. 20a). With increasing amounts of MMS, wildtype worms show reduced percentages of worms at L4 stage, with rising percentages of worms at L3 stage and lower stages (Fig. 20b, 20c, 20d). The *lin-52(n771)* mutant worms exhibited less developmental delay than wildtype for each dose of MMS exposure treatment. This difference was also significant (p- value < 0.05, Fisher´s exact test).

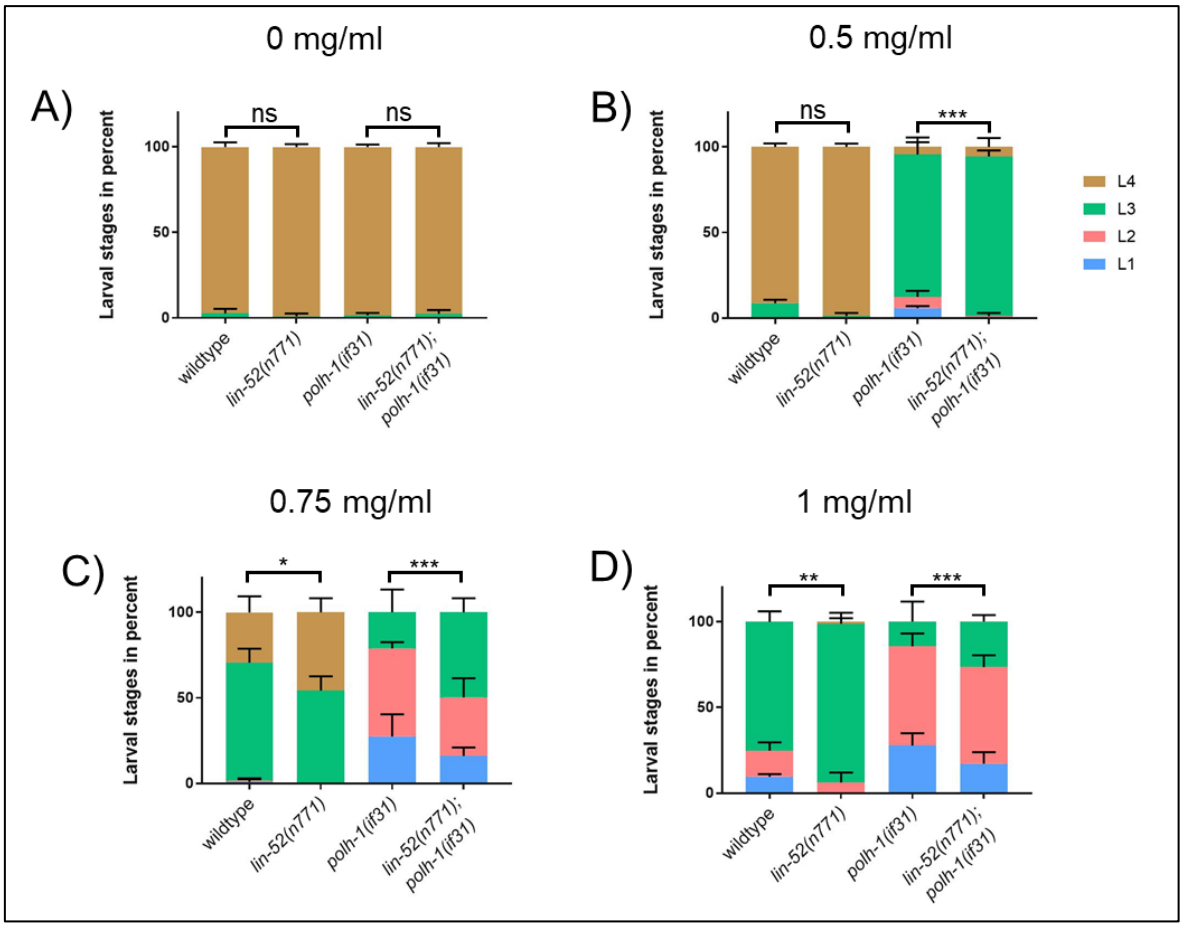

Figure 20. **MMS treatment of DRM- complex and *polh-1(if31)* mutant strains.**

20a), 20b), 20c) and 20d) Developmental assay, showing worm stages in percent of different mutants and wildtype. L1 worms were treated with different amounts of MMS for one hour. The *lin-52(n771)* mutant worms show faster development than wildtype after MMS treatment. The phenotype of *polh-1(if31)* mutant worms can be partial rescued by an intercross with the *lin-52(n771)* mutant strain. Experiment was performed in biological replicates. Error bars indicate standard deviation. Asterisks indicate significance in the Fisher´s exact test. p> 0.05 =ns, p<0.05 = *, p<0.01 = **, p<0.001 = ***. Further statistical analysis can be found in supplemental table 16.

At a dose of 0.5 mg/ml of MMS the *polh-1(if31)* mutant strain is almost unable to reach the L4 stage (Fig 20b). With higher doses of MMS, the number of worms at L3 stage also decreased in this mutants, and lower larval stages gain percentual higher numbers (Fig. 20c and 20d). Surprisingly, the *lin-52(n771); polh-1(if31)* intercrossed mutant shows a faster development under MMS treated conditions than the *polh-1(if31)* single mutant. The difference is also significant in the Fisher´s exact test (p- value < 0.001) for each treated group. However, the double mutant shows only a partial rescue in the developmental delay of *polh-1(if31)* mutant worms. The development in the *lin-52(n771); polh-1(if31)* mutant is more delayed than in wildtype or even the *lin-52(n771)* single mutant (Fig. 20b, 20c, 20d).

This result indicates that DRM- complex mutants exhibit a faster development after MMS treatment than wildtype. Thereby the phenotype of DRM- complex mutants is not only

limited to UV-B or UV-A irradiation and Trioxsalen treatment but can also be observed after chemically induced alkylating lesions. Furthermore, the *lin-52(n771); polh-1(if31)* intercrossed mutant showed a partial rescue of the *polh-1(if31)* single mutant phenotype after MMS treatment. Unpublished data by Arturo Bujarrabal revealed that UV- B irradiation of *lin-52(n771); polh-1(if31)* double mutants also show a partial developmental rescue compared to *polh-1(if31)* single mutant worms. Taken together, this indicates that DRM-complex mutants have a possible impact on the phenotype of *polh-1* mutant worms not only after UV-B irradiation but also after MMS treatment.

4.9.3 DRM- complex mutants can rescue the phenotype of *brc-1* deficient mutants after ionizing radiation

The human BRCA1 gene product functions in DNA double-strand break repair through homologous recombination (HR) and is a well-known risk gene for ovarian and breast cancer in women when mutated (110). Previous work showed that LIN9 appears elevated in triple- negative breast cancer cells (41) and that this overexpression is related to poor clinical outcome (42). In *C. elegans*, an ortholog to the human BRCA1 exists (111). Thus, it appeared interesting to investigate the effect of *brc-1* deficiency in DRM- complex mutants in *C. elegans*. For this experiment the *brc-1(tm1145)* mutant strain was used, which carries a deletion of 71 amino- acid C-terminal to the predicted RING domain (112). This is a common locus for mutations in BRCA1 deficient breast cancer (113). In addition, this mutant strain carries also the *brd-1(dw1)* deletion allele (80) which needs to be taken into account for interpretation of results.

For this experiment, the different activity of HR in *C. elegans* had to be considered, and therefore, the established developmental assay had to be adapted. DNA repair by HR is known to be active especially in dividing germ cells and not in somatic tissue (114). Within the first eight hours after an egg has been laid, the worm embryo exhibits rapid cell division. Thus, this time point appeared ideal to investigate DNA double-strand break repair by the HR in *C. elegans*. Therefore, early laid worm eggs were treated with ionizing radiation (IR) to induce DNA double-strand breaks. Hatched L1 worms were counted 24 hours after irradiation and were compared to the number of unhatched eggs.

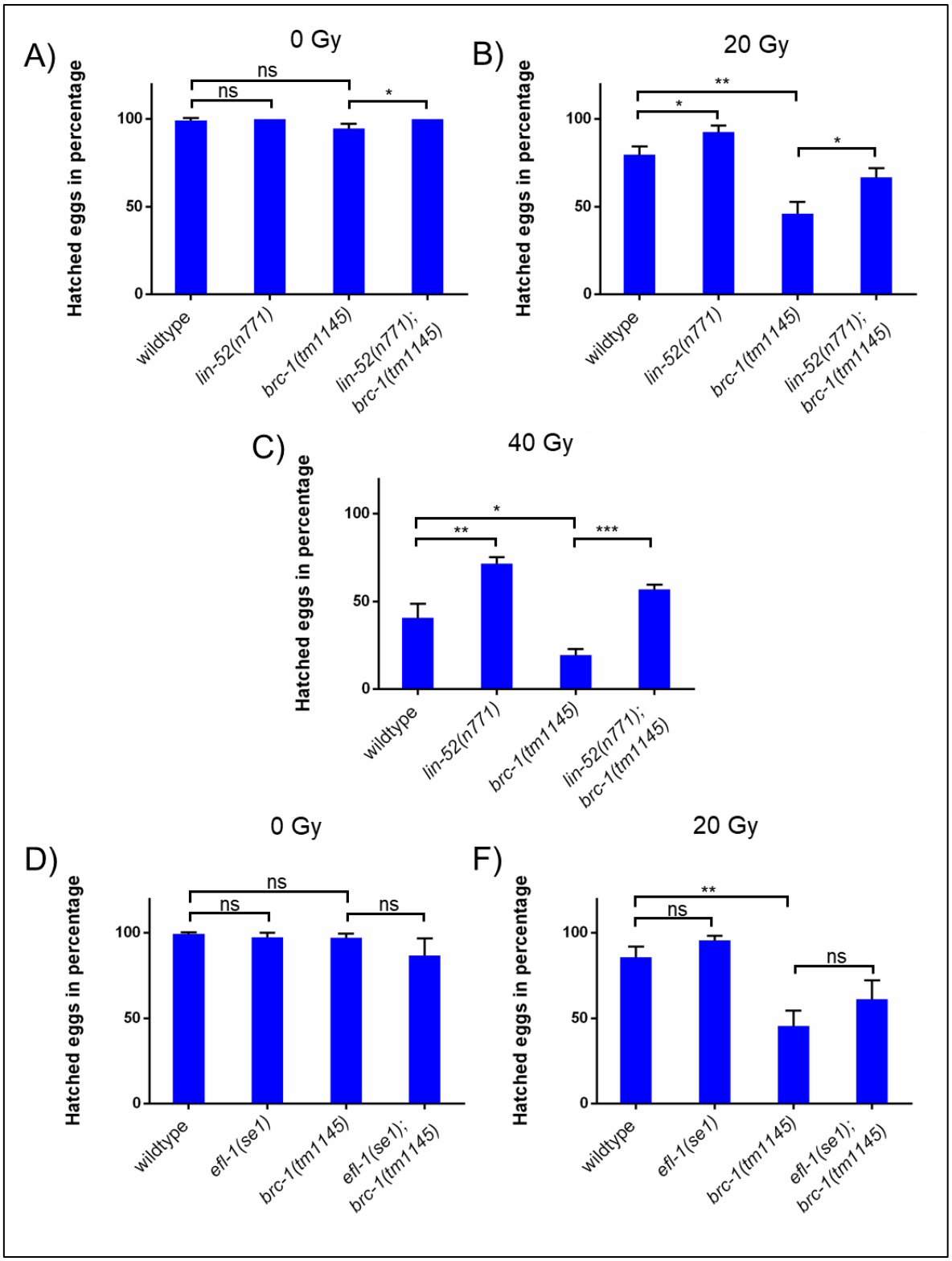
A)
0 Gy
Hatched eggs in percentage
ns
ns
*
100
50
0
wildtype
lin-52(n771)
brc-1(tm1145)
lin-52(n771); brc-1(tm1145)
B)
20 Gy
Hatched eggs in percentage
**
*
*
100
50
0
wildtype
lin-52(n771)
brc-1(tm1145)
lin-52(n771); brc-1(tm1145)
C)
40 Gy
Hatched eggs in percentage
*
**
***
100
50
0
wildtype
lin-52(n771)
brc-1(tm1145)
lin-52(n771); brc-1(tm1145)
D)
0 Gy
Hatched eggs in percentage
ns
ns
ns
100
50
0
wildtype
efl-1(se1)
brc-1(tm1145)
efl-1(se1); brc-1(tm1145)
F)
20 Gy
Hatched eggs in percentage
**
ns
ns
100
50
0
wildtype
efl-1(se1)
brc-1(tm1145)
efl-1(se1); brc-1(tm1145)

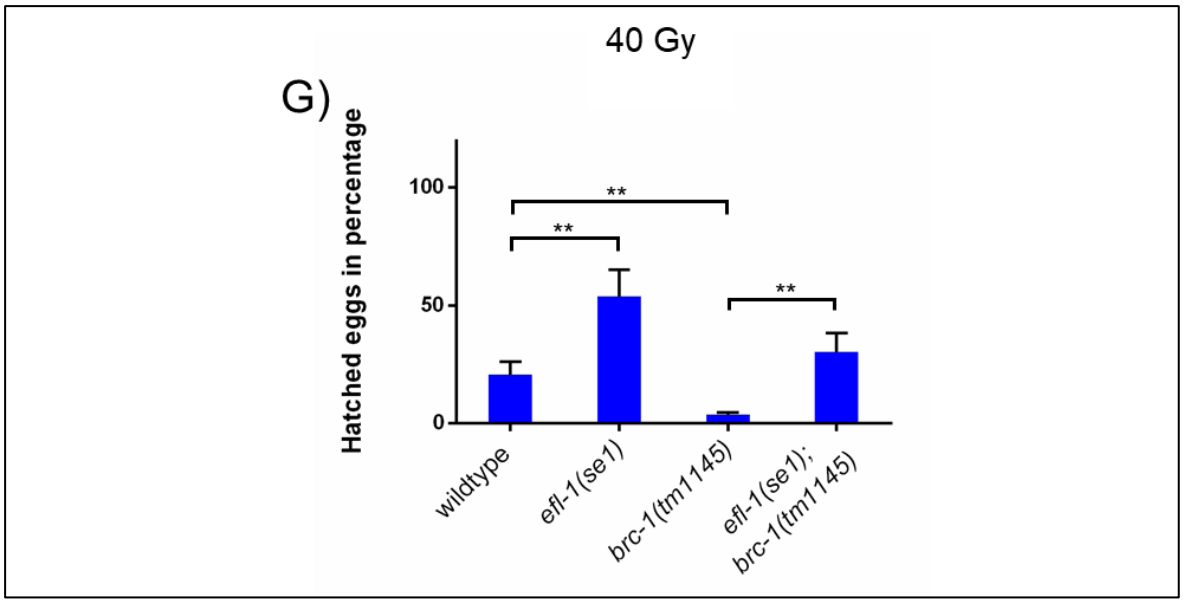

Figure 21. **Ionizing radiation of eggs in *brc-1* deficient and DRM- complex mutant background**

Percentage of hatched eggs in wildtype and different mutant strains after ionization radiation (IR) of eggs with 20 or 40 Gy. 21b), 21c), 21e), 21 f) *Lin-52(n771)* and *efl-1(se1)* mutant worms exhibit higher percentages of hatched eggs after IR than wildtype. The brc-1(tm1145) mutant worms can be partial rescued by an intercross with DRM- complex mutant strains. Error bars indicate standard deviation. Experiment was performed in biological replicates. Asterisks indicate significance in the unpaired two- tailed t- test. p> 0.05 =ns, p<0.05 = *, p<0.01 = **, p<0.001 = ***.

Under standard conditions, all strains exhibited a similar outcome as wildtype (Fig. 21a). After IR at a dose of 20 Gray (Gy), wildtype shows a reduced percentage of hatched L1 worms (Fig. 21b). This percentage decreased when a dose of 40 Gy of irradiation was given to the eggs (Fig. 21c). Surprisingly, the *lin-52(n771)* mutant exhibits higher percentages of hatched worms after IR than wildtype (Fig. 21b and 21c). This difference is also significant (p- value < 0.05) in a two- tailed t- test.

As expected, the *brc-1(tm1145)* single mutant appeared hypersensitive after IR treatment. The percentage of hatched worms is significantly (p- value < 0.05) lower than wildtype (Fig. 21b and 21c). Intercrossing this mutant strain with the *lin-52(n771)* mutant worms leads to a partial rescue of the single mutant. This double mutant shows a higher percentage of hatched worms than the *brc-1(tm1145)* single mutant after IR. This difference is also significant (p- value < 0.05, two- tailed t- test). At a dose of 40 Gy, the *lin-52(n771); brc-1(tm1145)* mutant even exhibits higher percentages of hatched worms than wildtype (Fig. 21c). However, a full rescue of the *brc-1(tm1145)* single mutant up to the DRM- complex mutant phenotype could not be observed in the intercrossed *lin-52(n771); brc-1(tm1145)* mutant strain. This indicates that DRM- complex mutants can rescue the hypersensitive phenotype of *brc-1(tm1145)* mutant worms which could be due to additional DNA repair mechanisms beyond HR. This experiment was also repeated with the *efl-1(se1)* and *efl-*

1(se1); brc-1(tm1145) mutant strains and shows consistency with the previous results (Fig. 21d, 21f and 21g). Therefore, it can be concluded that DRM- complex mutants are more resistant to IR than wildtype. This observation expands again the knowledge of DRM-complex mutants´ phenotype after UV-B irradiation towards IR resistance. These results are also important for clinical cancer research and the development of new tumor therapies.

In summary, these results indicate that DRM- complex mutants show resistance to DNA damage beyond UV-B irradiation using UV-A and Trioxsalen, IR or MMS treatment. They support the hypothesis that the apparently more efficient DNA repair in DRM- complex mutants is not only limited to the NER, but also affects other DNA repair mechanisms such as the HR.

4.10 Establishment of a Lin52 knock-out model in mouse embryonic stem cells

The experiments with *C. elegans* showed that DRM- complex mutants can repair DNA damage faster than wildtype resulting in a faster development. This phenotype was discovered first after UV-B irradiation but can be also seen after IR, MMS or UV-A irradiation and Trioxsalen treatment. At this point it may be interesting to investigate these results in other experimental organisms and models, such as mouse embryonic stem cells (mESC), which also have the capacity to differentiate. This would expand the present study and could give further insights by reaching closer to human cell biology. To test whether improved response to DNA damage also occurs in mouse cells with a loss of function of the DREAM-complex, mESC could be differentiated to e.g. neuronal stem cells. The time course or qualitive parameters of differentiation during neuronal differentiation could then be compared to wildtype mESC. UV-C irradiation or IR could be applied to mESC for DNA damage. This would give more insights in the function of the DREAM- complex in another organism.

To create a possible DREAM- complex knock-out model in mouse stem cells, I used CRISPR- Cas9 approach in mESC. This was intended to produce a 4350 base pair deletion in Lin52 affecting exon 2,3 and 4. Unfortunately, it was not possible to obtain this deletion for both alleles, but only as a heterozygote. This could mean and most likely indicates that this deletion is not viable for mESC. Further experiments with this heterozygote cell line were not followed up because these cells exhibited similar transcript levels of Lin52 compared to wildtype when tested by qRT-PCR analysis (data not shown).

5. Discussion

5.1 Summary of experiments

In this study, a new phenotype of DRM- complex mutant worms has been investigated. My results indicate that *C. elegans* mutant worms with defects in genes for components of the DRM-complex exhibit decreased larval arrest than wildtype after different DNA damage exposures such as UV-B irradiation, MMS and UV-A irradiation in combination with Trioxsalen treatment. Furthermore, treatment of DRM- complex mutant worms with ionizing radiation (IR) have also led to reduced embryonic lethality compared to wildtype. This improved larval development in DRM- complex mutants is not a consequence of disturbed cell cycle regulation but rather of a more efficient or faster DNA repair. This is based on the observation that DRM- complex mutant worms do not exhibit a faster cell division up to 24 hours after UV-B treatment compared to wildtype (Fig. 8). Furthermore, the accelerated development in DRM- complex mutant worms after DNA damage is abolished when XPA-1, a central mediator of the nucleotide excision repair (NER), is depleted in these worms (Fig. 14). Multiple genes involved in different repair mechanisms appear upregulated at transcript levels in DRM- complex mutants (92). Therefore, mutant *C. elegans* models with defects in different types of DNA repair mechanisms were tested in a developmental assay by intercrossing. This procedure was used in order to test the impact of DRM- complex mutant worms in different DNA repair mechanisms and to investigate the corresponding phenotype. Surprisingly, intercrossing DRM- complex mutants with these mutant models could partially rescue the developmental delay caused by inefficient DNA repair. As an exemplary model, the NER was further investigated in this assay because it is the main repair mechanism for UV-B irradiation dependent DNA damage. Interestingly, the TC- and GG-NER seem to be involved in the faster larval development of DRM- complex mutants. A knock-out of one NER sub-branch is associated with a partial developmental rescue after intercrossing with DRM- complex mutant worms (Fig. 12, 13). Furthermore, when the NER is completely abolished by a *xpa-1* knock-out model, DRM- complex mutants cannot rescue this larval delay anymore. This indicates that the NER plays a central role in DRM- complex mutants' developmental phenotype upon UV damage. Gene expression at transcript levels exhibited only upregulated levels of *csa-1* expression (Fig. 15), confirming previous RNAseq datasets from *lin-52(n771)* mutant worms. *In-vivo* measurement of GFP- tagged XPA-1 protein expression revealed indeed enhanced levels of this protein at different larval stages in DRM- complex mutants. However, this could not be confirmed by *in-vitro* western blot analyses. Attempts to expand these experiments to mouse embryonic stem cells were not successful, probably because cells with disruption of DREAM- complex functions via

homozygous Lin52 knock-out mutation using a CRISPR- Cas 9 approach were not viable. In addition, this negative result also argues for an important role of a functional DREAM-complex in cells from higher organisms.

A central focus of this thesis was to investigate the role of the DRM- complex in DNA repair in *C. elegans*. Indeed, DRM- complex mutant worms exhibit a faster or more efficient DNA repair after DNA damage exposure. This phenotype was not only investigated using an assay for larval development but also studied by analyzing differences in survival and health span (92). Analysis of gene expression in DRM- complex mutants revealed several upregulated transcripts that are known for their involvement in different types of DNA repair mechanisms (64,92). Furthermore, the results of this study show that many of these elevated DDR gene products are usually expressed exclusively in the germline in *C. elegans* (92). This is in agreement with and expands existing knowledge about the function of the DRM- complex in *C. elegans* as repressor of germline genes (66,67).

One DNA repair sub-pathway that is also known to be more relevant in germline cells is the GG-NER (54). In the experimental work of this thesis DRM- complex mutants do not only improve the GG-NER but also TC-NER response after UV irradiation. Surprisingly, the TC-NER is known to be more active in non- dividing somatic cells in *C.* elegans (54). Thus, this may expand the known function of DRM- complex as a repressor of germline genes towards a regulator for DNA repair genes in somatic tissues after UV- damage.

However, investigations of the mechanisms by which the DRM- complex in *C. elegans* regulates gene expression of components of the NER remained elusive. In mammalian cells the DREAM- complex is known to control gene expression of XPC, a component of the NER, via E2F mediated repression at the promoter region (39,40). Furthermore, target gene repression by DREAM- complex is mediated via cell cycle dependent elements (CDEs) and cell cycle gene homology regions (CHRs) (32,71,115). Similar repression mechanisms in *C. elegans* have not be investigated in detail so far. Interestingly, it has been shown that most of the DDR genes in *C. elegans* indeed exhibit an enrichment of CDE-CHR binding motifs (92). Previous studies have shown that the DRM- complex in *C. elegans* causes an enrichment of H2A.Z binding at gene bodies for target genes repression (74). Also, H3K4me3 modification may be especially relevant for mechanisms by which the DRM-complex regulates gene transcription activity (72). It is currently not fully resolved how this enrichment of CDE-CHR binding motifs and histone modifications are connected. Further investigation of this chromatin modification and binding motifs could give more insights into the regulative manner of DRM- complex in *C. elegans.*

5.2 Different DRM- complex mutants result in distinct phenotypes after UV-B irradiation

DRM- complex mutants exhibit faster larval development after UV-B exposure compared to wildtype. Interestingly, each mutant reveals an individual degree of faster larval development after UV-B exposure. However, this larval development was consistently faster in all mutant worms of the DRM- complex compared to wildtype (Fig. 5). The *lin-9(n112)*, *lin-35(n745)* and *lin-37(n758)* mutant worms exhibited a delay in growth when compared to wildtype or other DRM- complex mutant strains under standard conditions (Fig. 5a). Surprisingly, after UV-B irradiation these mutant worms reveal faster larval development than wildtype worms (Fig. 5b and 5c). However, this faster larval development after DNA damage exposure was less pronounced than e.g. in *lin-52(n771)* mutant worms. This observation suggests that different components of the DRM- complex exhibit other regulatory cellular functions beyond those of the classical DRM- complex. A previous study showed that some DRM- complex mutants exhibit L1 larval arrest at high temperature (26°C) (67). The sensitive period for this larval arrest was suggested to be in embryogenesis and L1 stage, as adult worms revealed normal progeny when downshifted from 26°C to 20°C (67). In contrast to this, upshifting from 20°C to 26°C in L1 mutant worms resulted in distinct alterations of larval arrest (67). In fact, the mutants which exhibit lower rescue levels in the developmental assay in my experiments also show larval arrest in the previous study at increased levels at high temperature. Thus, the arrest at high temperature could also correlate with alterations in larval development in these distinct strains. However, this previous study did not use 20°C as a reference standard condition but 24°C which already induced mild temperature stress. Unfortunately, this study misses a detailed determination of the different larval stages. Only the number of arrested L1 stage worms was counted at 24°C and 26°C. Even though less L1 larval arrest was detected at 24°C it is still possible that larval development is altered at higher larval stages. Differences in larval development with a delay especially at the L3 stage was found in DRM- complex mutant worms in the work for my thesis (Fig. 5a). Indeed, parallels between the analyzed DRM- complex mutant strains and the high temperature arrested mutant strains in the previous study are apparent.

Interestingly, in the same paper the levels of ectopic misexpression of “p- granule proteins”, gene products which usually are exclusively found in germline cells, were found to be elevated in somatic cells in different DRM- complex mutant worms. The high temperature larval arrest does also correlate positively with the upregulated germline related genes in the somatic tissue (67,72). Elevated somatic expression of these “p-granule proteins” was already detected at high levels at 20°C in *lin-35(n745)* and *lin-37(n758)* mutant strain whereas the strain *lin-52(n771)* revealed upregulated levels only at 26°C (67). The fact that

different DRM- complex mutant models vary strongly in the levels of “p- granule proteins” in somatic cells and high temperature arrest, supports the idea of an interindividual co-function among DRM- complex components which is more likely than a result of a full DRM-complex disruption in the mutants. Thus, this investigation could explain the differences in larval development of different DRM- complex mutant strains at 20°C.

However, the *lin-54(n2231)* mutant strain appeared as an exception. These mutant worms show larval arrest at the L1 stage at high temperature (67) but reveal increased larval development after UV-B exposure compared to wildtype in my experiments. Previous studies (64) have shown that this mutant produces less progeny which is consistent with observations in my study. In addition it has been shown that the *lin-54(n2231)* mutant strain is predicted to be a null mutant, carrying a mutation in the DNA binding CXC domain and an additional point mutation (87). However, these mutations do not affect the assembly of other components of the DRM- complex (87). More likely, the direct regulation of many genes, which is promoted together with E2F/DP interaction and over a T- enriched motif, is disrupted in the *lin-54(n2231)* mutant strain (87). Furthermore, this mutant strain exhibits the highest percentage of arrested L1 larvae of all DRM- complex mutant strains at 26°C and also ectopic expression of germline- related genes on 20°C and on 26°C (67). These three characteristics, disruption of direct gene regulation, ectopic expression of germline related genes and high temperature arrest, appear especially different in the *lin-54(n2231)* mutant strain compared to other DRM- complex mutant strains used in my experiments. Thus, it is possible that LIN-54 represses different subsets of genes. This could explain the strong phenotype of *lin-54(n2231)* mutant worms after UV-B irradiation but also the larval arrest at high temperature. This hypothesis is also based on the observation that *efl-1(se1)* mutant worms do not exhibit high temperature larval arrest (67) but also increased larval development after UV-B irradiation. Most likely this mutant strain deregulates other subsets of genes beyond the classical DRM- complex genes leading to decreased larval arrest after different DNA damage exposures.

The *lin-52(n771)* mutant worms showed no larval arrest at high temperature and only ectopic expression of germline- related genes at 26°C (67). Furthermore LIN-52 is also not known to directly regulate genes but only indirectly over E2F/DP binding sites together with other partners in the DRM- complex. Thus, the possibility of reduced activation of cofactors in the *lin-52(n771)* mutant strains could explain the phenotype observed in different experiments performed for this thesis.

5.3 Impact of germline related gene expression in somatic tissues in DRM-complex mutant worms

As explained above, the DRM- complex in *C. elegans* is also known to repress germline related genes in the somatic tissue (67). Consequently, many, but not all, DRM- complex mutants exhibit ectopic expression of distinct “p- granule genes” in somatic cells. Histone modifiers such as MES-4 or MET-2 are of central relevance for this regulation (67,72). This can be seen by reduction of the high temperature induced larval arrest when the chromatin modifier MES-4 is knocked-down by a RNAi approach. Similarly, the high temperature induced arrest is restored by knock-down of MET-2. For future experiments, this knock-down could be applied to DRM- complex mutant strains with high temperature arrest to test whether developmental delay could be rescued under standard conditions.

RNAi mediated knock-down of *mep-1*, which is part of the NuRD- complex, but also synMuvB mutant worms exhibit expression of germline related genes in somatic tissues. Such mutant worms also show larval arrest at high temperature (67,116). However, the DRM- complex mutants’ phenotype investigated in this thesis seems to be distinct from the NuRD- complex and other synMuvB mutant worms (Fig. 6 and 7). Interestingly, *efl-1(se1)* mutant worms do not exhibit high temperature induced larval arrest and ectopic expression of germline related genes in somatic cells which were tested in this previous study (67). These *efl-1(se1)* mutant worms reveal a similar phenotype as other DRM- complex mutants after UV-B irradiation or IR. Taken together, this indicates that high temperature induced expression of distinct germline related genes in somatic tissue in synMuvB mutant worms is not likely to explain the faster larval development of DRM- complex mutants after DNA damage.

It is possible that the DRM- complex also represses subsets of genes which are not regulated by other synMuvB or NuRD components. H3K9me2 modifications, which are enriched at promoter sites for repressing germline related genes in somatic tissue, appear more relevant in *lin-15B* mutant worms than in DRM- complex mutants (72). There is some evidence that DRM- complex mutants exhibit deregulation of a subset of genes which act on the modification of H3K4me3 (72). Experimental analysis of this subset of genes could give further insights into the developmental DRM- complex mutants phenotype. Such experiments appear interesting because misexpression of germline related genes in somatic cells is also relevant for human disease and clinical research. It has been shown that gametogenic gene expression in breast cancer in humans is linked to poor clinical outcome (117). Even though it is still unknown whether these genes are regulated by the DREAM- complex, several lines of evidence indicate that especially LIN9 is of central relevance for breast cancer (41,42). Therefore, further investigations on the causal

relationships between gametogenic gene expression and DREAM- complex functions in mammalian cells could give insights in future cancer research.

5.4 Explanation for distinct results of *in-vivo* and *in-vitro* experiments in DRM-complex mutants

The experiments performed in this thesis showed that DRM- complex mutant worms do not only improve the function of NER after UV-B irradiation but also after UV-A and Trioxsalen exposure (Fig. 14, 19). In mammalian cells, the DREAM- complex controls the expression of XPC, a component of the NER, via E2F mediated repression at the promoter region (39,40). However, explicit investigations on the mechanisms of how the DRM- complex regulates the NER in *C. elegans* remained inconclusive: Whereas the analyses of altered transcript levels in DRM- complex mutants could not give clear results, experiments on protein levels revealed distinct *in-vivo* (Fig. 17) and *in-vitro* results (Fig. 18). It is known that synMuvB mutants show silencing of repetitive GFP labeled transcriptional reporters in somatic cells (66). For this reason, I investigated whether subtypes of cells in the DRM-complex mutant worm show different XPA-1::GFP expression. DRM- complex mutant worms crossed with the transgenic strain *xpa-1(ok698); sbjIn27[pBS128(xpa-1::GFP) + pBS174(myo-2::tdTomato)]* were analyzed at the L4 stage under the microscope. Stable XPA-1::GFP expression was found in all somatic cells in these worms (data not shown). However, *in- vitro* analysis by western blot analysis revealed similar levels of XPA-1 in DRM-complex mutant and in *xpa-1(syb788)[CR(xpa-1::V5+TEV+linker+Ypet)]* mutant worms. It is possible that I could not detect a significant difference because the expression of XPA-1 in these worms is generally low. Furthermore, nuclear bounded XPA-1 could not be enriched for this western blot approach. This also could result in low sensitivity (118). Optimized buffer composition could help to enrich fractionation of chromatin bound XPA-1 for western blot analysis (119). It would be also interesting to investigate how XPA-1 and other NER candidates are degraded. It is possible that the DRM- complex affects this degradation and thus modulates the number of components of the NER in the cell.

5.5 Role of DRM-/DREAM- complex in DNA damage response

5.5.1 Multiple DNA- repair mechanisms and their function in DRM- complex mutant worms

In mammals, the DREAM- complex is involved in the p53-p21-DREAM-E2F/CHR pathway (36). Activation of the tumor suppressor p53 increases the expression of p21 (36). This protein inhibits cyclin- dependent kinases which results in a hypo-phosphorylated state of p130 and p107 (36). This then leads to formation of the DREAM- complex. As a consequence, transcriptional repression of multiple genes induces transition into the G0 phase (36). However, the central function of this pathway is to promote cell cycle arrest for allowing repair of the DNA damage. As described before, the DREAM- complex in mammals is also functioning in the repression of XPC (39,40). Furthermore, other DNA repair genes such as BRCA1 or BRCA2 appear as targets that are repressed by the p53-p21-DREAM-E2F/CHR pathway (36,120-122). In this thesis I have shown that UV-B irradiation induced developmental delay in TC-NER or GG-NER mutant worms can be rescued partially by DRM- complex mutants. This partial rescue is abolished when both of the NER sub-pathways are depleted in DRM- complex mutants. Furthermore, a deficit of gene products involved in DNA repair mechanisms that lead to homologous recombination (HR) or base excision repair (BER) can be partially rescued by intercrossing with DRM- complex mutants (Fig. 10, 11 and 21). The data shown in figure 11 demonstrate that larval delay by deficiency in *parp-1* is almost completely rescued by an additional intercross with DRM- complex mutant worms. This double mutant exhibits nearly equal results than the single DRM-complex mutant. Since DRM- complex mutants exhibit upregulated transcript levels of gene products involved in different DNA repair mechanisms (92), it is possible that other DNA repair mechanism replace the function of abolished DNA repair pathways to promote faster DNA repair in DRM- complex mutants than in wildtype. Analysis at transcript levels in TC-NER and DRM- complex mutants revealed that gene expression of transcripts involved in the GG-NER are upregulated when the TC-NER is abolished by knock-out of *csb-1* (Fig. 16). Even though this was independent from DRM- complex function, a synergistical and modifying role of these sub-branches became apparent. Similar mechanisms appear likely for DRM- complex mutants. This hypothesis is based on the observation that *xpa-1* and *brc-1* deficient worms exhibit stronger developmental defects and lower survival rates under standard conditions than single mutants (123). The study by Lans et al (123) has shown that mutants of *xpa-1* exhibit a small delay in development whereas *brc-1* deficient worms exhibit wildtype like larval development. Interestingly, crossing both mutants with each other leads to a much higher delay in development than that observed in single *xpa-1* deficient worms (123). Furthermore, the survival is also reduced in these double-crossed mutants

compared to the single mutants (123). The conclusion that could be drawn by these observations is discussed below.

In mammalian cells, members of the NER but also homologous recombination (HR) repair and translesion synthesis function together in the repair of interstrand cross links (ICL) (124). This special type of DNA damage is induced by Trioxsalen and UV-A irradiation (105), cisplatin and other chemotherapeutic agents (124), endogenous stress (125), but also IR is discussed as a trigger (126). During the repair, ERCC1 and XPF, two proteins which are working in the NER pathway, function together with other partners to eliminate the crosslinked base (124). During this process the ICL is transformed in a double-strand break as a secondary lesion which then is repaired by members of the HR repair pathway (127,128). It remains unclear, whether individual components of the NER play the crucial role for inducing DSB during the ICL repair (127,129). In *C. elegans, xpf-1* and *xpg*-1 mutant worms exhibit sensitivity to IR (123). It is tempting to speculate that this sensitivity is a reason of unrepaired ICLs. During my work it became apparent that IR induced embryonic lethality of *brc-1(tm1145)* mutant strains could be partially rescued by intercross with DRM-complex mutant worms (Fig. 21). It is possible that other DNA repair pathways could replace the function of HR by repairing or overcoming the DNA damage. Furthermore, it is known that *xpa-1 or ercc-1* defective worms exhibit high sensitivity to UV-A and Trioxsalen treatment which induces ICL formations (83). The same study also provided evidence that BRCA-1 is involved in this type of repair. In DRM- complex mutant worms, larval development is improved after UV-A and Trioxsalen treatment (Fig. 19). However, an additional intercross with a *xpa-1(gk698)* led to larval arrest similar than in NER single mutant worms (Fig. 19). This may emphasize the impact of the NER in the ICL repair. It is possible that the delayed development of *xpa-1* and *brc-1* deficient worms (123) is a consequence of inefficient repair of endogenous ICLs. An alternative pathway of DSB repair by ERCC-1 and XPF-1 could also come into play as revealed by studies with *C. elegans* (130). This study showed that *xpf-1; brc-1* double mutants exhibit a less effective repair than *brc-1* single mutant worms. This suggest that XPF-1 acts synergistically with BRC-1. In addition, this study also indicated that under conditions of deficient HR repair, DSBs can be transformed and repaired in a XPF-1 dependent manner (130). Unfortunately, this study does not provide evidence for the contribution of the ICL repair pathway.

Another study has shown that a combined knock-out of *xpa-1* and *polh-1* leads to decreased embryonic survival after UV-C treatment in comparison to the corresponding single mutants (131). Interestingly, DNA damage could be repaired in an adapted way in *polh-1* mutants by polymerase theta- mediated end joining (131). In DRM- complex mutant worms transcript levels of *polh-1* appeared upregulated compared to wildtype (92). MMS treatment of *polh-1* mutant worms causes reduced larval development. This is partially rescued by intercross

with *lin-52(n771)* mutant strain (Fig. 20). Further studies on transcript regulations of other potential repair mediators such as XPA-1 and polymerase theta mediated end joining could give more insights into this.

However, many details about the ICL and the HR- independent ICL repair pathway still remain unknown and unclear. Thus, previous observations and hypotheses need to be expanded by future research. The fact, that different repair mechanisms act together to repair a special type of DNA damage, such as ICLs, expands the current understanding of static repair pathways towards dynamic synergistic roles. Thus, it is possible that upregulated DNA repair genes in DRM- complex mutants show similar mechanisms. This could lead to improved DNA repair in DRM- complex mutant worms even though other DNA repair mechanisms such as the HR are defective by knock-out.

Furthermore, the results of this study show that in particular mutants of *exo-3* do also exhibit UV-B hypersensitivity compared to wildtype. This hypersensitivity can be partially rescued by DRM- complex mutants (Fig. 10). This improved response is most likely mediated through a more efficient NER. However, this DNA repair pathway could not normalize the faster larval development of DRM- complex mutant worms in *lin-52(n771); exo-3(ok3559)* double mutants. This suggests that not only the NER but also other repair mechanisms, such as the BER, have an impact on the DRM- complex mutant phenotype after UV-B irradiation. Further experiments need to test the expression of other DNA repair genes at transcript levels of *exo-3* and its double mutant with DRM- complex mutants to investigate the regulation of DNA repair mechanisms.

5.5.2 The DRM- complex function as a repressor for DNA repair genes in somatic tissue

In all organisms, including *C. elegans*, the germline is of central relevance to produce progeny. Therefore, these cells have to be protected in a different manner than somatic cells. IR- induced damage in *C. elegans* results in predominant DDR signaling in the germline in adult worms but not in the somatic tissue (132). In this study, germline and somatic tissue were exposed to IR in similar way. Interestingly, only germline cells exhibited apoptosis and activation of the ATM- pathway or other important DDR signaling proteins (132). In contrast to this, somatic cells showed lower rates of cell death and thus exhibit higher stress resistance (133). On an evolutionary sight this makes sense considering only the short life- cycle of *C. elegans.* Therefore, the germline cells are protected in a more efficient way to keep the following generation sustainable. Thus, this also explains the privileged role of germline cells using different DNA repair mechanism than somatic cells in

C. elegans (54). The study of Lans et al showed, that the GG-NER is more relevant for germline cells and early embryos whereas the TC-NER is more relevant for DNA repair during larval development (54). Interestingly, UV induced apoptosis was stimulated by both DNA repair sub-branches: TC- and GG-NER (54).

As described above, many synMuvB mutants are known to express germline related genes in somatic tissue in *C. elegans* (66,67). From these studies, it was concluded that subsets of genes are predominantly regulated by the DRM- complex (72). Thus, it is possible that DDR genes, which are normally repressed in somatic cells, are active in somatic cells in DRM- mutants. Indeed, the expression of many DDR genes appears upregulated in DRM- complex mutants compared to wildtype. These genes also contain DRM- complex specific binding motifs (92). Among these, many DDR genes encode for DNA repair mechanisms. This appears as an explanation for the more efficient or faster DNA repair in DRM- complex mutants after DNA damage exposure. Furthermore, multiple active DNA repair mechanisms in somatic tissue might also compensate when other DNA repair pathways are inhibited by knock-out approaches. However, this does not imply that DRM- complex mutants have similar DDR capacities in somatic cells, in comparison to germline cells (132). In DRM- complex mutants no change in ATM-1 or ATL-1 kinase activities were observed in somatic cells, as shown by lack of phosphorylation of target substrates at corresponding serine/ threonine sites (132). Unfortunately, the authors of this study only investigated the ATM-1 and ATL-1 kinase activity in *lin-35(n745)* and *lin-15b(n744)* mutant worms but did not further study the impact of the DRM- complex on DDR gene regulation. Experiments in this thesis with *atm-1* deficient mutants in DRM- complex mutant background revealed no impact on larval development compared to DRM- complex single mutants (Fig. 9). However, ATL-1, the homolog of ATR in *C. elegans* (134), is supposed to be more active than ATM-1 after UV- related DNA damage (135). Unfortunately, intercross with *atl-1* mutant worms in a DRM- complex mutant background was not possible during my experimental work. This experiment could give further insights in DDR signaling in DRM- complex mutants in *C. elegans*.

5.6 DRM-/DREAM- complex in modern cancer research

5.6.1 *C. elegans* as an established organism for studying cancer therapies and cell cycle regulation

The DRM- complex in *C. elegans* functions as a transcriptional repressor for DDR genes (92). In mammalian cells p53 is known to function together with the DREAM-complex in the p53-p21-DREAM-E2F/CHR pathway within the response to DNA damage (36). As a consequence, it appears tempting to speculate, whether similar pathways can be found in *C. elegans*. In this organism a potential p53 homolog has been identified and named *cep-1* (136). The corresponding gene product triggers germ cell apoptosis after IR and UV-C induced DNA damage (135,136). Furthermore, it has been shown that CEP-1 also represses DNA repair genes after UV-C irradiation (137). Interestingly, components of the DRM- complex like LIN-35, DPL-1 and EFL-1 are supposed to act as downstream targets of CEP-1 to promote DNA damage induced germ cell apoptosis (138). In particular, LIN-35 exhibits pro-apoptotic activity in germ cells by repressing *ced-9* transcription (138). Furthermore, DPL-1 and EFL-1 show pro-apoptotic activity by activating expression of *ced-3* and *ced-4* (138). These findings point to a link between DRM- complex and CEP-1 mediated germ cell apoptosis in *C. elegans*, and the function of the p53-p21-DREAM-E2F/CHR pathway in mammalian cells. However, this link needs to be confirmed by further research.

The mammalian p53-p21-DREAM-E2F/CHR pathway does not only promote cell cycle inhibition but also represses DNA repair genes such as BRCA1/ BRCA2 (36,120-122,139). Interestingly, BRCA1 and BRCA2 mutated ovarian and breast cancer cells are sensitive to cisplatin therapies (140). Experiments with *C. elegans* and cisplatin treatment revealed that DRM- complex mutants are less sensitive to this drug than wildtype which could be due to improved and more efficient DNA repair (92). Thus, in both organisms the repression of DNA repair genes appears to be a common mechanism that is mediated through the DRM-/DREAM- complex. These studies indicate, that *C. elegans* could be used as a model organism for studying the DRM-/ DREAM- complex in cancer and in particular for therapeutic strategies.

So far, cell cycle regulation by the DRM- complex in *C. elegans* is not fully understood, but analysis at transcript level reveals upregulated expression of multiple cell cycle related genes in DRM- complex mutants (64,92). The results of this thesis indicate that uncontrolled cell division is not a result of an impaired DRM- complex function. Thus, it would be interesting to analyze additional mechanisms which are necessary for cell cycle regulation. This could improve the knowledge about DREAM- complex mutated cancer cells in humans

and their progression that causes poor clinical prognosis. To analyze cell cycle regulation in *C. elegans*, experiments in germline cells might be more useful, as these cells divide at high levels during reproductive lifespan of the worms.

5.6.2 Cancer research and future therapeutic strategies involving the DREAM-complex

The MuvB complex in mammalian cells has a dual function: Repression or activation of cell cycle genes, depending on which subcomplex it is working with. G0 phase can be achieved by cell cycle repression through the DREAM- complex assembly, consisting of MuvB, p130 and E2F4/ DP1 (30). Activation of cell cycle genes is mediated via MuvB- B-MYB and MuvB-FOXM1 binding (29). Thus, this dual function implies also different options for cancer development beyond the established idea of uncontrolled cell division. Several studies have shown that cancer cells in G0 phase are resistant to chemotherapeutical drugs: Epithelial ovarian cancer cells are more viable in cellular aggregates (spheroid) when these cells arrest in G0 phase (28). Under these conditions, the DREAM- complex is assembled and active (28). This finding suggests that cancer cells in G0 phase are more resistant against chemotherapy and other stress conditions because they are arrested in G0 phase (28). Clinical observations indicate that epithelial ovarian cancer cells can invade to pelvic and abdomen sites and cause ascites production (141). Treatment with dual specificity tyrosine (Y)-phosphorylation-regulated kinase 1A (DYRK1A) inhibitors reduce the phosphorylation of S28 in LIN-52, resulting under normal conditions in the assembly of the DREAM-complex. As a consequence, these cells cannot arrest in G0 phase and appear to be more susceptible to chemotherapeutic treatment. Indeed, additional treatment of these epithelial ovarian cancer cells with carboplatin decreases spheroid viability, which may be interesting for further clinically studies (28). Another positive impact of DYRK1A inhibitors has been discovered in gastrointestinal stroma tumors (142). These tumor cells undergo DREAM-complex mediated G0 phase and exhibit imatinib resistance (142). This resistance could be bypassed by cotreatment with DYRK1A inhibitors (142). Similar results were also observed in breast cancer cells from tumors with poor clinical outcome and paclitaxel resistance (42). These cells exhibit overexpression of LIN9 (42). However, the assembly of the DREAM-complex and its interaction with B-MYB and FOXM1 was not investigated in this study (42). Therefore, it can only be speculated whether modulation of DREAM- complex function is involved when cancer cells become more sensitive to chemotherapeutic drugs.

Interestingly, use of DYRK1A inhibitors is not restricted to tumor therapies but is currently also studied in neurodegenerative diseases (143). However, in this clinical context, the focus of DYRK1A inhibition is not directed towards modulation of DREAM- complex function. DYRK1A is also known to phosphorylate tau in mammalian neurons. Hyperphosphorylated tau is the core component of neurofibrillary tangles, the pathological hallmark of Alzheimer disease (144,145). Interestingly, DYRK1A also increases the expression of tau by ensuring the stability of tau mRNA (146). Due to the fact that *DYRK1A* is located on chromosome 21, people with Down Syndrome exhibit higher protein levels of DYRK1A, which could explain the high risk of developing the Alzheimer disease (143). Therefore, DYRK1A inhibitors appear also as a future therapeutic candidate for treatment of Alzheimer´s disease (147).

In contrast to repression of cell cycle genes, MuvB, a subcomplex of the DREAM- complex, also activates gene expression together with B-MYB and FOXM1 (29). Overexpression of B-MYB and FOXM1 can be found in multiple types of tumors (148-150). Interestingly, infections with the human papilloma Virus type 16 (HPV16) leads also to perturbations of the DREAM- complex. The HPV16 E7 protein mediates protein degradation of DREAM-complex subunits and supports MuvB- B-MYB and FOXM1 interaction for regulation of corresponding gene expression (151,152). This finding underlines the pro- cancerous effect of B-MYB and FOXM1 when they act together with MuvB. The high impact of B-MYB for tumors can be also seen by the fact that this transcription factor is found frequently in breast cancer test panels (153). It is tempting to speculate that switching the stoichiometry from B-MYB/FOXM1- MuvB complex to DREAM- complex assembly by knock-down of B-MYB downstream targets could also be a potential therapeutic target for cancer therapy (154,155). As an example, MuvB- B-MYB interaction was found to induce cell proliferation in oncogenic K-RAS and p53 mutated lung cancer cells in mice (156). Deletion of B-MYB or p53 wildtype leads to inhibition of this proliferation, indicating that this mechanism is an option for a therapeutic target (156). However, it needs to be considered that this deletion may also have other effects on the organism. This can be also seen from my results: Homozygous knock-out of Lin52 in mouse embryonic stem cells appears not to be compatible with viability. Similar results were also observed in a Lin9 knock-out mouse model which revealed major cytokinetic and embryonic defects (90). Therefore, inhibition of the MuvB- B- MYB downstream target KIF23 which also results in a proliferation stop in lung cancer cells appears as a better target for future tumor therapies (156). Another interesting chemotherapeutic target has been identified with the drug palbociclib. This drug reduces phosphorylation of different DREAM- complex proteins and therefore blocks the disassembly of the DREAM- complex leading to an inhibition of cell cycle (157). However, negative side effects of palbociclib in the direction of chemotherapeutic resistance are

theoretical possible, as explained before with the observation made with epithelial ovarian cancer cells or gastrointestinal stroma tumors.

These findings point to multiple functions of the MuvB complex and its interactive partners for repression and activation of cell cycle and DDR genes. Perturbations in both ways are important for understanding cancer development and pharmacological treatment. Further biomedical research on this complex could therefore reveal new insights into cancer cell biology to develop new therapies. The upregulated expression of multiple cell cycle related genes in DRM- complex mutant worms (64,92) appears as a good starting point into such research directions.

5.7 Conclusion

The DREAM- complex is not only a master regulator for cell cycle regulation (29) but also modulates the expression of DNA repair genes. In *C. elegans* the DRM- complex does not only repress germline related genes in somatic tissues but also functions as a repressor for several DNA repair genes in somatic cells. Therefore, DRM- complex mutants reveal resistance to different types of DNA damage exposure such as UV-B irradiation, IR or MMS. Of central importance in this thesis was the interaction between the NER and the DRM- complex: DRM- complex mutants can rescue a loss of one NER sub-branch. However, DRM- complex mutant worms were not able to compensate for a full loss of NER. Attempts to study the mode how the NER and DRM- complex functions are connected, revealed complex interactions *in-vitro* and *in-vivo.* Also, other DNA repair mechanism such as HR or BER may be repressed by the DRM- complex. The observation that the loss of the NER in DRM- complex mutant worms stopped the improved larval development after UV- mediated DNA damage supports the hypothesis that the NER is of central relevance in DRM- complex mutants. It remains open if this repair mechanism is the central compensatory mechanism when other repair mechanisms are defective. However, other compensatory repair pathways could also come into play. As an example, it cannot be excluded that the BER also contributes to the improved response of DRM- complex mutants to DNA damage. Previous reports suggest alternative DNA repair pathways involving proteins of the NER or HR. It remains unclear why the DRM- complex, a cell cycle inhibitor, represses genes for DNA repair instead of ensuring a proper repair while promoting cell cycle arrest. It is tempting to speculate that arrested cells may be less susceptible to tumorigenesis because of their non-dividing behavior. Therefore, multiple DNA repair mechanisms could be repressed by the DRM- complex. Future research on DRM- complex mediated gene repression by histone modifications could give further insights into the regulation of DDR

genes. Furthermore, the role of the NER in DDR and DRM- complex functions might be an interesting target for future research. The nematode *C. elegans* is a well-established and ideal model for analyzing the function and regulation mechanisms of the DRM- complex. This could help to obtain new insights in DREAM- complex function that are also important for development of future therapies for tumors and other diseases.

6. References

1. Jackson SP, Bartek J. The DNA-damage response in human biology and disease. *Nature* 2009; **461**(7267): 1071-8.

2. Kraemer KH, Patronas NJ, Schiffmann R, Brooks BP, Tamura D, DiGiovanna JJ. Xeroderma pigmentosum, trichothiodystrophy and Cockayne syndrome: a complex genotype-phenotype relationship. *Neuroscience* 2007; **145**(4): 1388-96.

3. DiGiovanna JJ, Kraemer KH. Shining a light on xeroderma pigmentosum. *J Invest Dermatol* 2012; **132**(3 Pt 2): 785-96.

4. Brooks BP, Thompson AH, Bishop RJ, et al. Ocular manifestations of xeroderma pigmentosum: long-term follow-up highlights the role of DNA repair in protection from sun damage. *Ophthalmology* 2013; **120**(7): 1324-36.

5. Bradford PT, Goldstein AM, Tamura D, et al. Cancer and neurologic degeneration in xeroderma pigmentosum: long term follow-up characterises the role of DNA repair. *J Med Genet* 2011; **48**(3): 168-76.

6. Totonchy MB, Tamura D, Pantell MS, et al. Auditory analysis of xeroderma pigmentosum 1971-2012: hearing function, sun sensitivity and DNA repair predict neurological degeneration. *Brain* 2013; **136**(Pt 1): 194-208.

7. Riley DJ, Lee EY, Lee WH. The retinoblastoma protein: more than a tumor suppressor. *Annual review of cell biology* 1994; **10**: 1-29.

8. Kamihara J, Bourdeaut F, Foulkes WD, et al. Retinoblastoma and Neuroblastoma Predisposition and Surveillance. *Clinical cancer research : an official journal of the American Association for Cancer Research* 2017; **23**(13): e98-e106.

9. Rastogi RP, Richa, Kumar A, Tyagi MB, Sinha RP. Molecular mechanisms of ultraviolet radiation-induced DNA damage and repair. *J Nucleic Acids* 2010; **2010**: 592980.

10. Lo HL, Nakajima S, Ma L, et al. Differential biologic effects of CPD and 6-4PP UV-induced DNA damage on the induction of apoptosis and cell-cycle arrest. *BMC Cancer* 2005; **5**: 135.

11. Garinis GA, Mitchell JR, Moorhouse MJ, et al. Transcriptome analysis reveals cyclobutane pyrimidine dimers as a major source of UV-induced DNA breaks. *EMBO J* 2005; **24**(22): 3952-62.

12. Branzei D, Foiani M. Regulation of DNA repair throughout the cell cycle. *Nat Rev Mol Cell Biol* 2008; **9**(4): 297-308.

13. Lans H, Vermeulen W. Nucleotide Excision Repair in Caenorhabditis elegans. *Mol Biol Int* 2011; **2011**: 542795.

14. Marteijn JA, Lans H, Vermeulen W, Hoeijmakers JH. Understanding nucleotide excision repair and its roles in cancer and ageing. *Nat Rev Mol Cell Biol* 2014; **15**(7): 465-81.

15. Wittschieben BO, Iwai S, Wood RD. DDB1-DDB2 (xeroderma pigmentosum group E) protein complex recognizes a cyclobutane pyrimidine dimer, mismatches,

apurinic/apyrimidinic sites, and compound lesions in DNA. *J Biol Chem* 2005; **280**(48): 39982-9.

16. Mizukoshi T, Kodama TS, Fujiwara Y, Furuno T, Nakanishi M, Iwai S. Structural study of DNA duplexes containing the (6-4) photoproduct by fluorescence resonance energy transfer. *Nucleic Acids Res* 2001; **29**(24): 4948-54.

17. Spivak G. Nucleotide excision repair in humans. *DNA Repair (Amst)* 2015; **36**: 13-8.

18. Geijer ME, Marteijn JA. What happens at the lesion does not stay at the lesion: Transcription-coupled nucleotide excision repair and the effects of DNA damage on transcription in cis and trans. *DNA Repair (Amst)* 2018; **71**: 56-68.

19. Mathieu N, Kaczmarek N, Ruthemann P, Luch A, Naegeli H. DNA quality control by a lesion sensor pocket of the xeroderma pigmentosum group D helicase subunit of TFIIH. *Curr Biol* 2013; **23**(3): 204-12.

20. Sugasawa K, Akagi J, Nishi R, Iwai S, Hanaoka F. Two-step recognition of DNA damage for mammalian nucleotide excision repair: Directional binding of the XPC complex and DNA strand scanning. *Molecular cell* 2009; **36**(4): 642-53.

21. Camenisch U, Dip R, Schumacher SB, Schuler B, Naegeli H. Recognition of helical kinks by xeroderma pigmentosum group A protein triggers DNA excision repair. *Nat Struct Mol Biol* 2006; **13**(3): 278-84.

22. Scharer OD. Nucleotide excision repair in eukaryotes. *Cold Spring Harb Perspect Biol* 2013; **5**(10): a012609.

23. Staresincic L, Fagbemi AF, Enzlin JH, et al. Coordination of dual incision and repair synthesis in human nucleotide excision repair. *EMBO J* 2009; **28**(8): 1111-20.

24. Schafer KA. The cell cycle: a review. *Vet Pathol* 1998; **35**(6): 461-78.

25. Giacinti C, Giordano A. RB and cell cycle progression. *Oncogene* 2006; **25**(38): 5220-7.

26. Classon M, Harlow E. The retinoblastoma tumour suppressor in development and cancer. *Nature reviews Cancer* 2002; **2**(12): 910-7.

27. Wei P, Zhang N, Wang Y, et al. FOXM1 promotes lung adenocarcinoma invasion and metastasis by upregulating SNAIL. *Int J Biol Sci* 2015; **11**(2): 186-98.

28. MacDonald J, Ramos-Valdes Y, Perampalam P, Litovchick L, DiMattia GE, Dick FA. A Systematic Analysis of Negative Growth Control Implicates the DREAM Complex in Cancer Cell Dormancy. *Mol Cancer Res* 2017; **15**(4): 371-81.

29. Sadasivam S, DeCaprio JA. The DREAM complex: master coordinator of cell cycle-dependent gene expression. *Nature reviews Cancer* 2013; **13**(8): 585-95.

30. Litovchick L, Sadasivam S, Florens L, et al. Evolutionarily conserved multisubunit RBL2/p130 and E2F4 protein complex represses human cell cycle-dependent genes in quiescence. *Molecular cell* 2007; **26**(4): 539-51.

31. Litovchick L, Florens LA, Swanson SK, Washburn MP, DeCaprio JA. DYRK1A protein kinase promotes quiescence and senescence through DREAM complex assembly. *Genes & development* 2011; **25**(8): 801-13.

32. Muller GA, Quaas M, Schumann M, et al. The CHR promoter element controls cell cycle-dependent gene transcription and binds the DREAM and MMB complexes. *Nucleic Acids Res* 2012; **40**(4): 1561-78.

33. Knight AS, Notaridou M, Watson RJ. A Lin-9 complex is recruited by B-Myb to activate transcription of G2/M genes in undifferentiated embryonal carcinoma cells. *Oncogene* 2009; **28**(15): 1737-47.

34. Sadasivam S, Duan S, DeCaprio JA. The MuvB complex sequentially recruits B-Myb and FoxM1 to promote mitotic gene expression. *Genes & development* 2012; **26**(5): 474-89.

35. Charrasse S, Carena I, Brondani V, Klempnauer KH, Ferrari S. Degradation of B-Myb by ubiquitin-mediated proteolysis: involvement of the Cdc34-SCF(p45Skp2) pathway. *Oncogene* 2000; **19**(26): 2986-95.

36. Engeland K. Cell cycle arrest through indirect transcriptional repression by p53: I have a DREAM. *Cell Death Differ* 2018; **25**(1): 114-32.

37. Quaas M, Muller GA, Engeland K. p53 can repress transcription of cell cycle genes through a p21(WAF1/CIP1)-dependent switch from MMB to DREAM protein complex binding at CHR promoter elements. *Cell cycle* 2012; **11**(24): 4661-72.

38. Mannefeld M, Klassen E, Gaubatz S. B-MYB is required for recovery from the DNA damage-induced G2 checkpoint in p53 mutant cells. *Cancer Res* 2009; **69**(9): 4073-80.

39. Cam H, Balciunaite E, Blais A, et al. A common set of gene regulatory networks links metabolism and growth inhibition. *Molecular cell* 2004; **16**(3): 399-411.

40. Dominguez-Brauer C, Chen YJ, Brauer PM, Pimkina J, Raychaudhuri P. ARF stimulates XPC to trigger nucleotide excision repair by regulating the repressor complex of E2F4. *EMBO Rep* 2009; **10**(9): 1036-42.

41. Sahni JM, Gayle SS, Webb BM, et al. Mitotic Vulnerability in Triple-Negative Breast Cancer Associated with LIN9 Is Targetable with BET Inhibitors. *Cancer Res* 2017; **77**(19): 5395-408.

42. Lai H, Wang R, Li S, et al. LIN9 confers paclitaxel resistance in triple negative breast cancer cells by upregulating CCSAP. *Sci China Life Sci* 2019.

43. Corsi AK, Wightman B, Chalfie M. A Transparent Window into Biology: A Primer on Caenorhabditis elegans. *Genetics* 2015; **200**(2): 387-407.

44. Byerly L, Cassada RC, Russell RL. The life cycle of the nematode Caenorhabditis elegans. I. Wild-type growth and reproduction. *Dev Biol* 1976; **51**(1): 23-33.

45. Johnson TE, Mitchell DH, Kline S, Kemal R, Foy J. Arresting development arrests aging in the nematode Caenorhabditis elegans. *Mech Ageing Dev* 1984; **28**(1): 23-40.

46. Golden JW, Riddle DL. The Caenorhabditis elegans dauer larva: developmental effects of pheromone, food, and temperature. *Dev Biol* 1984; **102**(2): 368-78.

47. Fielenbach N, Antebi A. C. elegans dauer formation and the molecular basis of plasticity. *Genes & development* 2008; **22**(16): 2149-65.

48. Cassada RC, Russell RL. The dauerlarva, a post-embryonic developmental variant of the nematode Caenorhabditis elegans. *Dev Biol* 1975; **46**(2): 326-42.

49. Schindler AJ, Sherwood DR. Morphogenesis of the caenorhabditis elegans vulva. *Wiley Interdiscip Rev Dev Biol* 2013; **2**(1): 75-95.

50. Sulston JE, Horvitz HR. Post-embryonic cell lineages of the nematode, Caenorhabditis elegans. *Dev Biol* 1977; **56**(1): 110-56.

51. Kimble J, Hirsh D. The postembryonic cell lineages of the hermaphrodite and male gonads in Caenorhabditis elegans. *Dev Biol* 1979; **70**(2): 396-417.

52. Gartner A, Milstein S, Ahmed S, Hodgkin J, Hengartner MO. A conserved checkpoint pathway mediates DNA damage--induced apoptosis and cell cycle arrest in C. elegans. *Molecular cell* 2000; **5**(3): 435-43.

53. Mueller MM, Castells-Roca L, Babu V, et al. DAF-16/FOXO and EGL-27/GATA promote developmental growth in response to persistent somatic DNA damage. *Nat Cell Biol* 2014; **16**(12): 1168-79.

54. Lans H, Marteijn JA, Schumacher B, Hoeijmakers JH, Jansen G, Vermeulen W. Involvement of global genome repair, transcription coupled repair, and chromatin remodeling in UV DNA damage response changes during development. *PLoS Genet* 2010; **6**(5): e1000941.

55. Babu V, Hofmann K, Schumacher B. A C. elegans homolog of the Cockayne syndrome complementation group A gene. *DNA Repair (Amst)* 2014; **24**: 57-62.

56. Astin JW, O'Neil NJ, Kuwabara PE. Nucleotide excision repair and the degradation of RNA pol II by the Caenorhabditis elegans XPA and Rsp5 orthologues, RAD-3 and WWP-1. *DNA Repair (Amst)* 2008; **7**(2): 267-80.

57. Rieckher M, Bujarrabal A, Doll MA, Soltanmohammadi N, Schumacher B. A simple answer to complex questions: Caenorhabditis elegans as an experimental model for examining the DNA damage response and disease genes. *Journal of Cellular Physiology* 2018; **233**(4): 2781-90.

58. Harrison MM, Ceol CJ, Lu X, Horvitz HR. Some C. elegans class B synthetic multivulva proteins encode a conserved LIN-35 Rb-containing complex distinct from a NuRD-like complex. *Proc Natl Acad Sci U S A* 2006; **103**(45): 16782-7.

59. Fay DS, Yochem J. The SynMuv genes of Caenorhabditis elegans in vulval development and beyond. *Dev Biol* 2007; **306**(1): 1-9.

60. Ferguson EL, Horvitz HR. The multivulva phenotype of certain Caenorhabditis elegans mutants results from defects in two functionally redundant pathways. *Genetics* 1989; **123**(1): 109-21.

61. Korenjak M, Taylor-Harding B, Binne UK, et al. Native E2F/RBF complexes contain Myb-interacting proteins and repress transcription of developmentally controlled E2F target genes. *Cell* 2004; **119**(2): 181-93.

62. Lu X, Horvitz HR. lin-35 and lin-53, two genes that antagonize a C. elegans Ras pathway, encode proteins similar to Rb and its binding protein RbAp48. *Cell* 1998; **95**(7): 981-91.

63. Ceol CJ, Horvitz HR. dpl-1 DP and efl-1 E2F act with lin-35 Rb to antagonize Ras signaling in C. elegans vulval development. *Molecular cell* 2001; **7**(3): 461-73.

64. Goetsch PD, Garrigues JM, Strome S. Loss of the Caenorhabditis elegans pocket protein LIN-35 reveals MuvB's innate function as the repressor of DREAM target genes. *PLoS Genet* 2017; **13**(11): e1007088.

65. Kipreos ET, van den Heuvel S. Developmental Control of the Cell Cycle: Insights from Caenorhabditis elegans. *Genetics* 2019; **211**(3): 797-829.

66. Wang D, Kennedy S, Conte D, Jr., et al. Somatic misexpression of germline P granules and enhanced RNA interference in retinoblastoma pathway mutants. *Nature* 2005; **436**(7050): 593-7.

67. Petrella LN, Wang W, Spike CA, Rechtsteiner A, Reinke V, Strome S. synMuv B proteins antagonize germline fate in the intestine and ensure C. elegans survival. *Development* 2011; **138**(6): 1069-79.

68. Shi Y, Mello C. A CBP/p300 homolog specifies multiple differentiation pathways in Caenorhabditis elegans. *Genes & development* 1998; **12**(7): 943-55.

69. von Zelewsky T, Palladino F, Brunschwig K, Tobler H, Hajnal A, Muller F. The C. elegans Mi-2 chromatin-remodelling proteins function in vulval cell fate determination. *Development* 2000; **127**(24): 5277-84.

70. Solari F, Ahringer J. NURD-complex genes antagonise Ras-induced vulval development in Caenorhabditis elegans. *Curr Biol* 2000; **10**(4): 223-6.

71. Muller GA, Engeland K. The central role of CDE/CHR promoter elements in the regulation of cell cycle-dependent gene transcription. *FEBS J* 2010; **277**(4): 877-93.

72. Rechtsteiner A, Costello ME, Egelhofer TA, Garrigues JM, Strome S, Petrella LN. Repression of Germline Genes in Caenorhabditis elegans Somatic Tissues by H3K9 Dimethylation of Their Promoters. *Genetics* 2019; **212**(1): 125-40.

73. Liu T, Rechtsteiner A, Egelhofer TA, et al. Broad chromosomal domains of histone modification patterns in C. elegans. *Genome Res* 2011; **21**(2): 227-36.

74. Latorre I, Chesney MA, Garrigues JM, et al. The DREAM complex promotes gene body H2A.Z for target repression. *Genes & development* 2015; **29**(5): 495-500.

75. Brenner S. The genetics of Caenorhabditis elegans. *Genetics* 1974; **77**(1): 71-94.

76. Dorsett M, Westlund B, Schedl T. METT-10, a putative methyltransferase, inhibits germ cell proliferative fate in Caenorhabditis elegans. *Genetics* 2009; **183**(1): 233-47.

77. Springhorn A, Hoppe T. Western blot analysis of the autophagosomal membrane protein LGG-1/LC3 in Caenorhabditis elegans. *Methods Enzymol* 2019; **619**: 319-36.

78. Thomas JH, Ceol CJ, Schwartz HT, Horvitz HR. New genes that interact with lin-35 Rb to negatively regulate the let-60 ras pathway in Caenorhabditis elegans. *Genetics* 2003; **164**(1): 135-51.

79. Consortium CeDM. large-scale screening for targeted knockouts in the Caenorhabditis elegans genome. *G3 (Bethesda)* 2012; **2**(11): 1415-25.

80. Janisiw E, Dello Stritto MR, Jantsch V, Silva N. BRCA1-BARD1 associate with the synaptonemal complex and pro-crossover factors and influence RAD-51 dynamics during Caenorhabditis elegans meiosis. *PLoS Genet* 2018; **14**(11): e1007653.

81. Page BD, Guedes S, Waring D, Priess JR. The C. elegans E2F- and DP-related proteins are required for embryonic asymmetry and negatively regulate Ras/MAPK signaling. *Molecular cell* 2001; **7**(3): 451-60.

82. Porta-de-la-Riva M, Fontrodona L, Villanueva A, Ceron J. Basic Caenorhabditis elegans methods: synchronization and observation. *J Vis Exp* 2012; (64): e4019.

83. Wilson DM, 3rd, Rieckher M, Williams AB, Schumacher B. Systematic analysis of DNA crosslink repair pathways during development and aging in Caenorhabditis elegans. *Nucleic Acids Res* 2017; **45**(16): 9467-80.

84. Taylor SC, Posch A. The design of a quantitative western blot experiment. *Biomed Res Int* 2014; **2014**: 361590.

85. Schmittgen TD, Livak KJ. Analyzing real-time PCR data by the comparative C(T) method. *Nat Protoc* 2008; **3**(6): 1101-8.

86. Cohen J. Statistical power analysis for the behavioral sciences. New York: Lawrence Erlbaum assaociates; 1988.

87. Tabuchi TM, Deplancke B, Osato N, et al. Chromosome-biased binding and gene regulation by the Caenorhabditis elegans DRM complex. *PLoS Genet* 2011; **7**(5): e1002074.

88. Huang LS, Tzou P, Sternberg PW. The lin-15 locus encodes two negative regulators of Caenorhabditis elegans vulval development. *Mol Biol Cell* 1994; **5**(4): 395-411.

89. Schmit F, Korenjak M, Mannefeld M, et al. LINC, a human complex that is related to pRB-containing complexes in invertebrates regulates the expression of G2/M genes. *Cell cycle* 2007; **6**(15): 1903-13.

90. Reichert N, Wurster S, Ulrich T, et al. Lin9, a subunit of the mammalian DREAM complex, is essential for embryonic development, for survival of adult mice, and for tumor suppression. *Mol Cell Biol* 2010; **30**(12): 2896-908.

91. Mages CF, Wintsche A, Bernhart SH, Muller GA. The DREAM complex through its subunit Lin37 cooperates with Rb to initiate quiescence. *Elife* 2017; **6**.

92. Bujarrabal A, Sendtner G, Meyer H, Schumacher B. The DREAM complex functions as conserved master regulator of somatic DNA repair capacities. (submitted). *Science* 2021.

93. Stergiou L, Doukoumetzidis K, Sendoel A, Hengartner MO. The nucleotide excision repair pathway is required for UV-C-induced apoptosis in Caenorhabditis elegans. *Cell Death And Differentiation* 2007; **14**: 1129.

94. Shatilla A, Ramotar D. Embryonic extracts derived from the nematode Caenorhabditis elegans remove uracil from DNA by the sequential action of uracil-DNA glycosylase and AP (apurinic/apyrimidinic) endonuclease. *Biochem J* 2002; **365**(Pt 2): 547-53.

95. Shatilla A, Leduc A, Yang X, Ramotar D. Identification of two apurinic/apyrimidinic endonucleases from Caenorhabditis elegans by cross-species complementation. *DNA Repair (Amst)* 2005; **4**(6): 655-70.

96. Schlotterer A, Hamann A, Kukudov G, et al. Apurinic/apyrimidinic endonuclease 1, p53, and thioredoxin are linked in control of aging in C. elegans. *Aging Cell* 2010; **9**(3): 420-32.

97. Durkacz BW, Omidiji O, Gray DA, Shall S. (ADP-ribose)n participates in DNA excision repair. *Nature* 1980; **283**(5747): 593-6.

98. Benjamin RC, Gill DM. ADP-ribosylation in mammalian cell ghosts. Dependence of poly(ADP-ribose) synthesis on strand breakage in DNA. *J Biol Chem* 1980; **255**(21): 10493-501.

99. Haince JF, Kozlov S, Dawson VL, et al. Ataxia telangiectasia mutated (ATM) signaling network is modulated by a novel poly(ADP-ribose)-dependent pathway in the early response to DNA-damaging agents. *J Biol Chem* 2007; **282**(22): 16441-53.

100. Vodenicharov MD, Ghodgaonkar MM, Halappanavar SS, Shah RG, Shah GM. Mechanism of early biphasic activation of poly(ADP-ribose) polymerase-1 in response to ultraviolet B radiation. *J Cell Sci* 2005; **118**(Pt 3): 589-99.

101. Bryant HE, Schultz N, Thomas HD, et al. Specific killing of BRCA2-deficient tumours with inhibitors of poly(ADP-ribose) polymerase. *Nature* 2005; **434**(7035): 913-7.

102. Farmer H, McCabe N, Lord CJ, et al. Targeting the DNA repair defect in BRCA mutant cells as a therapeutic strategy. *Nature* 2005; **434**(7035): 917-21.

103. Gagnon SN, Hengartner MO, Desnoyers S. The genes pme-1 and pme-2 encode two poly(ADP-ribose) polymerases in Caenorhabditis elegans. *Biochem J* 2002; **368**(Pt 1): 263-71.

104. Dequen F, Gagnon SN, Desnoyers S. Ionizing radiations in Caenorhabditis elegans induce poly(ADP-ribosyl)ation, a conserved DNA-damage response essential for survival. *DNA Repair (Amst)* 2005; **4**(7): 814-25.

105. Huang J, Liu S, Bellani MA, et al. The DNA translocase FANCM/MHF promotes replication traverse of DNA interstrand crosslinks. *Molecular cell* 2013; **52**(3): 434-46.

106. Kato K, Strauss B. Accumulation of an intermediate in DNA synthesis by HEp.2 cells treated with methyl methanesulfonate. *Proc Natl Acad Sci U S A* 1974; **71**(5): 1969-73.

107. Holway AH, Kim SH, La Volpe A, Michael WM. Checkpoint silencing during the DNA damage response in Caenorhabditis elegans embryos. *J Cell Biol* 2006; **172**(7): 999-1008.

108. Waters LS, Minesinger BK, Wiltrout ME, D'Souza S, Woodruff RV, Walker GC. Eukaryotic translesion polymerases and their roles and regulation in DNA damage tolerance. *Microbiol Mol Biol Rev* 2009; **73**(1): 134-54.

109. Roerink SF, Koole W, Stapel LC, Romeijn RJ, Tijsterman M. A broad requirement for TLS polymerases eta and kappa, and interacting sumoylation and nuclear pore proteins, in lesion bypass during C. elegans embryogenesis. *PLoS Genet* 2012; **8**(6): e1002800.

110. Semmler L, Reiter-Brennan C, Klein A. BRCA1 and Breast Cancer: a Review of the Underlying Mechanisms Resulting in the Tissue-Specific Tumorigenesis in Mutation Carriers. *J Breast Cancer* 2019; **22**(1): 1-14.

111. Boulton SJ, Martin JS, Polanowska J, Hill DE, Gartner A, Vidal M. BRCA1/BARD1 orthologs required for DNA repair in Caenorhabditis elegans. *Curr Biol* 2004; **14**(1): 33-9.

112. Li Q, Saito TT, Martinez-Garcia M, et al. The tumor suppressor BRCA1-BARD1 complex localizes to the synaptonemal complex and regulates recombination under meiotic dysfunction in Caenorhabditis elegans. *PLoS Genet* 2018; **14**(11): e1007701.

113. Hashizume R, Fukuda M, Maeda I, et al. The RING heterodimer BRCA1-BARD1 is a ubiquitin ligase inactivated by a breast cancer-derived mutation. *J Biol Chem* 2001; **276**(18): 14537-40.

114. Clejan I, Boerckel J, Ahmed S. Developmental modulation of nonhomologous end joining in Caenorhabditis elegans. *Genetics* 2006; **173**(3): 1301-17.

115. Schmit F, Cremer S, Gaubatz S. LIN54 is an essential core subunit of the DREAM/LINC complex that binds to the cdc2 promoter in a sequence-specific manner. *FEBS J* 2009; **276**(19): 5703-16.

116. Unhavaithaya Y, Shin TH, Miliaras N, Lee J, Oyama T, Mello CC. MEP-1 and a homolog of the NURD complex component Mi-2 act together to maintain germline-soma distinctions in C. elegans. *Cell* 2002; **111**(7): 991-1002.

117. Maine EA, Westcott JM, Prechtl AM, Dang TT, Whitehurst AW, Pearson GW. The cancer-testis antigens SPANX-A/C/D and CTAG2 promote breast cancer invasion. *Oncotarget* 2016; **7**(12): 14708-26.

118. Bass JJ, Wilkinson DJ, Rankin D, et al. An overview of technical considerations for Western blotting applications to physiological research. *Scand J Med Sci Sports* 2017; **27**(1): 4-25.

119. Holden P, Horton WA. Crude subcellular fractionation of cultured mammalian cell lines. *BMC Res Notes* 2009; **2**: 243.

120. Valenti F, Ganci F, Fontemaggi G, et al. Gain of function mutant p53 proteins cooperate with E2F4 to transcriptionally downregulate RAD17 and BRCA1 gene expression. *Oncotarget* 2015; **6**(8): 5547-66.

121. Wu K, Jiang SW, Couch FJ. p53 mediates repression of the BRCA2 promoter and down-regulation of BRCA2 mRNA and protein levels in response to DNA damage. *J Biol Chem* 2003; **278**(18): 15652-60.

122. Fischer M, Steiner L, Engeland K. The transcription factor p53: not a repressor, solely an activator. *Cell cycle* 2014; **13**(19): 3037-58.

123. Lans H, Lindvall JM, Thijssen K, et al. DNA damage leads to progressive replicative decline but extends the life span of long-lived mutant animals. *Cell Death Differ* 2013; **20**(12): 1709-18.

124. Lopez-Martinez D, Liang CC, Cohn MA. Cellular response to DNA interstrand crosslinks: the Fanconi anemia pathway. *Cell Mol Life Sci* 2016; **73**(16): 3097-114.

125. Pang Q, Andreassen PR. Fanconi anemia proteins and endogenous stresses. *Mutat Res* 2009; **668**(1-2): 42-53.

126. Dextraze ME, Gantchev T, Girouard S, Hunting D. DNA interstrand cross-links induced by ionizing radiation: an unsung lesion. *Mutat Res* 2010; **704**(1-3): 101-7.

127. Niedernhofer LJ, Odijk H, Budzowska M, et al. The structure-specific endonuclease Ercc1-Xpf is required to resolve DNA interstrand cross-link-induced double-strand breaks. *Mol Cell Biol* 2004; **24**(13): 5776-87.

128. De Silva IU, McHugh PJ, Clingen PH, Hartley JA. Defining the roles of nucleotide excision repair and recombination in the repair of DNA interstrand cross-links in mammalian cells. *Mol Cell Biol* 2000; **20**(21): 7980-90.

129. Rothfuss A, Grompe M. Repair kinetics of genomic interstrand DNA cross-links: evidence for DNA double-strand break-dependent activation of the Fanconi anemia/BRCA pathway. *Mol Cell Biol* 2004; **24**(1): 123-34.

130. Pontier DB, Tijsterman M. A robust network of double-strand break repair pathways governs genome integrity during C. elegans development. *Curr Biol* 2009; **19**(16): 1384-8.

131. van Bostelen I, Tijsterman M. Combined loss of three DNA damage response pathways renders C. elegans intolerant to light. *DNA Repair (Amst)* 2017; **54**: 55-62.

132. Vermezovic J, Stergiou L, Hengartner MO, d'Adda di Fagagna F. Differential regulation of DNA damage response activation between somatic and germline cells in Caenorhabditis elegans. *Cell Death Differ* 2012; **19**(11): 1847-55.

133. Johnson TE, Hartman PS. Radiation effects on life span in Caenorhabditis elegans. *J Gerontol* 1988; **43**(5): B137-41.

134. Garcia-Muse T, Boulton SJ. Distinct modes of ATR activation after replication stress and DNA double-strand breaks in Caenorhabditis elegans. *EMBO J* 2005; **24**(24): 4345-55.

135. Stergiou L, Doukoumetzidis K, Sendoel A, Hengartner MO. The nucleotide excision repair pathway is required for UV-C-induced apoptosis in Caenorhabditis elegans. *Cell Death Differ* 2007; **14**(6): 1129-38.

136. Schumacher B, Hofmann K, Boulton S, Gartner A. The C. elegans homolog of the p53 tumor suppressor is required for DNA damage-induced apoptosis. *Curr Biol* 2001; **11**(21): 1722-7.

137. Derry WB, Bierings R, van Iersel M, Satkunendran T, Reinke V, Rothman JH. Regulation of developmental rate and germ cell proliferation in Caenorhabditis elegans by the p53 gene network. *Cell Death Differ* 2007; **14**(4): 662-70.

138. Schertel C, Conradt B. C. elegans orthologs of components of the RB tumor suppressor complex have distinct pro-apoptotic functions. *Development* 2007; **134**(20): 3691-701.

139. Jaber S, Toufektchan E, Lejour V, Bardot B, Toledo F. p53 downregulates the Fanconi anaemia DNA repair pathway. *Nat Commun* 2016; **7**: 11091.

140. Mylavarapu S, Das A, Roy M. Role of BRCA Mutations in the Modulation of Response to Platinum Therapy. *Front Oncol* 2018; **8**: 16.

141. Shield K, Ackland ML, Ahmed N, Rice GE. Multicellular spheroids in ovarian cancer metastases: Biology and pathology. *Gynecol Oncol* 2009; **113**(1): 143-8.

142. Boichuk S, Parry JA, Makielski KR, et al. The DREAM complex mediates GIST cell quiescence and is a novel therapeutic target to enhance imatinib-induced apoptosis. *Cancer Res* 2013; **73**(16): 5120-9.

143. Abbassi R, Johns TG, Kassiou M, Munoz L. DYRK1A in neurodegeneration and cancer: Molecular basis and clinical implications. *Pharmacol Ther* 2015; **151**: 87-98.

144. Ryoo SR, Jeong HK, Radnaabazar C, et al. DYRK1A-mediated hyperphosphorylation of Tau. A functional link between Down syndrome and Alzheimer disease. *J Biol Chem* 2007; **282**(48): 34850-7.

145. Park J, Yang EJ, Yoon JH, Chung KC. Dyrk1A overexpression in immortalized hippocampal cells produces the neuropathological features of Down syndrome. *Mol Cell Neurosci* 2007; **36**(2): 270-9.

146. Qian W, Jin N, Shi J, et al. Dual-specificity tyrosine phosphorylation-regulated kinase 1A (Dyrk1A) enhances tau expression. *J Alzheimers Dis* 2013; **37**(3): 529-38.

147. Branca C, Shaw DM, Belfiore R, et al. Dyrk1 inhibition improves Alzheimer's disease-like pathology. *Aging Cell* 2017; **16**(5): 1146-54.

148. Musa J, Aynaud MM, Mirabeau O, Delattre O, Grunewald TG. MYBL2 (B-Myb): a central regulator of cell proliferation, cell survival and differentiation involved in tumorigenesis. *Cell Death Dis* 2017; **8**(6): e2895.

149. Zhang J, Zhang J, Cui X, et al. FoxM1: a novel tumor biomarker of lung cancer. *Int J Clin Exp Med* 2015; **8**(3): 3136-40.

150. Huang C, Du J, Xie K. FOXM1 and its oncogenic signaling in pancreatic cancer pathogenesis. *Biochim Biophys Acta* 2014; **1845**(2): 104-16.

151. Pang CL, Toh SY, He P, et al. A functional interaction of E7 with B-Myb-MuvB complex promotes acute cooperative transcriptional activation of both S- and M-phase genes. (129 c). *Oncogene* 2014; **33**(31): 4039-49.

152. Nor Rashid N, Yusof R, Watson RJ. Disruption of repressive p130-DREAM complexes by human papillomavirus 16 E6/E7 oncoproteins is required for cell-cycle progression in cervical cancer cells. *J Gen Virol* 2011; **92**(Pt 11): 2620-7.

153. Paik S, Shak S, Tang G, et al. A multigene assay to predict recurrence of tamoxifen-treated, node-negative breast cancer. *N Engl J Med* 2004; **351**(27): 2817-26.

154. Iness AN, Felthousen J, Ananthapadmanabhan V, et al. The cell cycle regulatory DREAM complex is disrupted by high expression of oncogenic B-Myb. *Oncogene* 2019; **38**(7): 1080-92.

155. Iness AN, Litovchick L. MuvB: A Key to Cell Cycle Control in Ovarian Cancer. *Front Oncol* 2018; **8**: 223.

156. Iltzsche F, Simon K, Stopp S, et al. An important role for Myb-MuvB and its target gene KIF23 in a mouse model of lung adenocarcinoma. *Oncogene* 2017; **36**(1): 110-21.

157. Schade AE, Oser MG, Nicholson HE, DeCaprio JA. Cyclin D-CDK4 relieves cooperative repression of proliferation and cell cycle gene expression by DREAM and RB. *Oncogene* 2019; **38**(25): 4962-76.

7. Appendix

7.1 Supplemental figures

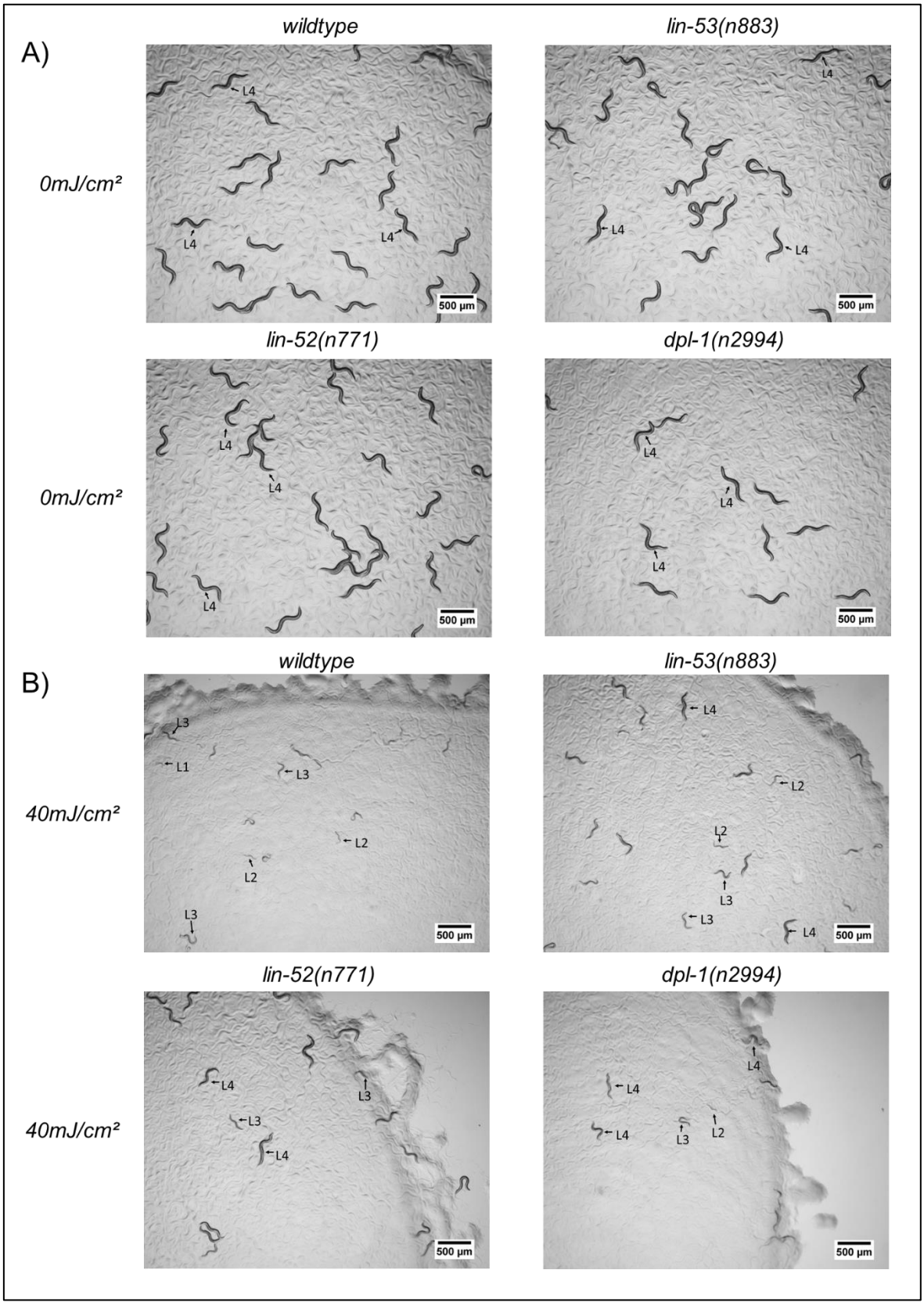

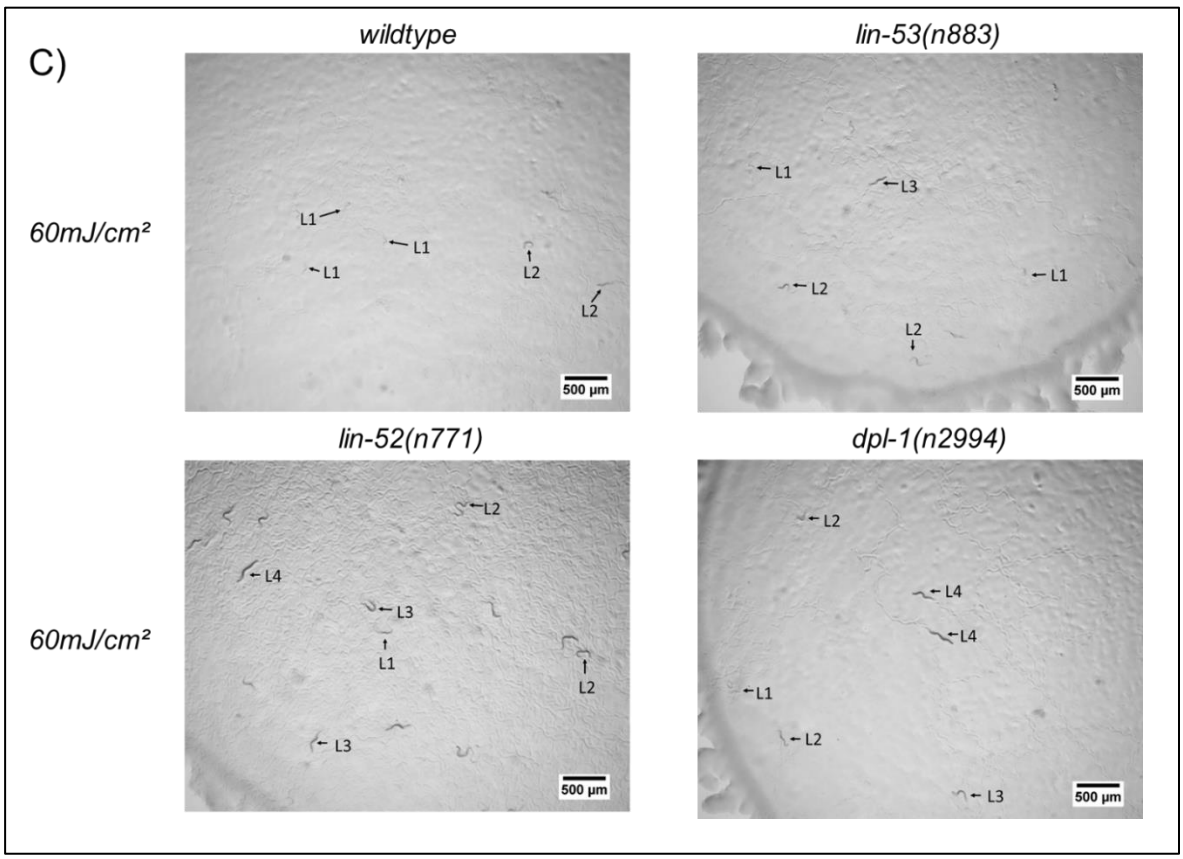

Supplemental figure 1. **Representative pictures of different DRM- complex mutant worms and wildtype.**

Starved L1 worms were irradiated with UV-B and fed for 48 hours under standard conditions. Pictures were taken 48 hours after irradiation which equates the normal developmental assay setup to determine the larval stages. Arrows indicate examples for different larval stages.
1a) Development of mutant strains and wildtype under standard conditions 1b) Development of mutant strains and wildtype after 40 mJ/cm² of UV-B irradiation 1c) Development of mutant strains and wildtype after 60 mJ/cm² of UV-B irradiation. All pictures were done with the same magnification. Overall magnification: 38.5x. Scale bar showing length of 500µm.

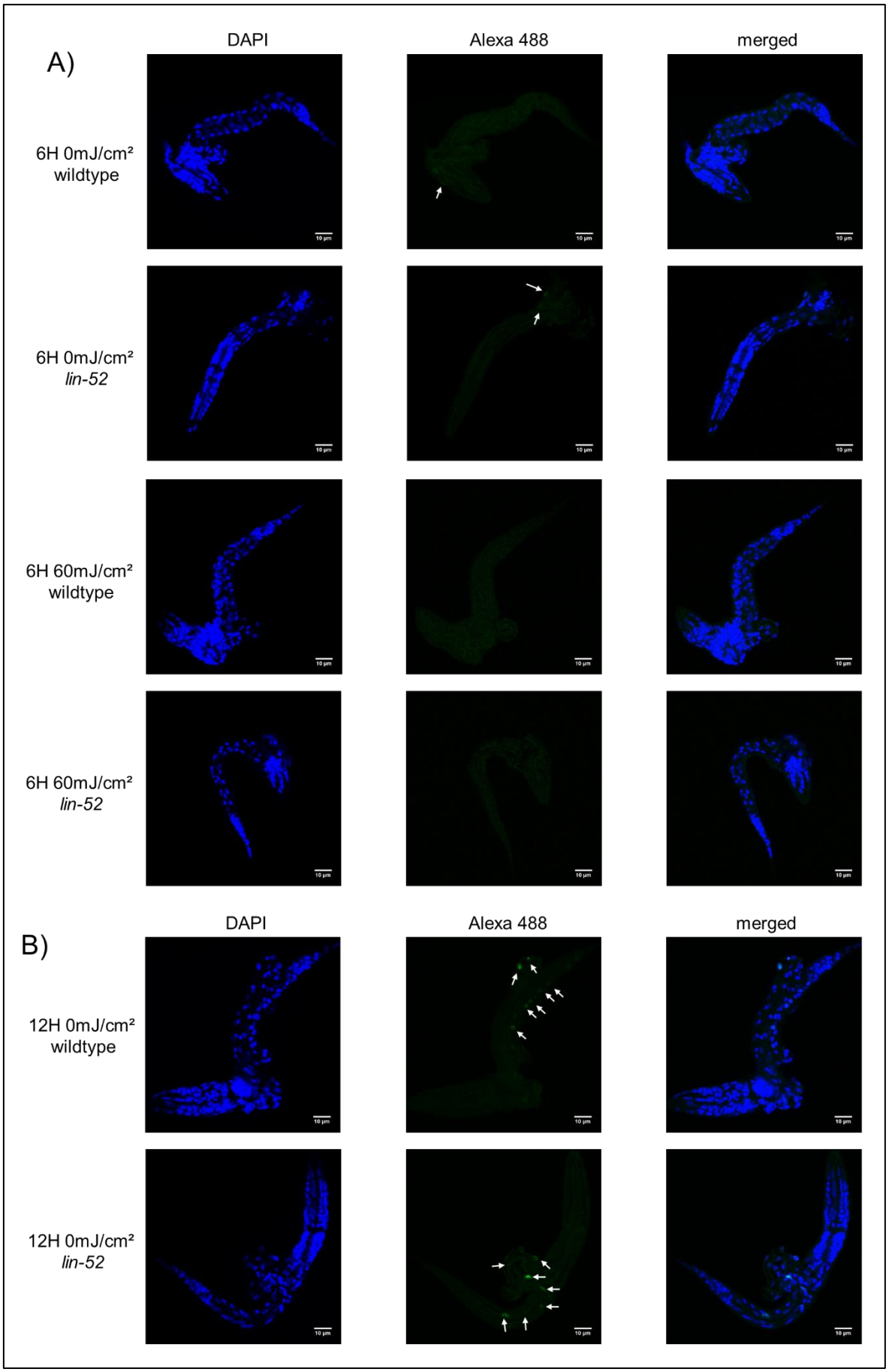
A)
DAPI
Alexa 488
merged
6H 0mJ/cm²
wildtype
6H 0mJ/cm²
lin-52
6H 60mJ/cm²
wildtype
6H 60mJ/cm²
lin-52
B)
DAPI
Alexa 488
merged
12H 0mJ/cm²
wildtype
12H 0mJ/cm²
lin-52

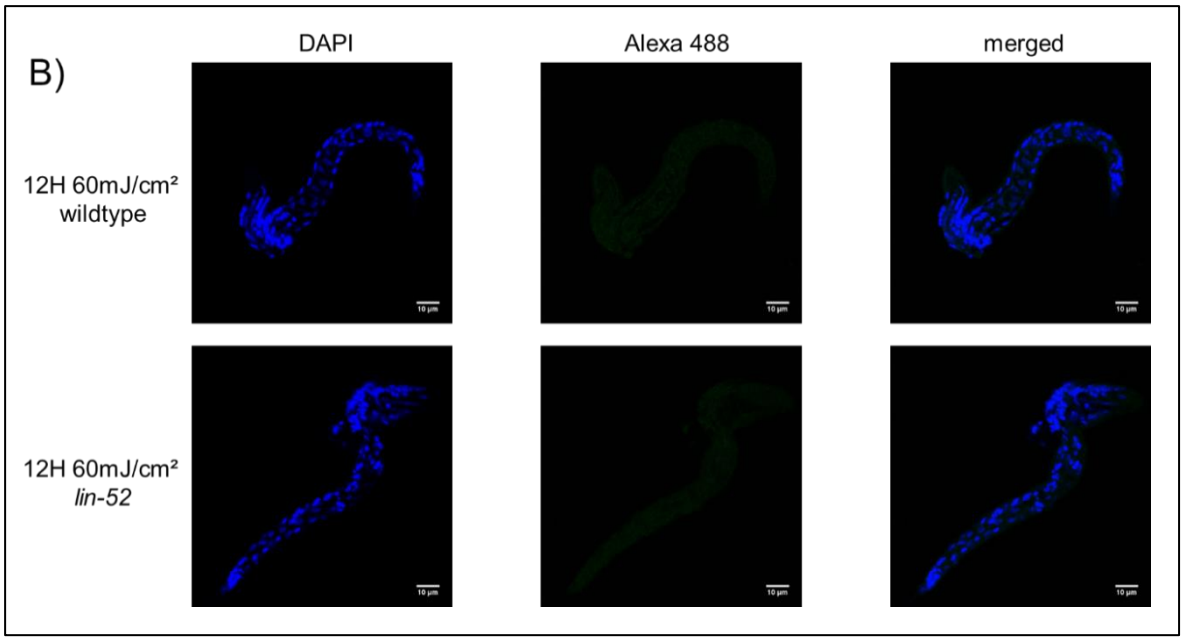

Supplemental figure 2. **Representative pictures of wildtype and *lin-52(n771)* mutant worms in an EdU Alexa Fluor 488 assay.**

Nuclei were stained with DAPI, new divided cells were labeled with Alexa 488. Arrows indicate Alexa 488 positive cells, scale bar showing length of 10 µm. 2a) 6 hours after UV-B irradiation, treatment and unirradiated controls. 2b) 12 hours after UV-B irradiation, treatment and unirradiated controls. All pictures were done with the same magnification. Overall magnification 630x.

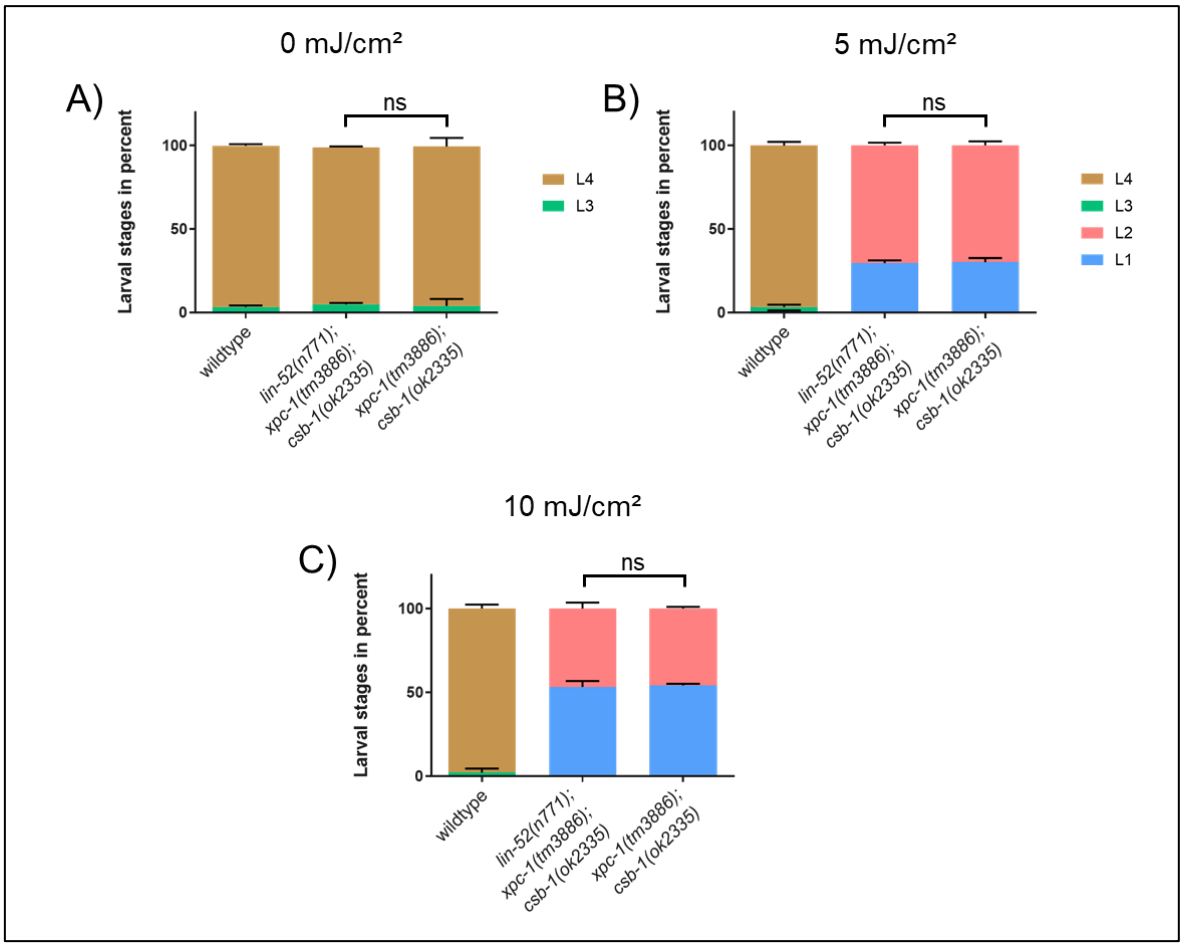

Supplemental figure 3. **Developmental assay of *lin-52(n771)* and NER deficient mutants following UV-B irradiation.**

The developmental assay shows the different larval stages in percent of mutant and wildtype worms. Starved L1 worms were irradiated with UV-B and fed for 48 hours under standard conditions before different larval stages were determined. 3a) Development of *xpc-1(tm3886); csb-1(ok2335)*, *lin-52(n771); xpc-1(tm3886); csb-1(ok2335)* mutant worms and wildtype under standard conditions. 3b) and 3c) Development of NER deficient mutant worms and wildtype after 5 mJ/cm² or 10 mJ/cm² of UV-B irradiation. The *lin-52(n771); xpc-1(tm3886); csb-1(ok2335)* shows similar behavior as the *xpc-1(tm3886); csb-1(ok2335)* mutant worms. The Fisher´s exact test shows no significant (ns) difference (p- value > 0.05). This experiment was performed in biological replicates. Error bars represent standard deviation. Further statistical analysis can be found in the supplemental table 17.

7.2 Supplemental tables

This supplemental chapter shows the statistical analysis of different experiments of this thesis. If not described otherwise, table exhibits statistical analysis of different development assays using different amounts of UV-B irradiation (mJ/cm^2). The Fisher´s exact test reveals overall differences between stages. To compare single stages with each other, the two-tailed t-test was used. For both statistical tests asterisks indicate following significance: p> 0.05 =ns, p<0.05 = *, p<0.01 = ** p<0.001 = ***.

Supplemental table 1:

Two-tailed t-test		**L1**	**L2**	**L3**	**L4**	**Fisher´s exact test**
wildtype vs *lin-52(n771)*	0mJ/cm²		ns	ns	ns	ns
	40mJ/cm²	*	**	**	***	***
	60mJ/cm²	ns	ns	**	ns	***
wildtype vs *dpl-1(n2994)*	0mJ/cm²		ns	ns	ns	ns
	40mJ/cm²	*	**	***	***	***
	60mJ/cm²	*	**	**	**	***
wildtype vs *efl-1(se1)*	0mJ/cm²		ns	ns	ns	ns
	40mJ/cm²	ns	ns	ns	**	*
	60mJ/cm²	ns	ns	ns		*
wildtype vs *lin-35(n745)*	0mJ/cm²			***	***	***
	40mJ/cm²	ns	**	***		***
	60mJ/cm²	ns	ns	*		***
wildtype vs *lin-37(n758)*	0mJ/cm²		ns	**	**	***
	40mJ/cm²	ns	*	*	ns	***
	60mJ/cm²	ns	ns	ns	ns	***
wildtype vs *lin-54(n2231)*	0mJ/cm²		ns	ns	ns	ns
	40mJ/cm²	**	**	**	***	***
	60mJ/cm²	ns	*	**	*	***
wildtype vs *lin-53(n833)*	0mJ/cm²		ns	ns	ns	ns

	40mJ/cm²	ns	*	**	**	***
	60mJ/cm²	ns	ns	ns		ns
wildtype vs *lin-9(n112)*	0mJ/cm²		ns	***	***	***
	40mJ/cm²	ns	ns	*		***
	60mJ/cm²	ns	ns	ns		***

Supplemental table 1: Statistical analysis of developmental assay in figure 5 containing two-tailed t- test and Fisher´s exact test. Asterisks indicate following significance: p> 0.05 =ns, p<0.05 = *, p<0.01 = ** p<0.001 = ***.

Supplemental table 2:

Two-tailed t-test		**L1**	**L2**	**L3**	**L4**	**Fisher´s exact test**
wildtype vs *hpl-2(tm1489)*	0mJ/cm²			ns	ns	ns
	40mJ/cm²	ns	ns	ns	*	*
	60mJ/cm²	ns	ns	ns		ns
wildtype vs *lin-13(n770)*	0mJ/cm²			ns	ns	ns
	40mJ/cm²	*	ns	ns	ns	*
	60mJ/cm²	ns	ns	ns		ns
wildtype vs *lin-15B(n765)*	0mJ/cm²			ns	ns	ns
	40mJ/cm²	ns	ns	ns	ns	ns
	60mJ/cm²	*	ns	ns		ns

Supplemental table 2: Statistical analysis of developmental assay in figure 6 containing two-tailed t- test and Fisher´s exact test. Asterisks indicate following significance: p> 0.05 =ns, p<0.05 = *, p<0.01 = ** p<0.001 = ***.

Supplemental table 3

Two-tailed t-test		**L1**	**L2**	**L3**	**L4**	**Fisher´s exact test**
wildtype vs *let-418(n3536)*	0mJ/cm²		ns	**	**	**
	40mJ/cm²	ns	ns	ns	ns	ns
	60mJ/cm²	ns	ns	ns	***	ns

wildtype vs *hda-1(e1795)*	0mJ/cm²			***	***	***
	40mJ/cm²	ns	ns	ns	ns	ns
	60mJ/cm²	ns	ns	ns	ns	ns

Supplemental table 3: Statistical analysis of developmental assay in figure 7 containing two-tailed t- test and Fisher´s exact test. Asterisks indicate following significance: p> 0.05 =ns, p<0.05 = *, p<0.01 = ** p<0.001 = ***.

Supplemental table 4

Two-tailed t-test		**L1**	**L2**	**L3**	**L4**	**Fisher´s exact test**
wildtype vs *lin-52(n771)*	0mJ/cm²			ns	ns	ns
	40mJ/cm²	**	*	**	ns	***
	60mJ/cm²	**	*	***		***
wildtype vs *atm-1(gk186)*	0mJ/cm²			ns	ns	ns
	40mJ/cm²	ns	ns	ns		ns
	60mJ/cm²	ns	ns	ns		ns
wildtype vs *lin-52(n771);atm-1(gk186)*	0mJ/cm²			ns	ns	ns
	40mJ/cm²	*	**	***	ns	***
	60mJ/cm²	ns	**	***		***
lin-52(n771) vs *atm-1(gk186)*	0mJ/cm²			ns	ns	ns
	40mJ/cm²	*	**	***	*	***
	60mJ/cm²	*	*	***		***
lin-52(n771) vs *lin-52(n771);atm-1(gk186)*	0mJ/cm²			ns	ns	ns
	40mJ/cm²	ns	ns	ns	ns	ns
	60mJ/cm²	**	ns	ns		ns
atm-1(gk186) vs *lin-52(n771);atm-1(gk186)*	0mJ/cm²			ns	ns	ns
	40mJ/cm²	ns	**	***	ns	***
	60mJ/cm²	ns	***	***		***

Supplemental table 4: Statistical analysis of developmental assay in figure 9 containing two-tailed t- test and Fisher´s exact test. Asterisks indicate following significance: p> 0.05 =ns, p<0.05 = *, p<0.01 = ** p<0.001 = ***.

Supplemental table 5

Two-tailed t-test		**L1**	**L2**	**L3**	**L4**	**Fisher´s exact test**
wildtype vs *lin-52(n771)*	0mJ/cm²		***	ns	ns	ns
	40mJ/cm²	***	***	ns	***	***
	60mJ/cm²	ns	***	***	***	***
wildtype vs *exo-3(ok3559)*	0mJ/cm²		*	**	***	***
	40mJ/cm²	*	*	*		**
	60mJ/cm²	ns	ns	ns		***
wildtype vs *lin-52(n771); exo-3(ok3559)*	0mJ/cm²		***	*	**	ns
	40mJ/cm²	ns	***	***	***	***
	60mJ/cm²	ns	***	***	*	***
lin-52(n771) vs *exo-3(ok3559)*	0mJ/cm²		**	*	**	***
	40mJ/cm²	**	**	ns	**	***
	60mJ/cm²	**	**	***	***	***
lin-52(n771) vs *lin-52(n771);exo-3(ok3559)*	0mJ/cm²			ns	ns	*
	40mJ/cm²	ns	*	ns	ns	*
	60mJ/cm²	*	ns	ns	*	**
exo-3(ok3559) vs *lin-52(n771);exo-3(ok3559)*	0mJ/cm²		**	***	***	***
	40mJ/cm²	*	***	**	**	***
	60mJ/cm²	*	**	***	*	***

Supplemental table 5: Statistical analysis of developmental assay in figure 10 containing two-tailed t- test and Fisher´s exact test. Asterisks indicate following significance: p> 0.05 =ns, p<0.05 = *, p<0.01 = ** p<0.001 = ***.

Supplemental table 6

Two-tailed t-test		**L1**	**L2**	**L3**	**L4**	**Fisher´s exact test**
wildtype vs *lin-52(n771)*	0mJ/cm²			*	*	*
	40mJ/cm²	**	**	***	***	***
	60mJ/cm²	***	**	*	***	***
wildtype vs *parp-1(ok988)*	0mJ/cm²			*	*	**
	40mJ/cm²	**	ns	ns	*	***
	60mJ/cm²	ns	ns	ns		ns
wildtype vs *lin-52(n771)**;** parp-1(ok988)*	0mJ/cm²			ns	ns	ns
	40mJ/cm²	***	**	*	**	***
	60mJ/cm²	*	**	***	**	***
lin-52(n771) vs *parp-1(ok988)*	0mJ/cm²			***	***	***
	40mJ/cm²	***	***	***	***	***
	60mJ/cm²	**	ns	*	***	***
lin-52(n771) vs *lin-52(n771);parp-1(ok988)*	0mJ/cm²			ns	ns	ns
	40mJ/cm²	ns	ns	ns	ns	ns
	60mJ/cm²	ns	ns	ns	**	ns
parp-1(ok988) vs *lin-52(n771);parp-1(988)*	0mJ/cm²			**	**	***
	40mJ/cm²	***	***	*	***	***
	60mJ/cm²	*	ns	**	**	***

Supplemental table 6: Statistical analysis of developmental assay in figure 11 containing two-tailed t- test and Fisher´s exact test. Asterisks indicate following significance: p> 0.05 =ns, p<0.05 = *, p<0.01 = ** p<0.001 = ***.

Supplemental table 7

Two-tailed t-test		**L1**	**L2**	**L3**	**L4**	**Fisher´s exact test**
wildtype vs *lin-52(n771)*	0mJ/cm^2			ns	ns	ns
	15mJ/cm^2			ns	ns	ns
	30mJ/cm^2	*	*	ns	*	**
wildtype vs *csa-1(tm4539)*	0mJ/cm^2			ns	ns	ns
	15mJ/cm^2	ns	ns	ns	*	**
	30mJ/cm^2	**	**	ns	***	***
wildtype vs *lin-52(n771)*; *csa-1(tm4539)*	0mJ/cm^2			ns	ns	ns
	15mJ/cm^2	ns		ns	ns	ns
	30mJ/cm^2	*	***	**	***	***
lin-52(n771) vs *csa-1(tm4539)*	0mJ/cm^2			ns	ns	ns
	15mJ/cm^2	ns	ns	ns	*	**
	30mJ/cm^2	***	**	ns	***	***
lin-52(n771) vs *lin-52(n771)*; *csa-1(tm4539)*	0mJ/cm^2			ns	ns	ns
	15mJ/cm^2			ns	ns	*
	30mJ/cm^2	**	***	**	***	***
csa-1(tm4539) vs *lin-52(n771)*; *csa-1(tm4539)*	0mJ/cm^2			ns	ns	ns
	15mJ/cm^2	ns	ns	ns	ns	ns
	30mJ/cm^2	ns	ns	*	ns	**

Supplemental table 7: Statistical analysis of developmental assay in figure 12 containing two-tailed t- test and Fisher´s exact test. Asterisks indicate following significance: p> 0.05 =ns, p<0.05 = *, p<0.01 = ** p<0.001 = ***.

Supplemental table 8

Two-tailed t-test		**L1**	**L2**	**L3**	**L4**	**Fisher´s exact test**
wildtype vs *lin-52(n771)*	0mJ/cm^2			ns	ns	ns
	15mJ/cm^2			ns	ns	ns
	30mJ/cm^2	***	***	**	**	***
wildtype vs *csb-1(ok2335)*	0mJ/cm^2			ns	ns	ns
	15mJ/cm^2	**	**	***	***	***
	30mJ/cm^2	***	***	**	***	***
wildtype vs *lin-52(n771)*; *csb-1(ok2335)*	0mJ/cm^2			ns	ns	ns
	15mJ/cm^2	*	*	***	***	***
	30mJ/cm^2	***	***	**	***	***
lin-52(n771) vs *csb-1(ok2335)*	0mJ/cm^2			ns	ns	ns
	15mJ/cm^2	**	**	***	***	***
	30mJ/cm^2	***	***	*	***	***
lin-52(n771) vs *lin-52(n771)*; *csb-1(ok2335)*	0mJ/cm^2			ns	ns	ns
	15mJ/cm^2	*	*	***	***	***
	30mJ/cm^2	***	***	ns	***	***
csb-1(ok2335) vs *lin-52(n771)*; *csb-1(ok2335)*	0mJ/cm^2			ns	ns	ns
	15mJ/cm^2	ns	ns	***	***	***
	30mJ/cm^2	**	ns	**		***

Supplemental table 8: Statistical analysis of developmental assay in figure 12 containing two-tailed t- test and Fisher´s exact test. Asterisks indicate following significance: p> 0.05 =ns, p<0.05 = *, p<0.01 = ** p<0.001 = ***.

Supplemental table 9

Two-tailed t-test		**L1**	**L2**	**L3**	**L4**	**Fisher´s exact test**
wildtype vs *lin-52(n771)*	0mJ/cm²			ns	ns	ns
	40mJ/cm²	***	**	ns	**	***
	60mJ/cm²	**	ns	**		***
wildtype vs *xpc-1(tm3886)*	0mJ/cm²			ns	ns	ns
	40mJ/cm²	*	**	**	**	***
	60mJ/cm²	ns	ns			ns
wildtype vs *lin-52(n771)*; *xpc-1(tm3886)*	0mJ/cm²			ns	ns	ns
	40mJ/cm²	ns	ns	*	**	***
	60mJ/cm²	**	**	ns		***
lin-52(n771) vs *xpc-1(tm3886)*	0mJ/cm²			ns	ns	ns
	40mJ/cm²	***	***	**	**	***
	60mJ/cm²	***	ns	**		***
lin-52(n771) vs *lin-52(n771)*; *xpc-1(tm3886)*	0mJ/cm²			ns	ns	ns
	40mJ/cm²	**	**	**	**	***
	60mJ/cm²	ns	*	*		***
xpc-1(tm3886) vs *lin-52(n771)*; *xpc-1(tm3886)*	0mJ/cm²			ns	ns	ns
	40mJ/cm²	ns	ns	ns		*
	60mJ/cm²	***	***	ns		***

Supplemental table 9: Statistical analysis of developmental assay in figure 13 containing two-tailed t- test and Fisher´s exact test. Asterisks indicate following significance: p> 0.05 =ns, p<0.05 = *, p<0.01 = ** p<0.001 = ***.

Supplemental table 10

Two-tailed t-test		**L1**	**L2**	**L3**	**L4**	**Fisher´s exact test**
wildtype vs *lin-52(n771)*	0mJ/cm^2			ns	ns	ns
	5mJ/cm^2			ns	ns	ns
	10mJ/cm^2			ns	ns	ns
wildtype vs *xpa-1(ok698)*	0mJ/cm^2			ns	ns	ns
	5mJ/cm^2	***	***	ns	***	***
	10mJ/cm^2	***	***	ns	***	***
wildtype vs *lin-52(n771); xpa-1(ok698)*	0mJ/cm^2			ns	ns	ns
	5mJ/cm^2	***	***	ns	***	***
	10mJ/cm^2	***	**	ns	***	***
lin-52(n771) vs *xpa-1(ok698)*	0mJ/cm^2			ns	ns	ns
	5mJ/cm^2	***	***	ns	***	***
	10mJ/cm^2	***	***	ns	***	***
lin-52(n771) vs *lin-52(n771); xpa-1(ok698)*	0mJ/cm^2			ns	ns	ns
	5mJ/cm^2	***	***	ns	***	***
	10mJ/cm^2	***	**	ns	***	***
xpa-1(ok698) vs *lin-52(n771); xpa-1(ok698)*	0mJ/cm^2			ns	ns	ns
	5mJ/cm^2	ns	ns			ns
	10mJ/cm^2	ns	ns			ns

Supplemental table 10: Statistical analysis of developmental assay in figure 14 containing two-tailed t- test and Fisher´s exact test. Asterisks indicate following significance: p> 0.05 =ns, p<0.05 = *, p<0.01 = ** p<0.001 = ***.

Supplemental table 11-14

The supplemental tables 11-14 show statistical results using the Multi-Range Large Particle Flow Cytometer (BioSorter). Abbreviated forms of strains were used. The *xpa-1(ok698); sbjIn27[pBS128(xpa-1::GFP) + pBS174(myo-2::tdTomato)]* transgene mutant strain was abbreviated as "*xpa-1(ok698); sbjIn27*". Numbers in brackets of the double mutant transgene strains indicate crossing number. The data from the BioSorter were first transformed into a logarithmic function. To test for possible significant differences an one-way Anova was performed, comparing the single and double mutant worms for each larval stage. Subsequently, a Tukey test was applied to compare two different groups from one larval stage with each other. Asterisks indicate following significance: p> 0.05 =ns, p<0.05 = *, p<0.01 = ** p<0.001 = ***.

To determine the effect size, the Cohens d was determined. The original fixed intervals of Cohen were used for this analysis (86): d ≥ 0.2 = "small", d ≥ 0.5 = "medium", d ≥ 0.8 = "large".

Supplemental table 11

L1 stage	**Tukey´s Test**	**Cohens d**
xpa-1(ok698);sbjIn27 vs *lin-52(n771);xpa-1*(ok698);sbjIn27 (#10)	***	1.16569076
xpa-1(ok698);sbjIn27 vs *lin-52(n771);xpa-1(ok698);sbjIn27* (#11)	***	1.36709338
lin-52(n771);xpa-1(ok698);sbjIn27 (#10) vs *lin-52(n771);xpa-1(ok698);*sbjIn27 (#11)	***	0.30632359

Supplemental table 11: Statistical analysis of experiment shown in figure 17a.

Supplemental table 12

L3 stage	**Tukey´s test**	**Cohens d**
xpa-1(ok698);sbjIn27 vs *lin-52(n771);xpa-1(ok698);sbjIn27* (#10)	***	0.98761313
xpa-1(ok698);sbjIn27 vs *lin-52(n771);xpa-1(ok698);sbjIn27* (#11)	***	0.58175131
lin-52(n771);xpa-1(ok698);sbjIn27 (#10) vs *lin-52(n771);xpa-1(ok698);sbjIn27* (#11)	***	0.47209428

Supplemental table 12: Statistical analysis of experiment shown in figure 17b.

Supplemental table 13

L4 stage	**Tukey´s test**	**Cohens d**
xpa-1(ok698);sbjIn27 vs *lin-52(n771);xpa-1(ok698);sbjIn27* (#10)	***	0.6707703
xpa-1(ok698);sbjIn27 vs *lin-52(n771);xpa-1(ok698);sbjIn27* (#11)	***	0.54265225
lin-52(n771);xpa-1(ok698);sbjIn27 (#10) vs *lin-52(n771);xpa-1(ok698);sbjIn27* (#11)	ns	0.11805803

Supplemental table 13: Statistical analysis of experiment shown in figure 17c.

Supplemental table 14

Adult stage	**Tukey´s test**	**Cohens d**
xpa-1(ok698);sbjIn27 vs *lin-52(n771);xpa-1(ok698);sbjIn27* (#10)	***	0.595205972
xpa-1(ok698);sbjIn27 vs *lin-52(n771);xpa-1(ok698);sbjIn27* (#11)	***	0.539689591
lin-52(n771);xpa-1(ok698);sbjIn27 (#10) vs *lin-52(n771);xpa-1(ok698);sbjIn27* (#11)	**	0.251693153

Supplemental table 14: Statistical analysis of experiment shown in figure 17d.

Supplemental table 15

Two-tailed t-test		**L1**	**L2**	**L3**	**L4**	**Fisher´s exact test**
wildtype vs *lin-52(n771)*	0 min			ns	ns	ns
	4 min		ns	ns	ns	*
	6 min		ns	**	**	***
wildtype vs *xpa-1(ok698)*	0 min			ns	ns	ns
	4 min	ns	**	***	***	***
	6 min	**	*	ns	***	***
wildtype vs *lin-52(n771)*; *xpa-1(ok698)*	0 min			ns	ns	ns
	4 min	ns	*	***	***	***
	6 min	*	***	*	***	***
lin-52(n771) vs *xpa-1(ok698)*	0 min			ns	ns	**
	4 min	ns	*	***	***	***
	6 min	**	*	*	***	***
xpa-1(ok698) vs *lin-52(n771); xpa-1(ok698)*	0 min			ns	ns	*
	4 min	ns	ns	ns	ns	ns
	6 min	ns	ns	ns	ns	ns

Supplemental table 15: Statistical analysis of developmental assay using the drug Trioxsalen and UV-A irradiation (per time) shown in figure 19. This table shows only the results of the Trioxsalen + UV-A irradiated group. Trioxsalen negative control is not shown. Asterisks indicate following significance: p> 0.05 =ns, p<0.05 = *, p<0.01 = ** p<0.001 = ***.

Supplemental table 16

Two-tailed t-test		**L1**	**L2**	**L3**	**L4**	**Fisher´s exact test**
wildtype vs *lin-52(n771)*	0 mg/ml			ns	ns	ns
	0.5 mg/ml			**	**	ns
	0.75 mg/ml	ns	ns	ns	ns	*
	1 mg/ml	***	ns	*	ns	**
wildtype vs *polh-1(if31)*	0 mg/ml			ns	ns	ns
	0.5 mg/ml	***	*	***	***	***
	0.75 mg/ml	*	***	**	**	***
	1 mg/ml	*	**	**		***
wildtype vs *lin-52(n771)*; *polh-1(if31)*	0 mg/ml			ns	ns	ns
	0.5 mg/ml		ns	***	***	***
	0.75 mg/ml	**	**	*	**	***
	1 mg/ml	ns	**	***		***
lin-52(n771) vs *polh-1(if31)*	0 mg/ml			ns	ns	ns
	0.5 mg/ml	***	*	***	***	ns
	0.75 mg/ml	*	***	*	***	***
	1 mg/ml	**	***	***	ns	*
lin-52(n771) vs *lin-52(n771)*; *polh-1(if31)*	0 mg/ml			ns	ns	ns
	0.5 mg/ml		ns	***	***	***
	0.75 mg/ml	**	**	ns	***	***
	1 mg/ml	*	***	***	ns	***
polh-1(if31) vs *lin-52(n771)*; *polh-1(if31)*	0 mg/ml			ns	ns	ns
	0.5 mg/ml	***	ns	ns	ns	***
	0.75 mg/ml	ns	ns	*		***
	1 mg/ml	ns	ns	ns		***

Supplemental table 16: Statistical analysis of development assay using different amounts of MMS (mg/ml) shown in figure 20. Asterisks indicate following significance: p> 0.05 =ns, p<0.05 = *, p<0.01 = ** p<0.001 = ***.

Supplemental table 17

Two-tailed t-test		**L1**	**L2**	**L3**	**L4**	**Fisher´s exact test**
wildtype vs *lin-52(n771); xpc-1(tm3886); csb-1(ok2335)*	0mJ/cm^2		ns	ns	*	ns
	5mJ/cm^2	***	***			***
	10mJ/cm^2	***	***			***
wildtype vs *xpc-1(tm3886); csb-1(ok2335)*	0mJ/cm^2		ns	ns	ns	ns
	5mJ/cm^2	***	***			***
	10mJ/cm^2	***	***			***
lin-52(n771); xpc-1(tm3886); csb-1(ok2335) vs *xpc-1(tm3886); csb-1(ok2335)*	0mJ/cm^2		ns	ns	ns	ns
	5mJ/cm^2	ns	ns			ns
	10mJ/cm^2	ns	ns			ns

Supplemental table 17: Statistical analysis of development assay shown in supplemental figure 3. Asterisks indicate following significance: p> 0.05 =ns, p<0.05 = *, p<0.01 = ** p<0.001 = ***.